ELUCIDATING THE ANTI-INFLAMMATORY MECHANISM AND TARGETS OF DT-13 IN LPS STIMULATED RAW264.7 CELLS

Inaugural Dissertation

to obtain the academic degree

Doctor rerum naturalium (Dr. rer. nat.)

Submitted to the Department of Biology, Chemistry, Pharmacy

of Freie Universität Berlin

By

SHIKHA RAINA

Berlin 2024

This thesis was performed from June 2020 to December 2023 under the supervision of Prof. Dr. Hendrik Fuchs, Institute of Diagnostic Laboratory Medicine, Clinical Chemistry and Pathobiochemistry, Charité – Universitätsmedizin Berlin.

1st Reviewer:

Prof. Dr. Hendrik Fuchs

Charité – Universitätsmedizin Berlin

Institute of Diagnostic Laboratory Medicine, Clinical Chemistry and Pathobiochemistry

Augustenburger Platz 1

13353 Berlin Germany

2nd Reviewer:

Prof. Dr. Gerhard Wolber

Freie Universität Berlin

Computer-Aided Drug Design Institute of Pharmacy Pharmaceutical Chemistry

Königin-Luise-Str. 2+4/R275 VH

14195 Berlin, Germany

Date of defense: 04.12.2024

Acknowledgement

This thesis is not just an academic achievement for me instead it has been a wonderful journey that I started in Berlin after coming from India. In this time, I have had amazing experiences personally and professionally. First, I would like to express my immense gratitude to my supervisor Prof. Hendrik Fuchs for allowing me to pursue this doctoral thesis in his group. I have been fortunate to work under the guidance of such an amazing person, who not only helped to navigate through the experiments but also gave motivation and advice whenever needed.

I want to thank Prof. Gerhard Wolber, who accepted to be second supervisor and assisted me to pursue the thesis from Freie University.

This work could not have been possible without people who made each day funtastic. The PhD gang – Tuyen, Melanie, Phillip; the meeting coordinators and building blocks – Mazdak and Gregor; our know-it-all neighbours – Burak, Marten, Isa; our former labmates – Lena, Allesio, Alexandra, Nicole and Gaurav for their valuable comments and advice and my dear students Emely and Esther.

I also want to thank Dr. Jens Dernedde, who was always there to help and motivate me.

I want to express my thanks and love to my parents and my sister, who prayed and supported me from miles away.

Lastly, I dedicate this thesis to my husband Kumar, who stayed with me through the highs and lows, believed in me and supported me at each step. Also, to my son because of whom it could have finished little early. Love you both.

This work has been funded by the Deutsche Forschungsgemeinschaft (DFG) (Grant no: FU 408/11-1)

Declaration of Authorship

Herewith I certify that I have prepared and written my thesis independently and that I have not used any sources and aids other than those indicated by me.

Shikha Raina

Table of contents

Zusammenfassung

Saponine sind sekundäre Stoffwechselprodukte, die den Pflanzen helfen, sich vor Pflanzenfressern zu schützen und die bereits in der alten Medizin Verwendung fanden. Ginsenoside aus *Panax ginseng* C.A.MEY , Curcumin aus *Curcuma longa* L. und viele andere wurden wegen ihrer entzündungshemmenden, krebshemmenden und pilzhemmenden Eigenschaften erforscht. Vor allem triterpenoide Saponine wie Ginsenoside sind gut charakterisiert, während steroidale Saponine wie DT-13 weniger erforscht sind. Daher haben wir in dieser Studie den Mechanismus und die Zielstrukturen von DT-13 als entzündungshemmende Substanz untersucht. Zu diesem Zweck wurden Lipopolysaccharid(LPS)-stimulierte RAW264.7-Mausmakrophagen als In-vitro-Entzündungsmodell verwendet. Die mit DT-13 vorbehandelten Zellen wurden mit denen verglichen, die mit Rk1 (Ginseng-saponin) und Dexamethason (synthetisches entzündungshemmendes Medikament) vorbehandelt wurden. DT-13 hemmte pro-inflammatorische Zytokine effizienter als Rk1 und Dexamethason. DT-13 reduzierte die Genexpression von Tumornekrosefaktor alpha (TNFα) und Cyclooxygenases-2 (COX-2) um 85 % bzw. 99 %. Es hemmte auch die Freisetzung von IL-6 aus den Zellen um 89 %, gemessen mit einem enzymgekoppelten Immunadsorptionstest (ELISA). Wie Rk1 und Dexamethason hemmte DT-13 die nukleäre Lokalisierung von *phosphorylated-nuclear factor kappa B* (p-NFκB) wie mit Immunfluoreszenzmikroskopie beobachtet wurde.

Diese Ergebnisse deuten darauf hin, dass DT-13 als entzündungshemmendes Mittel über den NFκB-Signalweg wirkt. Die Bestätigung der Beeinflussung der NFκB-Signalisierung durch DT-13 führte zur Untersuchung anderer Gene, die durch NFκB-Aktivierung reguliert werden. Interessanterweise wurde beobachtet, dass DT-13 die Expression der nod like receptor family pyrin binding domain 3 (NLRP3)- und interleukin 1 beta (IL-1β) gene um 73 % bzw. 92 % reduzierte. Es hemmte auch signifikant die NLRP3-Inflammasom-induzierte Caspase1-Aktivierung und IL-1β-Freisetzung. Die Bildung des Membranangriffskomplexes wurde ebenfalls gehemmt, wie durch den alternate pathway (AP) Komplement-Test überprüft wurde. Dies lässt den Schluss zu, dass er auch an der Abschwächung der NLRP3-Inflammasombildung beteiligt ist. Es ist bekannt, dass der ligandenaktivierte Peroxisom-Proliferator-Rezeptor gamma (PPARγ) die durch LPS stimulierte NFκB-Genaktivierung durch

einen Mechanismus hemmt, der als "Transrepression" bezeichnet wird. DT-13 und Rk1 wurden als Liganden für die PPARγ-Aktivierung unter Verwendung des HEK-Transfektionsmodellsystems untersucht. Sowohl DT-13 als auch Rk1 induzierten signifikant die Expression von Luziferase-konjugierten PPARγ-Reaktionselementen und damit die Aktivierung von PPARγ. Dies wurde auch durch eine in silico-Studie bestätigt, die die Bindungsstelle für DT-13 in der PPARγ-Ligandenbindungstasche aufzeigt. Zusammenfassend lässt sich sagen, dass alle Ergebnisse erfolgreich auf die entzündungshemmende und Inflammasomen hemmende Eigenschaft von DT-13 über die Ligandenaktivierung von PPARγ in Mausmakrophagen schließen lassen.

Abstract

Saponins are secondary metabolites that aid in plants' defense against herbivory and have been used in ancient medical practices. Ginsenosides from *Panax ginseng* C.A.MEY, Curcumin from *Curcuma longa* L. and many more were explored for their anti-inflammatory, anti-cancer, and anti-fungal properties. Especially triterpenoid saponins like ginsenosides are well characterized whereas steroidal saponins like DT-13 are not well explored. Therefore, in this study we investigated the mechanism and targets of DT-13 as an anti-inflammatory compound. To achieve this, lipopolysaccharide (LPS) stimulated RAW264.7 mouse macrophages were used as in vitro inflammatory model. Cells pretreated with DT-13 were compared with those pretreated with Rk1 (ginseng saponin) and dexamethasone (synthetic anti-inflammatory drug). DT-13 inhibited pro-inflammatory cytokines more efficiently when compared to Rk1 and dexamethasone. DT-13 downregulated gene expression of tumor necrosis factor-alpha (TNFα), cyclooxygenases-2 (COX-2) by 85% and 99% respectively. It also inhibited interleukin-6 (IL-6) release from cells by 89% as measured by enzyme linked immunosorbent assay (ELISA). Like Rk1 and dexamethasone, DT-13 inhibited nuclear localization of phosphorylated-nuclear factor kappa B (p-NFκB), as observed with immunofluorescence microscopy. These results indicate that DT-13 acts as anti-inflammatory agent via NFκB signaling pathway. The confirmation of interference of NFκB signaling by DT-13 lead to investigation of other genes regulated by NFκB activation. Interestingly, it was observed that DT-13 reduced the expression of nod like receptor family pyrin binding domain 3 (NLRP3) and interleukin 1 beta (IL-1β) gene by 73% and 92% respectively. It also significantly inhibited NLRP3-inflammasome induced Caspase-1 activation and IL-1β release. Membrane attack complex formation was also inhibited as checked by alternate pathway (AP) complement assay. This concludes that it is involved in attenuation of NLRP3 inflammasome formation as well. It is known that ligand activated peroxisome proliferator activated receptor inhibits LPS stimulated NFκB gene activation by a mechanism called as 'trans-repression'. DT-13 and Rk1 were explored as ligands for PPARγ activation using HEK transfection model system. DT-13 and Rk1 both significantly induced the expression of luciferase conjugated PPARγ response elements and hence the activation of PPARγ. This was also concluded by in silico study that shows the binding affinity of DT-13 in PPARγ ligand binding pocket similar

to that of rosiglitazone. To summarise, all the results successfully concluded anti-inflammatory and anti-inflammasome properties of DT-13 via ligand activation of PPARγ in mouse macrophages.

Abbreviations

9-HODE	9-hydroxyoctadecadienoic acid
ACN	Acetonitrile
AIM2	Absent in melanoma 2
AP	Alternate pathway
ARG	Arginine
ASC	Apoptosis associated speck like protein
ATCC	American type culture collection
BSA	Bovine Serum Albumin
CD14	Cell differentiation factor 14
COX/2	Cyclooxygenase/2
CYS	Cysteine
DAMPs	Damage associated molecular patterns
DAPI	4′,6-diamidino-2-phenylindole
DMEM	Dulbecco’s minimal eagles’ medium
DMSO	Dimethylsulfoxide
ESI-MS	Electrospray ionization-mass spectrometry
FBS	Fetal bovine serum
FITC	Fluorescein isothiocyanate
GLU	Glutamic acid
HDAC3	Histone deacetylase 3
HPLC	High performance liquid chromatography
IF	Immunofluorescence
IKKB	A kappa B kinase
IL-1β	Interleukin 1 beta

IL-6	Interleukin-6
ILE	Isoleucine
iNOS	inducible Nitric oxide synthase
IκBα	I kappa B alpha
LBAmp	Lysogeny broth with ampicillin
LBD	Ligand binding domain
LBP	Lipopolysaccharide Binding Protein
LEU	Leucine
LOX	Lipoxygenase
LPS	Lipopolysaccharide
MAC	Membrane attack complex
MTT	3-(4,5-dimethylthiazol-2-yl)-2,5-diphenyltetrazolium bromide
MyD88	Myeloid differentiation response protein 88
N/n	biological repeats/technical repeats
NCOR	Nuclear receptor corepressor
NFκB	Nuclear factor kappa B
NLR	Nod like receptor
NLRP3	NLR family pyrin binding domain 3
NO	Nitric oxide
NSAIDs	Non-steroidal anti-inflammatory drugs
P/S	Penicillin/streptomycin
PAMPs	Pathogen associated molecular patterns.
PBS/T	Phosphate Buffer Saline / with Tween20
p-JNK	phosphorylated Jun-N terminal kinase
p-p38 MAPK	phosphorylated protein 38 mitogen activated kinase

PPARγ	Peroxisome proliferator-activated receptor gamma
PRRs	Pathogen recognition receptors
ROS	Reactive oxygen species
RXR	Retinoid-X-Receptor
SD	Standard deviation
SDS	Sodium dodecyl sulfate
SER	Serine
SEM	Standard error mean
TAE	tris(hydroxymethyl)-aminomethane-acetate-ethylenediaminetetraacetic acid buffer
TAK1	Transforming growth factor beta activated kinase 1
TFA	Trifluoroacetic acid
TICAM	Toll interleukin receptor containing domain adaptor molecule
TLR/4	Toll like receptor/4
TNFα	Tumor necrosis factor-alpha
TYR	Tyrosine
WB	Western blot
β-actin	Beta actin

List of Figures

Appendex Figures

List of Tables

1. Introduction

1.1 Inflammation and Immunity

Our immune system, like our body, is composed of two arms innate and adaptive immunity that responds to various external pathogens encountering our system [1]. Innate immune response is the first non-antigen specific response of the host cell to the pathogen that is comprised of macrophages and neutrophils [2]. Adaptive immunity or pathogen specific response is marked by the involvement of effector cells like T cells and B cells under the influence of innate immune system [3]. Inflammation, on the other hand, is characterized by the recruitment of immune cells by external stimuli like bacterial pathogens at the site of infection [4]. This response of the innate immune system acts as a defense mechanism to eliminate the cause of infection, restoration of the normal functioning of the body and for the development of adaptive immunity for the concerned pathogen [5] whereas persistent and immoderate increase in the immune cells leads to chronic inflammation [6].

1.2 Types of Inflammation

Inflammation is mainly categorised into acute and chronic inflammation. Acute Inflammation occurs via four different phases [7]. It is initiated first by the inducers of inflammation like external stimuli causing tissue injury or infection. The second stage of inflammation is the recognition of the stimuli by sensors, for example the receptors on macrophages and mast cells. The third stage is characterized by inflammation mediators like cytokines, prostaglandins that convey the message to the other cells and organelles (Figure 1).The last stage is the actual site of infection which shows the classic four symptoms of inflammation – rubor (redness), calor (heat), tumor (swelling), and dolor (pain) [7]. If the combined effect of inflammatory mediators is insufficient to resolve the infection, then a chronic inflammatory state takes over where pathogen persists and leads to tissue detriment [8] by forming tertiary lymphoid tissues for example [9, 10]

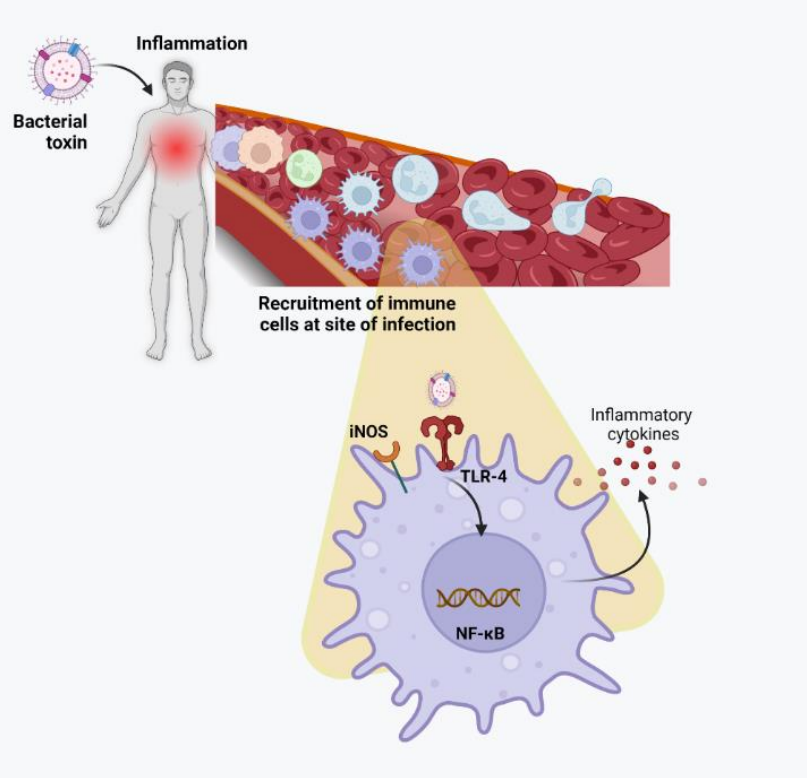

Figure 1: Bacterial LPS induced inflammation in macrophages.

Diagrammatic representation of a generalized bacterial toxin induced toll like receptor pathway in macrophages that leads to inflammation and production of inflammatory cytokines. Image information was retrieved from Rebeiro *et al*, José Luis *et al* [11, 12] and created with Biorender.com.

1.3 Inflammation associated diseases

The prolonged prevalence of any of the above-mentioned stages disbalances the innate immune functioning and thereby consummates to the formation of chronic inflammatory environment. This underlies various metabolic disorders including rheumatoid arthritis, diabetes, obesity, and neurodegenerative diseases (Figure 2). Reports suggest that increase in inflammatory cytokines lead to stress dependent loss of function of pancreatic beta cells progressing towards insulin resistance and type 2 diabetes [13]. In addition, chronic inflammation leads to formation of an environment suitable for cell mutagenesis, damage induced cell proliferation and tumorigenesis that aids in the development of cancer [14].

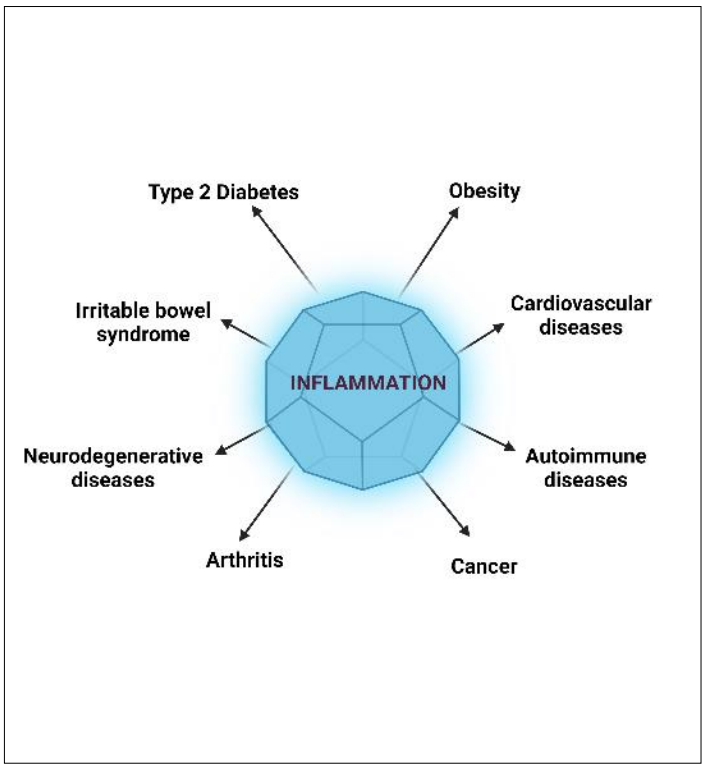

Figure 2: Graphical representation of diseases associated with inflammation.

The image was adapted from Liu C *et al*., 2017 [15], created with Biorender.com.

Vascular inflammation (atherosclerosis) can progress to stroke [16] and the increased proinflammatory cytokines can lead to cerebrovascular disease that causes neuroinflammation [17]. This in turn increases the risk factor for depression, dementia and neurodegenerative diseases like Alzheimer's [18]. Another major cause of these chronic immune disease is the preference of catabolic pathway over anabolic state [19].

1.4 Inflammatory pathway: TLR4/NFκB signaling

The pathways involved in inflammatory processes can vary depending on the type of stimuli. External pathogenic antigens or internal oxidative stress are responsible for the activation of certain receptor mediated pathways that initiate the release of proinflammatory mediators [20].

This is the first line of defense mechanism for the body to cope with the damage done by the pathogens whereas persistent infection leads to the cytokine storm and hence

the underlying severity of inflammation associated disorders [21]. The conventional inflammatory pathway involves the activation of Toll like receptors (TLRs) by bacterial pathogens and activation of nuclear factor kappa B (NFκB) signaling cascade in antigen presenting cells like macrophages [22]. In such a pathway, bacterial endotoxin lipopolysaccharide (LPS) (consisting of Lipid A and O antigen of outer wall of gram-negative bacteria) is recruited to the TLR4 via LPS binding protein (LBP) and cell differentiation protein 14 (CD14). This binding leads to dimerization of TLR4 receptor and further activation of myeloid differentiation response protein 88 (MyD88) [23].

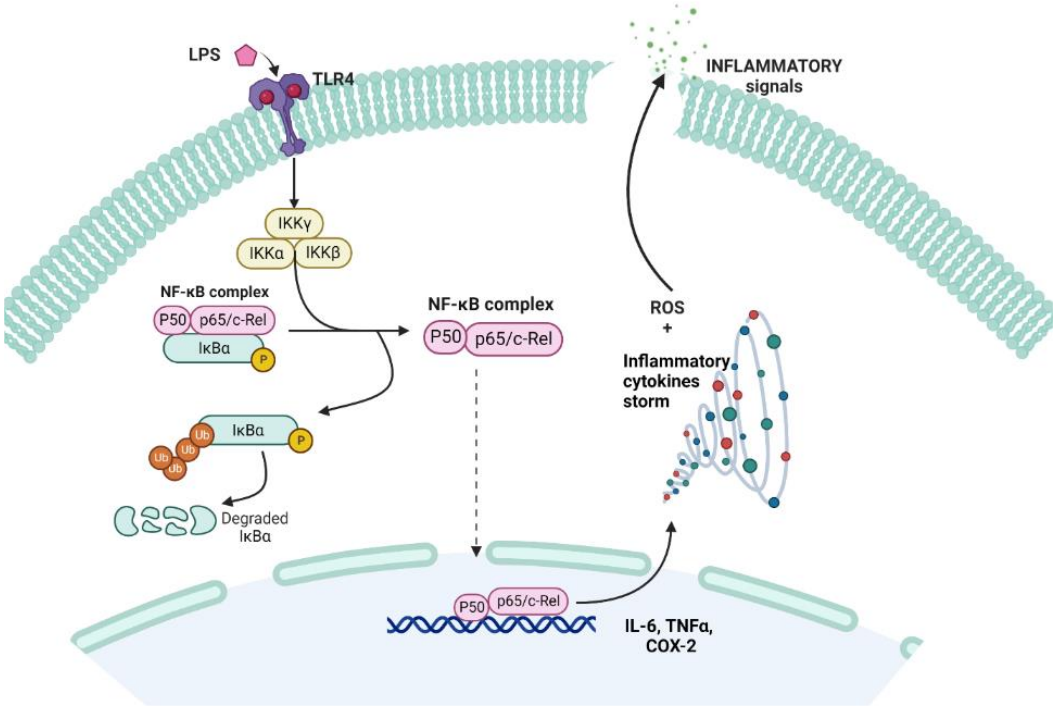

Figure 3 schematic illustration of LPS-induced TLR4/NFκB pathway responsible for production of Inflammatory signals by immune cells.

Image is created with Biorender.com and adapted from Kawai *et al* [22]

Further downstream upregulation of transforming growth factor beta activated kinase 1 (TAK1) triggers another kinase protein namely I kappa B kinase (IKK) complex. IKK protein activates I kappa B alpha (IκBα), a member of I kappa B protein. It binds NFκB protein and inhibits its activation, therefore also known as its repressor [24]. IκBα phosphorylation by IKK leads to its proteasomal degradation and release of NFκB. This ubiquitination of IκBα induces phosphorylation and activation of NFκB [25].

Phosphorylated NFκB further translocates from cytosol to nucleus acting as a transcription factor for the expression of pro-inflammatory genes like tumor necrosis factor-alpha (TNFα), interleukin-6 (IL-6), cyclooxygenase-2 (COX-2), inducible nitric oxide synthase (iNOS) and others. IκBα in turn undergoes ubiquitinylation followed by proteasomal degradation [25]. Therefore, inflammation is marked by the increased release of cytokines IL-6, TNFα and other inflammatory mediators like COX-2 and nitric oxide (NO). Additionally, there is mostly another pathway activated in parallel in response to the stress conditions that aggravate the production of these cytokines The severity of the inflammation associated disease is relative to the extent of the production of these inflammatory mediators [26].

1.5 Inflammasomes

In response to external pathogens like bacteria and viruses, multimeric cytosolic proteins are formed called as inflammasomes that initiate the activation and release of caspase-1 dependent IL-1β [27]. Bacterial and viral pathogens consisting of pathogen associated molecular patterns (PAMPs) or the damaged cells releasing damage associated molecular patterns (DAMPs) activate pathogen recognition receptors (PRRs).There are five types of PRRs that are associated in inflammasome assembly: Nod like receptor (NLR) member proteins – NLRP1, NLRP3 and NLRC4 – nucleotide binding oligomerization (NOD) protein central domain, absent in melanoma 2 protein (AIM2), pyrin domain, and apoptosis-associated speck like protein (ASC) [28]. As showed in Figure 4 an activated NLR family pyrin binding domain 3 (NLRP3) inflammasome molecule is mainly composed of NLR membrane protein- NLRP3, pro caspase-1 and ASC.

Inflammasomes activation is also known to work in parallel with the activation of the complement system. The recognition of PAMPs or DAMPs by PRRs activates the complement and the membrane attack complex (MAC) in presence of C5b9 component. This pore assembly in membranes consequently leads to a change in the membrane potential due to influx of calcium ions [29]. Also, efflux of adenosine triphosphates causes energy loss, which marks the beginning of pyroptosis [30] and eventually cell death [31, 32].

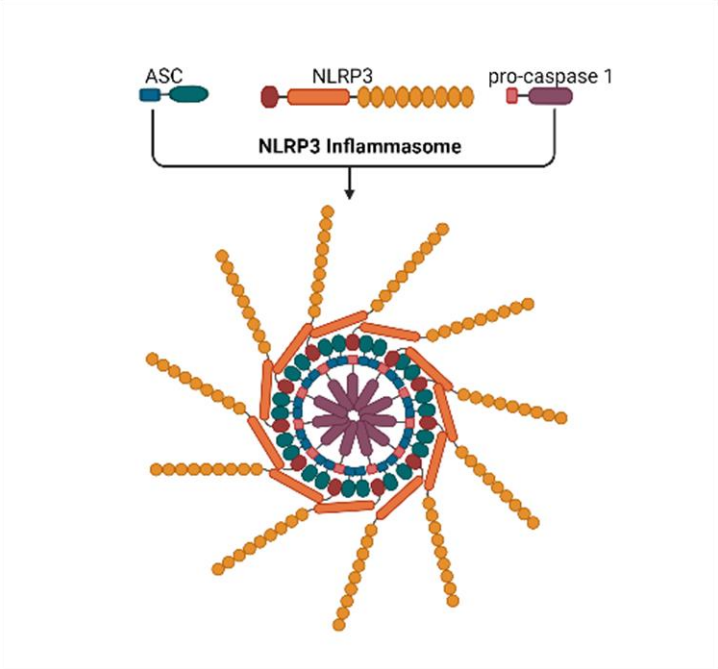

Figure 4: A diagrammatic representation of NLRP3 inflammasome

NLRP3-inflammasome structure consisting of three main components – ASC, NLRP3, pro-caspase-1. The image was derived from Seok,J.K *et al*., 2021 [33] and created with Biorender.com

1.6 NLRP3 inflammasome

Upon pathogen recognition, NFκB signaling cascade is activated. It is known to mediate the expression of the inflammasome specific genes NLRP3 and IL-1β. This in turn initiates the NLRP3 inflammasome cytosolic complex [34]. NLRP3 inflammasome activates proinflammatory caspase-1 which cleaves the pro-IL-1β into a mature form IL-1β and is released by the immune cells in parallel with other inflammatory cytokines [35]. Synthesis and release of IL-1β is associated with fever, pains, and inflammatory symptoms [36]. Further, activated caspase-1 along with AIM2, pyrin and ASC protein assembles activated inflammasomes that trigger the formation of pore like structure in the cells and thereby mediating pyroptosis [37] (Figure 5).

Inflammasome and complement mediated inflammation works in parallel creating a series of local inflammatory events that are responsible for disease pathophysiologies [32].

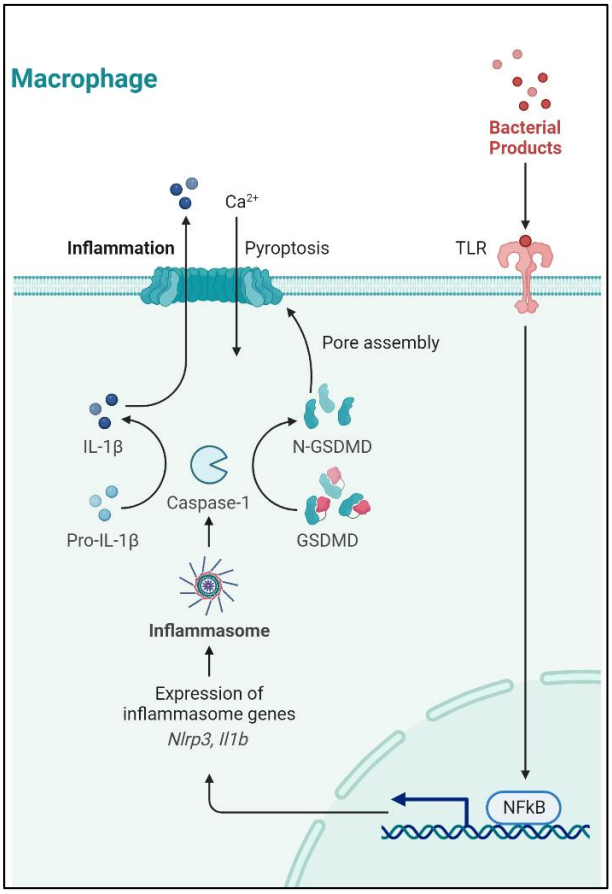

Figure 5: A schematic representation of the mechanism of NLRP3-inflammasome formation

NLRP3 inflammasome related genes are activated via NFκB pathway, initiating the formation of the inflammasome and activation of caspase-1. Inflammasome formation results in pore assembly and eventually cell death. The image is create with Biorender.com, adapted from [34] and "Inflammasome" template in BioRender.com (2020) and retrieved from https://app.biorender.com/biorender-templates.

.

1.7 Role in inflammation

There are numerous diseases that involve inflammasome formation leading to inflammation. Aggravated activation of NLRP3 inflammasome leads to an increase in reactive oxygen species mediated oxidative stress and cardiovascular dysfunction.
In addition to neurodegenerative diseases like Parkinson's diseases [38], Alzheimer's disease [39] [40], The NLRP3 inflammasome is also known to contribute to certain eye diseases like diabetic retinopathy, dry eyes [41-44] and cardiovascular diseases [45,

46]. Therefore, it is now researched as a therapeutic target for underlying autoinflammatory diseases [40, 47]. Inflammation and inflammasomes have also been implicated in SARS-CoV-2 [48]. Recently, Mieres-Castro and Mora-Poblete, in their review article, have explained the importance of saponins in the post COVID-19 era. They highlighted the risks of using steroidal and non-steroidal anti-inflammatory drugs (NSAIDs) and thereby emphasizing the role of natural compounds from plants as antiviral drugs [49].

1.8 NSAIDs and their effects

Depending on the type of inducers, inflammatory pathways are activated, namely the arachidonic acid and NFκB pathways. Induction of the arachidonic acid pathway activates leukotrienes and prostaglandins via lipoxygenases (LOX) and cyclooxygenases (COX) (Figure 6).

Synthetic drugs aim at inhibiting COX enzymes and thereby limiting the activation of local inflammatory responses. Such classical drugs available include ibuprofen, naproxen, diclofenac, celecoxib [50], and mefenamic acid [51].

These non-steroidal drugs are effective but constitute many side effects like stomach ulcers, hypertension, impaired wound healing, and others [52]. Therefore, as an alternative, naturally derived anti-inflammatory drugs are now being studied [53]. They are often considered more effective, specifically for long term pain relief. Flavonoids, alkaloids, terpenoids and polyphenols are a few types of natural chemicals found in plants known to have anti-inflammatory properties [54, 55]. Some known examples are azadirachtin [56], curcumin [57], embelin [58], resveratrol [59] and quercetin [60].

Inflammasome inhibitors for example thalidomide [61], anakinra [62], parthenolide [63], and canakinumab [64] are the examples of drugs used in clinical trials. Additionally, various caspase-1 inhibitors potentially have antitumor properties, for e.g. VX-765 (Balnacasan), and Ac-YVAD-CHO [65].

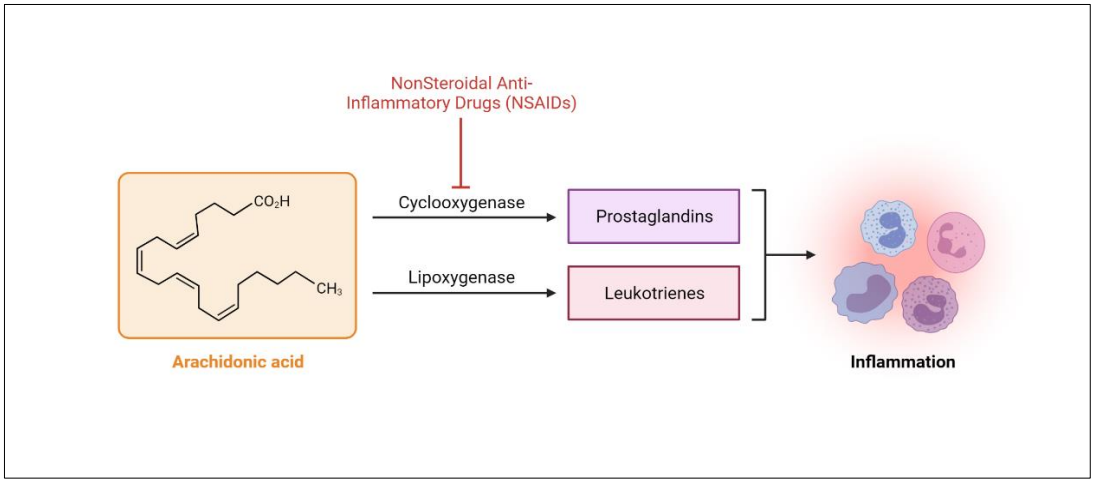

Figure 6: Mode of action of NSAIDs in inflammation

Synthetic anti-inflammatory drugs like ibuprofen inhibit cyclooxygenases in the arachidonic acid pathway and thereby preventing synthesis of prostaglandins-mediators of inflammation. Image is adapted [66] and retrieved from “Arachidonic Acid Induces Inflammation" template in Biorender.com

Due to many known side effects, compounds from natural sources like plants are preferred over synthetic ones [67]. Natural products are known to be structurally advantageous for drug discovery due to their rigid protein-protein interaction, higher molecular mass and optimized structure [68] in relevance with their anti-cancer and anti-inflammatory function [69]. These compounds have been used in ancient traditional medicine and therefore are referred to be safe and highly efficient to use.

1.9 Saponins

Saponins are soap-like structures mostly found in plants and some star fishes as well. These are structurally amphipathic molecules with sugar chains attached to a minimum of four hydrocarbon rings of steroidal or triterpenoidal origin. They form micelles in water and froth when agitated. Their glycosidic part is considered important for various functional properties. For example, presence of single sugar residues is known to form more froth in comparison to the one with more than one sugar residue [70]. Also, it was reported that the number and position of binding of sugar chain determines the cytotoxicity of the saponins [71].

These plant metabolites are generally known to prevent herbivory. They are also thought to kill microbes, fungi and insects affecting plant growth [72]. Saponins are studied widely for its medicinal properties. It is known to impart antifungal, antimicrobial, anti-inflammatory and anti-cancer effects. In contrast to its beneficial effects, lower membrane permeability and poor bioavailability makes it a challenging drug candidate [73]. Therefore, studies are focused on pure isoforms and compounds of saponins isolated from crude extracts to ensure maximum effectiveness and absorption in the cell. Also, saponin coated nanoparticles are being designed and studied for increasing the bioavailability of the saponins [74]. They are increasingly researched as an adjuvant for vaccines [75].

1.10 Saponin biosynthesis and metabolism

Saponins can be categorised into steroidal saponin and triterpenoid saponin based on the different aglycone part. They are biosynthesised via mevalonate pathway in cytosol of plants[76]. The pathway starts with acetyl-Coenzyme A (CoA) which is converted to precursor squalene. Squalene is further oxidized to 2,3-oxidosqualene which is later oxidized to cycloartanes. These cycloartenols are the precursor of cholesterol biosynthesis. Cholesterol is the main precursor of synthesis of steroidal saponins [77] and 2,3-oxidosqualene forms the precursor for the synthesis of triterpene aglycones [78]. Absorption and disposition of saponins are not well studied. However, it is known that saponins are poorly absorbed by intestinal lining [79] due to their complex structures and high molecular mass [80]. Natural ginsenosides for example are difficult to be directly absorbed and therefore need biotransformation into secondary saponins which is mainly done by intestinal microflora [81].

1.11 Properties of saponins

1.11.1 Anti-inflammatory

Saponins are known for its various medicinal properties and has been implicated in ancient Chinese and Indian (Ayurvedic) medicinal practices for example ginseng and curcumin. Saponins, mostly triterpenoids have already been studied for its anti-inflammatory properties, whereas steroidal saponins are now gaining attention [82].

The mechanism of anti-inflammatory saponins is majorly known and is thought to be acting via intervening the NFκB and phosphoinositide 3-kinases / AKT serine/threonine kinase 1 (PI3K/AKT) pathway [83]. Ginseng saponin from plant *Panax ginseng* C.A. MEY, among all is widely researched, whereas steroidal saponin DT-13 from plant *Liriope muscari (decne)* L.H. BAILEY is not well known. Therefore, this study focuses on understanding the mechanism and target of DT-13 in comparison with other known saponins and drugs.

1.11.2 Anti-diabetic

Saponins isolated from Momordica charantia (bitter gourd) stimulated insulin secretion in vitro [84]. Ethanolic extracts from *Bryonia laciniosa* LINN imparted anti-hyperglycemic and anti-hyperlipidemic activity in diabetic rats [85]. Zhang *et al*. isolated 33 saponins from *Trigonella foenum-graecum* L. (fenugreek) and observed three sapogenins and two saponins having inhibitory effects on α-glucosidase activity [86].

1.11.3 Anti-cancer

The cytotoxic properties of saponins have been investigated in association with anti-cancer activity [87] Diosgenin, a steroidal saponin, is known as one of the strong cytotoxic compounds inducing apoptosis in osteosarcoma cells [88] Hederagenin glycosides from Medicago species are studied as anticancer agents inhibiting the proliferation of Hela and MCF cell line invitro[89]. Xia-Jian *et al*. summarised triterpenoids as agents for potential reversal of anticancer drug resistance [90].

1.11.4 Anti-microbial

With antibiotic resistant bacterias on rise, the need for novel antimicriobial compounds has become necessary to reduce economic burden [91]. Therfore, more natural compounds are studied with respect to their anti-microbial properties. Extracts obtained from *Moringa oleifera* seeds showed significant inhibition of Staphylococcus aureus,Escherichia coli, Klebsiella, Streptococcus aureus,and Pseudomonas

aureginosa [92]. Joana et al studied the antimicrobial effect of phytochemicals in synegistic with antibiotics in biofilm state [93].

1.12 Saponins used in the study

1.12.1 DT-13

Steroidal saponin DT-13 is obtained from the roots of *Liriope muscari* L.H.BAILEY and has recently been studied for its medicinal properties. It consists of three sugar rings – xylose, mannose and glucose attached to the steroidal hydrophobic backbone. Oral toxicological studies have shown that it is of low toxicity and did not induce any mortality or any changes in organs of mice at a single dose of 5000 mg/kg [35]. Studies have shown that DT-13 attenuates inflammation via MAPK/NFκB pathway [36]. It has been implicated in studies with anti-thrombotic activity [37]. It is also known to inhibit TNFα induced NO and reactive oxygen species in vivo [38]. Figure 7 shows the structure of DT-13 and Rk1.

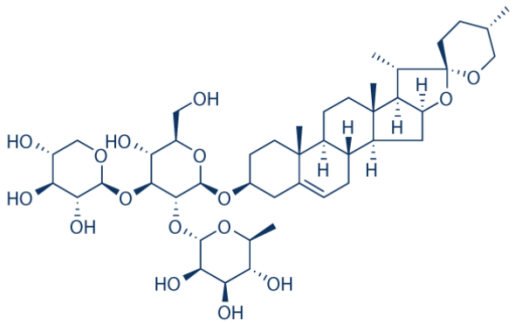

DT-13

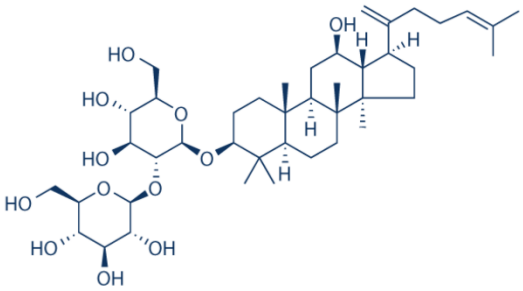

Rk1

Figure 7: Structure of saponins DT-13 and Rk1.

Adapted from Maeng et al 2013 and Khan et al 2018 [94, 95].

1.12.2 Rk1

Triterpenoidal ginsenoside Rk1 is obtained via heat processing of ginseng saponin Rg3 from plant *Panax ginseng* C.A.MEY. Rk1 consists of two glucose molecules attached to the triterpene backbone and a total molecular mass of 767 Da. Toxicological studies showed that the LD50 of the saponin is around 200 mg/kg [32]. It is known to have immunomodulatory effects in addition to anticancer, anti-influenza

and anti-inflammatory effects like other ginseng saponins [33]. Recently, its precursor Rg3 has been implicated in relation to inflammasome and SARS-CoV-2 [34].

1.13 Anti-inflammatory mode of action of saponins

Saponins are known to exert their anti-inflammatory properties by modulating NFκB signaling pathway (Figure 8). NFκB intermediate proteins are sequestered in the cytoplasm in inhibited state by IκB family proteins namely IκBα. Ginseng saponins and DT-13 are known to inhibit p65 NFκB and its inhibitor IκBα in TNFα induced cells. [96, 97]. The implication of these saponins in disease therapeutics makes it important to explore multiple targets and thereby functioning of these saponins as anti-inflammatory compounds. Interestingly, inflammation is related to the nuclear receptor signaling as well [98]. It is observed that activation of peroxisome proliferator-activated receptor gamma (PPARγ) uplifts the anti-inflammatory M2 macrophage phenotype [99] and downregulates the pro-inflammatory cytokines [100, 101].

PPARγ is a ligand-activated nuclear receptor and is known to have a significant role in the regulation of genes involved in lipid metabolism [102], insulin resistance and inflammation [103, 104]. It's therapeutic role has been implicated in cancer [105] and neurogenerative diseases [106]. PPARγ agonists rosiglitazone and pioglitazone are used to regulate the Type 2 diabetes [107]. Also, there is in silico evidence of PPARγ having hydrophobic pockets for binding of its natural ligands and saponins [85].

As described by Bailey and Ghosh [108], the PPARγ ligand activation is linked to the anti-inflammatory phenotype by repressing the NFκB signaling in LPS stimulated cells (Figure 9). It is observed that in normal conditions without any infection, NFκB signaling is in repressed state due to binding of repressors like histone deacetylases 3 (HDAC3), nuclear receptor corepressor (NCOR). Upon stimulation with LPS, the proteasomal degradation of repressor molecules and binding of activators of NFκB is initiated. This further promotes transcription of proinflammatory cytokine genes and consequently inflammation [108].

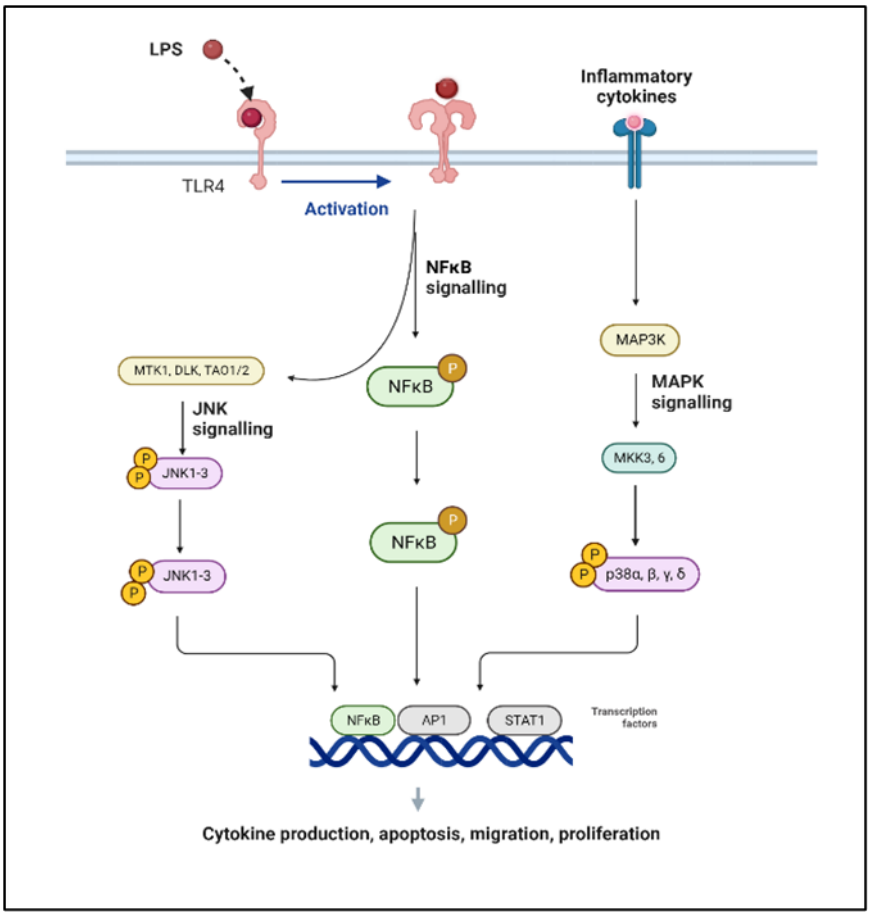

Figure 8: Inflammatory pathways involved in saponin functioning.

Various inflammatory pathways like NFκB, Jak/STAT and MAPK pathway mediators are known to be inhibited by anti-inflammatory saponins. Adapted and retrieved from "MAPK signaling pathway" template from Biorender.com

In contrast to this, ligand activated PPARγ receptor in an LPS stimulated condition acts as a transrepressor of NFκB signaling. It is known that ligand binding initiates sumoylation of PPARγ, which interacts with HDAC3-NCOR repressor complex and prevents it from ubiquitination thereby repressing the pro-inflammatory gene activation and progresses to anti-inflammation state [109, 110]. Recently, saponins are being investigated in relation to the PPARγ pathway activation with reference to their anti-inflammatory activity [111-113]. In silico studies have identified anti-diabetic saponins acting as partial agonist of PPARγ [114, 115]. Hence, the search for new agonistic molecules has formed part of the recent research therapeutics [116-118].

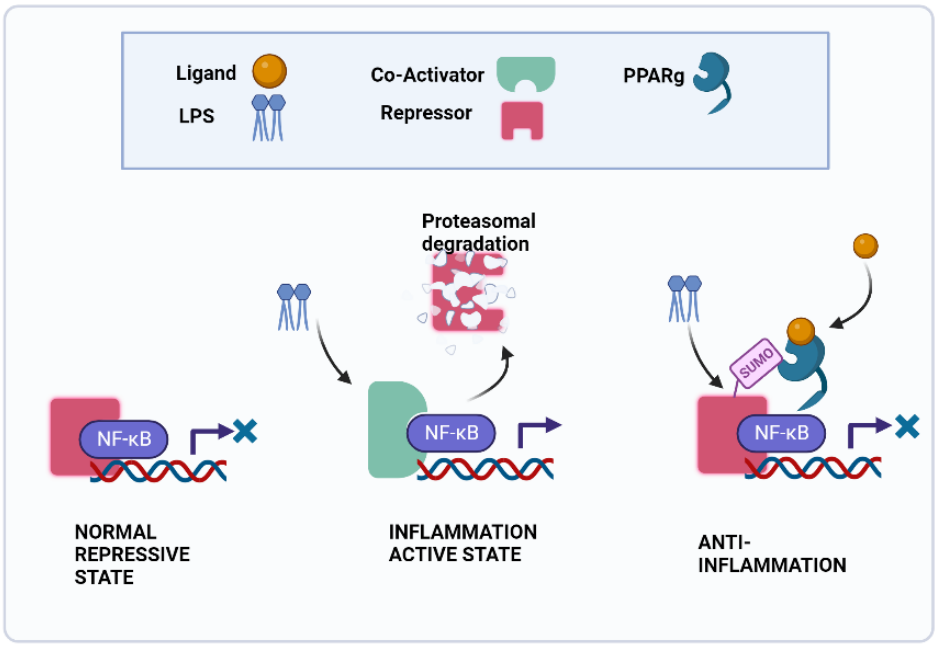

Figure 9: Role of PPARγ in transrepression of NFκB mediated inflammation.

Image was adapted from [108] and created with Biorender.com.

2. Objectives of the study

To avoid the side effects of the available synthetic anti-inflammatory drugs, major research has been shifted in understanding the mechanism of natural anti-inflammatory compounds for new drug discovery. The aim of the proposed study was to investigate the effect of saponins from different sources and understand their mechanism of action as an anti-inflammatory compound. To achieve this, the study was divided into two major objectives. The first objective focussed to investigate the role of DT-13 in inflammation and inflammasome in comparison to well-known ginseng saponin Rk1. The protein and gene expression of various pro-inflammatory cytokines like IL-6, TNF-α and COX-2 were analysed in saponin pretreated LPS stimulated mouse macrophages with the help of ELISA, Western blot, and real-time PCR. Furthermore, expression and activation of p-/NFκB was visualised via immunofluorescence. To understand the role of DT-13 in inflammasome inhibition, inflammasome related genes – NLRP3 and Il-1β were also analysed. A widely marketed anti-inflammatory drug dexamethasone was used as a positive control. As it is known previously and confirmed in this study that DT-13 has anti-inflammatory properties, it was interesting to know about the binding partners of DT-13 in vitro. It is known that nuclear receptors like PPARγ are involved in anti-inflammation. Therefore, the second objective was to explore DT-13 as a ligand of PPARγ to attenuate inflammation. To observe the gene activation mediated by ligand activated PPARγ, HEK293FT cells were used to overexpress PPARγ and PPARγ response element containing luciferase gene. Expression of luciferase gene was analysed in the presence of saponin corresponding to the measurement of PPARγ activity. Molecular docking was performed to visualise the putative binding of DT-13 to PPARγ protein. Furthermore, comparative analysis of binding efficiencies of PPARγ ligands were performed using fluorescent based PPARγ ligand competitive assay.

3. Materials and Methods

3.1 Materials

Cells lines

- RAW264.7 mouse macrophages (ATCC TIB-71)
- HEK293-FT (Invitrogen™ R70007)

Media and chemicals

- Acetic acid (Sigma-Aldrich)
- Acrylamide/Bis solution, 30% (Carl Roth, Karlsruhe, Germany)
- Albumin fraction V, ≥ 98% (Carl Roth, Karlsruhe, Germany)
- Ammoniumpersulfate (APS) (Merck, Darmstadt, Germany)
- Complete^{TM} Mini Protease Inhibitor (Roche)
- dexamethasone (Fisher Scientific, Waltham, US)
- Dexamethasone (Thermo Scientific, Waltham, US)
- Dimethylsulfoxide (DMSO) (Sigma Aldrich, St. Louis, US)
- Dimethylsulfoxide (DMSO, Carl Roth, Karlsruhe, Germany)
- DT-13 (Biosynth-Carbosynth, Staad, Switzerland)
- Dulbecco's minimal eagles' medium (Lonza Group, Basel, Switzerland)
- Opti-minimum essential media(MEM) (Gibco, life technologies, Carlsbad, US)
- Dulbecco's phosphate buffered saline (Lonza Group, Basel, Switzerland)
- Ethanol ≥99.8% (Baker)
- Fetal bovine serum (FBS) (Gibco, life technologies, Carlsbad, US)
- Ginsenoside Rk1 (Merck, Darmstadt, Germany)
- Glycine (Carl Roth, Karlsruhe, Germany)
- Isopropanol (Carl Roth, Karlsruhe, Germany)
- Lipopolysaccharides (Sigma Aldrich, St. Louis, US)
- Methanol (Carl Roth, Karlsruhe, Germany)
- Modified Griess reagent (Sigma Aldrich, St. Louis, US)
- MTS tetrazolium reagent (Abcam, Cambridge, UK)

- nitrocellulose membrane (Perkin Elmer, Waltham, US)
- PageRulerTM Plus Prestained protein ladder (Thermo Scientific, Waltham, US)
- Penicillin/streptomycin (P/S) (Gibco, life technologies, Carlsbad, US)
- Phosphatase Inhibitor PhosStop™ (Roche,Basel, Switzerland)
- Phosphate-buffered saline (Thermo Scientific, Waltham, US)
- Ponceau S (Sigma-Aldrich)
- Protease Inhibitor Cocktail cOmplete (Roche,Basel, Switzerland)
- RNase free water (Thermo Scientific, Waltham, US)
- SO1861-EMCH (Symeres, Nijmegen, Netherlands)
- Sodium carbonate (Thermo Scientific, Waltham, US)
- Sodium chloride (Thermo Scientific, Waltham, US)
- Sodium dodecyl sulfate (SDS) (Sigma Aldrich, St. Louis, US)
- Sodium nitrite (Sigma Aldrich, St. Louis, US)
- Stripping buffer (Merck, Darmstadt, Germany)
- TEMED (Cole-Parmer, Illinois, US)
- Tris Buffer (Carl Roth, Karlsruhe, Germany)
- Trypan blue (Gibco by life technologies, Carlsbad, US)
- Trypsin-EDTA (Gibco, life technologies, Carlsbad, US)
- Tween 20 (PanReac AppliChem, Darmstadt, Germany)
- Western Blot Pierce^{TM} ECL substrate (Thermo Scientific, Waltham, US)
- β-Mercaptoethanol (Carl Roth, Karlsruhe, Germany)

Devices

- Cell counter device (Luna™, logos biosystems, Annandale, US)
- Centrifuge (Sorvall Evolution RC, Thermo Scientific, Waltham, US)
- Fluoroscence polarisation detector (TECAN Spark Multimode plate reader, Männedorf, Switzerland)
- HPLC (1100 Series, Agilent, Santa Clara, US)
- Western blot imaging system (Molecular Imager ® VersaDoc™, Bio-Rad, Hercules, US)
- 37 °C cell incubator (Certomat® BS-1, Sartorius, Göttingen, Germany)

- Live-cell analysis system (Incucyte® S3 Sartorius, Göttingen, Germany)
- Luminometer (Fluoroscan Ascent FL, Thermo Scientific, Waltham, US)
- Lyophilizer (Alpha 1-2 LD plus, Martin Christ Gefriertrocknungsanlagen GmbH)
- MALDI-TOF-MS (Ultraflex III, Bruker, Billerica, US)
- ELISA microplate reader (SpectraMax 340P, Molecular Devices, San Jose, US)
- Rocker shaker (Rocky, Fröbel Labor Technik, Lindau, Germany)
- Spectrometer (NanoDrop®ND 1000, Thermo Scientific)
- Fluorescence microscope (Zeiss Axio, Carl Zeiss AG, Jena, Germany)
- Spectrophotometer (NanoDrop®ND 1000, Thermo Scientific, Waltham, US)

Antibodies

*Horse raddish peroxide (HRP) labelled

Fluorescein isothiocyanate (FITC) labelled

Antibody	Buffer	Dilution	Secondary antibody	Application
Phospho- Jun-N terminal kinase (p-JNK)	5% BSA in 1× TBS	1:1000	Goat anti-rabbit* (GAR) (1:5000)	Western Blot (WB)
phospho-p38 mitogen activated protein kinase (p-p38 MAPK)	5% BSA in 1× PBST	1:1000	GAR* (1:5000)	WB
I kappa B-alpha (IκBα)	5% BSA in 1× PBST	1:1000	GAR* (1:5000)	WB
Beta-actin(β-actin)	5% BSA in 1×PBST	1:3000	Rabbit anti-mouse* (1:2000)	WB

NFκB	5% BSA in 1× PBST	1:1000	GAR* (1:5000)	WB
p-NFκB	2% BSA in 1× PBST	1:500	Goat anti-rabbit# (1:2000)	Immunofluorescence (IF)
TLR4	2% BSA in 1×PBST	1:200	GAR# (1:2000)	IF

3.2 Cell culture maintenance

DMEM supplemented with 10% FBS and 1× P/S was used to cultivate cells in a 37 °C incubator (Certomat® BS-1, Sartorius, Göttingen, Germany) with 5% CO2 and 95% humidity. Cells were maintained in 100 mm polystyrene tisuue culture-treated dishes at a confluency of 80% before splitting. For splitting, cells were treated with Trypsin (0.25%) for 5 minutes at 37 °C or until detached. For cell seeding, cell suspension (10 µL) was mixed with trypan blue (10 µL), and number of cells were counted using cell counter (Luna™, logos biosystems, Annandale, US).

3.3 MTT assay

MTT, 3-(4,5-dimethylthiazol-2-yl)-2,5-diphenyltetrazolium bromide, a yellow-coloured dye was used to analyse the cytotoxicity of the compounds in vitro. The tetrazolium dye is used to measure the metabolic activity of the cells and therefore can be correlated as the viability of cells. MTT is reduced to purple formazan crystals by viable cells. For the experimental analysis, cells were seeded at a density of 1×10^4 cells per well in a 96 well plate. The plate was incubated overnight (~24 h) in 37 °C incubator. Next day, cells were renewed with complete media containing the saponins with various concentrations. The plate was kept for overnight incubation in 37 °C incubator. The media was removed and 50 µL of MTT solution (5 mg/mL in phosphate buffer saline (PBS)) was added in each well. The plate was kept for a maximum of 4 h at 37 °C until the purple-coloured formazan crystals appear. The MTT solution was removed from the wells and 50 µL of Formazan solubiliser (10% SDS – 25 mL, isopropanol – 20.5 mL, 0.1 M HCl – 2 mL for a total volume of 50 mL in water) was added to solubilize

the crystals. The plate was kept on shaker until all the crystals were solubilized evenly. The absorbance was measured at 570 nm using a microplate reader SpectraMax 340P.

3.4 Griess Reagent Assay

Griess Reagent: 10 g Griess reagent powder was mixed with 250 mL water (0.2 g Griess reagent with 5.0 mL). Standards were prepared from 1 mM $NaNO_2$ in DMEM (Table 1).

Table 1: Standards for Greiss Reagent Assay

$NaNO_2$ (µL)	Media (µL)	Final conc. (nmol /well)
0	400	0
4	396	1
8	392	2
16	384	4
24	376	6
32	368	8
40	360	10

3.5 SDS PAGE and Western Blotting

SDS-PAGE

10% resolving buffer: 1.5 M Tris-HCl, 0.4% [w/v] SDS, pH 8.8
4% stacking buffer: 0.5 M Tris-HCl, 0.6% [w/v] SDS, pH 6.8
Sample loading buffer: 40% glycerin, 8% SDS, 10 mM EDTA, 0.25 M Tris, 0.1% bromphenolblue
Running buffer: 20 mM TRIS, 192 mM glycine, 0.1% [w/v] SDS, pH 8.3
Running conditions:200 V, 80 mA for 70-90 minutes

In sodium dodecyl sulfate-polyacrylamide gel electrophoresis (SDS-PAGE) proteins are separated based on the molecular mass. SDS denatures and binds the protein, distributing the negative charge uniformly. When the current is applied, the proteins move towards the positive electrode. Smaller proteins move faster than the larger

through the acrylamide gel. This results in separation of proteins based on their size and molecular mass. Depending on the size of the protein, 10% or 12% SDS-PAGE gel is used. Buffer composition for the gel preparation of 10% resolving gel with 4% stacking gel is listed in Table 2. Samples (60 µg each) were diluted with nuclease free water and were mixed with 10 µL of 4 × sample loading buffer prior to denaturation. at 95 °C for 10 minutes. Pre-stained protein molecular ladder was added to the first well for reference, followed by the addition of the samples in the remaining wells. The proteins were separated at 200 V, 80 mA for 90 minutes or until the loading dye was run out.

Table 2: Composition of resolving and stacking gels for SDS-PAGE

	10% resolving gel (10 ml)	4% stacking gel (5 ml)
MilliQ water	3.98 ml	3 ml
30% Acrylamide	3.3 ml	660 µl
Tris buffer	2.5 ml (pH 8.8)	1.26 ml (pH 6.8)
10% ammoniumpersulfate	75 µl	25 µl
TEMED	7 µl	5 µl

Protein Transfer:

Ponceau S: 2% Ponceau S, 30% trichloroacetic acid, 30% sulfosalicylic acid

Transfer buffer (10×): 25 mM TRIS base (M 121,14 g/mol), 191.8 mM glycine, 10% Ethanol

ECL solution A:100 mM TRIS HCl, 14.11 mM luminol, pH 8.6

ECL solution B: 6 mM *p*-coumarin acid in DMSO

ECL solution C: 30% [v/v] H_2O_2

The proteins are transferred onto the nitrocellulose membrane using an electrophoretic transfer (350 mA, 90 minutes). Transmembrane Bio-Rad frame with white side facing upward direction was placed in transfer buffer in a separate tray. Layering was done with sponge, 2× filter papers, SDS gel, nitrocellulose membrane, 2× filter papers, sponge in the same order. The frame containing the stacked layers

was kept in the Bio-Rad transmembrane apparatus. The tank was filled with transfer buffer with an ice cool pack inserted to avoid overheating of the device. After the transfer was complete, the membrane was checked for the successful transfer of proteins using ponceau S staining for 5 minutes. Stain was removed by washing with 1× phosphate buffered saline with Tween 20 (PBST) or distilled water before using the membrane for protein detection.

Protein Detection:

The membrane was blocked using blocking buffer (5% bovine serum albumin (BSA)) and kept for shaking (40 min) using rocker shaker (Rocky, Fröbel Labor Technik, Lindau, Germany) at room temperature (RT). Primary antibody was added to the membrane and incubated overnight at 4 °C while shaking. Next day, membranes were washed with 1× PBST (thrice for 5 min each) prior to the addition of secondary antibody addition (1 h at RT). Membrane was developed at last using Enhanced Chemiluminescence. For the detection, ECL complete solution was made using ECL solution A: 1000 µL; ECL solution B: 150 µL and ECL solution C: 2 µL and the membrane was covered completely with the complete solution and incubated for 1 minute. The protein bands were visualised using Western blot imaging system (Molecular Imager ® VersaDoc™, Bio-Rad, Hercules, US)

3.6 Polymerase chain reaction(PCR)

PCR is a simple laboratory technique, where fragments of DNA are rapidly amplified and detected based on size. For the quantitative analysis of gene expression, real time PCR is performed using a fluorescent probe (SYBR green) that is incorporated in the newly amplified fragments and the gene is quantified in real time.

For gene amplification, Phusion® High-Fidelity PCR Kit (NEW ENGLAND Biolabs, Massachussets, US) was used and buffers for gene amplification were added as listed in Table 3. After setting up the reaction mixture in 0.5 mL eppendorf tubes, the individual tubes were kept in thermocycler with cycling conditions as mentioned in Table 4

Table 3: Components of PCR reaction mixture

Chemical	Concentration	Volume (per 20 µL)
HiFidelity buffer	5 ×	4 µL

Deoxyribonucleotides (dNTPs)	10 mM	0.4 µL
Gene specific primers (FP+RP)	10 µM	2 µL
template	50–100 ng	1 µL
MilliQ		12.4 µL
Phusion–FH Polymerase	2000 units/mL	0.2 µL

Table 4: Cycling conditions for PCR

Step	Temperature	Time
Initial Denaturation	98 °C	30 s
Cycles (25–35)	98 °C 45–72 °C 72 °C	10 s 30 s 30 s
Final Extension	72 °C	10 min
Hold	4 °C	

3.7 Agarose gel electrophoresis

The DNA fragments are separated with the help of agarose gel electrophoresis technique which uses electric field to separate the macromolecules based on size. DNA having negative charge due to the presence of phosphates in its backbone, moves towards anode. The agarose gel (1%) is stained with Synergy Brands Inc. (SYBR) Safe which is activated only when incorporated into DNA. The samples were mixed with DNA loading dye before running the agarose gel (80V, 40 min) in tris(hydroxymethyl)-aminomethane-acetate-ethylenediaminetetraacetic acid buffer (TAE). The bands were observed under UV light using Molecular Imager ® (VersaDoc™, Bio-Rad, Hercules, US).

3.8 Real time PCR reaction

GoTaq® Probe qPCR kit (Promega, Walldorf, Germany) was used. The reaction mixture was prepared as described in Table 5. All components were mixed and transferred in transparent 96-well PCR plate. The plate was kept in the thermal cycler and temperature conditions were applied as per Table 6. After completion of the experiment the cycle threshold values were used to generate the fold change in expression of gene of interest with respect to the house keeping gene (reference gene). The primers used are listed in Table 7.

The formula used to calculate the fold change is given below-

$$\delta cT(\ gene\ of\ interest) = \ avg\ ct\ (gene\ of\ interest) - avg\ cT(reference\ gene)$$

$$\delta\delta cT(\ gene\ of\ intrest) = \ \delta ct\ (test\ sample) - \delta cT(control\ sample)$$

$$fold\ change = 2^{-\delta\delta cT}$$

Table 5: Reaction mixture for real time PCR

Substance	Concentration	Volume per well
Go Taq Buffer	2 ×	10 µL
Nuclease free water		2.2 µL
Forward Primer	10 mM	0.15 µL
Reverse Primer	10 mM	0.15 µL
cDNA template	1:10 diluted	7.5 µL

Table 6: Cycling conditions for real time PCR thermal cycler.

*Annealing temperatures are primer specific

Step	No. Of cycles	Temperature	time
Denaturing	1	95 °C	10 min
Annealing	35	Annealing temperature*	30 s
Extension	1	72 °C	30 s
Hold	1	4 °C	10 min.

Table 7: List of genes and Primer pair

Gene	Primer Pair	Reference
iNOS	FP: 5'-ATGTCCGAAGCAAACATCAC-3' RP: 5'-TAATGTCCAGGAAGTAGGTG-3'	[119]
COX-2	FP: 5′-AAGACTTGCCAGGCTGAACT-3' RP: 5'-CTTCTGCAGTCCAGGTTCAA-3'	[120]
TNF-α	FP: 5′-CCCTCACACTCAGATCATCTTCT-3′ RP: 5'-GCTACGACGTGGGCTACAG-3′	[121]
IL-1β	FP: 5'-TGGACCTTCCAGGATGAGGACA-3' RP: 5'-GTTCATCTCGGAGCCTGTAGTG-3'	[122]
GAPDH	FP: 5′-AGGCCGGTGCTGAGTATGTC-3' RP: 5'-TGCCTGCTTCACCACCTTCT-3'	[123]
NLRP3	FP: 5'-TCACAACTCGCCCAAGGAGGAA-3' RP: 5'-AAGAGACCACGGCAGAAGCTAG-3'	[124]

3.9 Complement alternate pathway assay

This assay was used to understand how saponins affect the activation of the complement system and its role in membrane activation complex (MAC) formation. The complement system alternative pathway was measured using Wieslab® Complement system (COMPLAP330), an ELISA-based assay wherein the pre-coated strips with specific activator were provided. Patient serum* (provided in the kit) was diluted with specific blockers to ensure activation of only alternate pathway. Binding of patient serum with the precoated wells activate the pathway. C5b-9 (component of MAC) was detected with alkaline phosphatase labelled antibody. Activity of alkaline phosphatase using alkaline phosphatase substrate was observed as a difference in colour intensity. Absorbance at 405 nm was measured using ELISA microplate reader (SpectraMax 340P, Molecular Devices, San Jose, US) which corresponds to the amount of complement activation.

Saponins were diluted in the patient serum provided with the kit and incubated for 1 h at 37 °C onto the coated microtiter strips.

Saponin stocks: DT-13 and Rk1

1. **Stock 1**: 10 mg/mL – (3.5 mg in 350 µL DMSO)
2. **Stock 2:** 1 mg/mL

Working dilutions:

* patient serum provided with the kit

- **10 µg/mL**: take 2.5 µL from stock 2 in 250 µL serum*
- **50 µg/mL**: take 12.5 µL from stock 2 in 250 µL serum*
- **100 µg/mL**: take 2.5 µL from stock1 in 250 µL serum*
- ➢ Same equivalence for DMSO was used as a buffer control for compounds.
- ➢ Serum* dilution: 1/18 dilution in diluent AP provided in the kit

3.10 Caspase inflammasome assay

The Caspase-Glo® 1 Inflammasome Assay (Promega, Walldorf, Germany) is a bioluminescent assay, which measures inflammasome activity by detecting the caspase-1 release in the cell culture media treated with the test compounds. The assay involves two reactions, first cleavage of the given substrate Z-WEHD-aminoluciferin into Z-WEHD and aminoluciferin by caspase-1 present in the cell supernatants. Second, aminoluciferin, a substrate for luciferase, produces light.

All reagents used for the assay were prepared following the manufacturer protocol. Caspase-Glo 1 Reagent (100 µL) was added to the cell culture medium treated with test compounds. Caspase-Glo 1 Reagent mixed with caspase inhibitor Ac-YVAD-CHO (1:1) was used as a positive control for inflammasome inhibition.

The plate was sealed properly with foil, placed on a shaker (30 s) (Rocky, Fröbel Labor Technik, Lindau, Germany) to mix the contents in the plate. The plate was kept for incubation at RT and luminescence was measured within 60 min. using a luminescent plate reader (Fluoroscan Ascent FL, Thermo Scientific, Waltham, US)

3.11 Enzyme linked immunosorbent assay(ELISA)

Wash buffer: PBS with 0.05% tween-20

Blocking buffer: PBS containing bovine serum albumin (provided with kit as diluent A)

ELISA kits (TNF-α, IL-1β, IL-6) were purchased from BioLegend (San Diego, California) to detect the cytokines levels in cell culture supernatant of LPS stimulated cells pre-treated with compounds. A standard protocol for sandwich ELISA was followed as mentioned by the manufacturers protocol. First, capture antibody was diluted in coating buffer provided in the kit. Diluted capture antibody (100 µL) was added to the wells of a 96-well plate and was kept for overnight incubation at 4 °C. Next day, the capture antibody was removed by washing 4 times with wash buffer (300 µL) with in between gentle tapping of the plate on stacks of absorbent tissue. To avoid non-specific binding, blocking buffer (200 µL) was added to the wells and kept for incubation for 1 h, RT. The blocking buffer was removed by washing with wash buffer. A serial dilution of standards was prepared following manufacturer's instructions. Diluted standards (100 µL) and samples (cell culture supernatants) were added the respective wells and incubated for 2 h, RT. Further, after washing off the samples post incubation, detection antibody (100 µL, 1 h, RT) was added followed by avidin-HRP solution (100µL, 30 min, RT). Afterwards, 3,3′,5,5′-tetramethylbenzidine (TMB) substrate solution (100 µL, 15 min) was added until blue color appeared. The TMB reaction was stopped by 2 M sulfuric acid and the blue color was changed into yellow color. The absorbance was measured at 450 nm by ELISA microplate reader (SpectraMax 340P, Molecular Devices, San Jose, US) within 15 min of addition of stop solution.

3.12 Immunofluorescence (IF)

Washing Buffer: 1X PBS with 0.1% Triton-X

Blocking buffer: 2% bovine serum albumin (BSA)

Fixing solution: 3.4% formaldehyde

Cell culture experimental conditions: Cells were carefully seeded on glass coverslips kept in a 6 well cell culture dish, 3000 cells per well and kept for overnight incubation in the incubator at general cell culture conditions. Further treatments were done according to the type of assay to be performed. For LPS time kinetics, 200 ng/mL of LPS was used at various time points for detection of NFκB nuclear localization. To visualise the effect of saponin on NFκB localisation in presence of LPS, cells were pre-incubated with saponin at 10 µM conc. for 1 h and then 200 ng/mL LPS was added for 30 min or 60 min. (because we saw the nuclear localisation NFκB of at a time point of 30 min in presence of LPS alone).

The cells were treated according to the experimental setup as mentioned above. Post incubation, the cells were washed with cold PBS. Cells were fixed with 3.4% formaldehyde solution (500 µL) for 20 min at RT. The solution was further removed, and the cells were washed with cold washing buffer prior to addition of blocking buffer (500µL, 20 min). After the incubation time is over, the media is removed, and the cells are washed slowly with cold PBS twice. Further cells were incubated with primary antibody for 1.5 h at RT. Wash again twice with cold PBST. Secondary antibody was further added for 30 min at RT. Nuclear stain - 4′,6-diamidino-2-phenylindole (DAPI) (1:10,000 in PBS) was added for 5 min before mounting the coverslips onto the glass slides using immuno-mount mounting media. The cells were observed under fluorescence microscope (Zeiss Axio, Carl Zeiss AG, Jena, Germany)

This assay is commonly used to detect the proteins present in cell culture media as released by the cells. The sandwich ELISA is the most common type of ELISA used. The principle behind the assay is that antigen or a protein molecule is detected between two layers of antibodies, one is the capturing antibody coated on the surface of the plate and the other is the detection antibody that detects the antigen bound on the capture antibody. The detection antibody is further recognised by biotin labelled antibody. Streptavidin-HRP binds to biotin and the final enzymatic reaction leads to color formation measured via spectrometer.

3.13 Plasmid isolation

Plasmids used:

- pcDNA flag PPAR gamma (PPARγ gene cloned in pcDNA3.1 myc-His A vector by Bruce Spiegelman) [125], Addgene plasmid # 8895 ; RRID:Addgene_8895)
- PPRE X3-TK-luc (PPAR response elements (PPRE) consisting of three direct repeats cloned in ptkLUC modified vector by Bruce Spiegelman [126], Addgene plasmid # 1015; RRID:Addgene_1015)
- pGL4.73[hRluc/SV40] (Renilla luciferase reporter vector pGL4.73, Promega # E691A)

Buffers and medium:

- Lysogeny broth with ampicillin (LBAmp): 10 g/L peptone, 5 g/L yeast extract, 10 g/L NaCl, 50 µg/mL ampicillin
- LB agar plates: 40 g/L LB-Agar +50 µg/mL ampicillin

Plasmids were procured in DH5α bacteria as agar stabs. A small amount was streaked on LB agar plates (containing ampicillin), incubated overnight in 37 °C incubator and single colony was picked the day after. A single colony of bacteria was inoculated in 100 mL of Lysogeny broth with ampicillin (LBAmp) and shaken for overnight incubation (37 °C,200 rpm). Next day, bacterial cell pellet was obtained and processed further to isolate the plasmid using plasmid mini-prep kit (Qiagen, Hilden, Germany) using manufacturer's protocol.The concentration of plasmid DNA obtained was measured using spectrophotometer (NanoDrop®ND 1000, Thermo Scientific, Waltham, US)

3.14 Restriction digestion

Restriction enzyme digestion of plasmids is used to analyse the correct orientation of plasmids and to validate the presence of plasmids isolated using a plasmid isolation kit. The enzymes and reaction conditions used to digest the plasmids is shown in (**Table 3**). The digested plasmids were analysed using agarose gel electrophoresis.

Table 3 : Restriction Enzymes used for restriction digestion of plasmids

Plasmid	Enzyme	Temperature
pcDNA-PPARg (#8895)	Sma1, Nde1	Add Sma1 (1 µL) at 25°C then add Nde1 (1 µL) at 37°C in CutSmart Buffer for 1 h Inactivate at 65°C
PPRE-Tk-Luc (#1015)	Sca1, BamH1	Add Sca1 (1 µL) and BamH1 (1 µL) at 37°C in Cut Smart Buffer for 1 h. Inactivate at 65°C

3.15 Invitro Transfection assay

Invitro transfection technique is used for the introduction of nucleic acids into the cells using non-viral methods to analyse the expression and function of genes and their respective proteins. HEK293FT cells were used to transfect plasmids containing PPARγ gene and PPRE. The cells were seeded in 96 well plate (overnight incubation at 37 °C) and fresh media was added prior to the transfection protocol. Plasmids pcDNA flag PPAR-gamma (100 ng), PPRE X3-Tk-Luc (150 ng) and pGL4.73[hRluc/SV40] (0.05 ng) were mixed in 25 µL Opti-MEM. Diluted lipofectamine (2.5 µL in 25 µL Opti-MEM) was mixed with the plasmids (plasmid-lipo mix) and incubated for 15 min at RT. After incubation, 200 µL DMEM was added to the plasmid-lipo mix and incubated for 15 min at RT. Plasmid-Lipo mix (50µL) was slowly added in each well and the plate was incubated for 14–16 h. Post transfection, the transfection media was removed and fresh media containing test compounds were added (4 h). The luciferase activity of the cells was measured using Dual-Glo luciferase assay (Promega) following manufacturer's Dual-Glo luciferase assay from Promega, following the manufacturer's protocol.

3.16 Molecular modelling

Docking was carried out using AutoDock methodology on Autodock tools 1.4.2. The X-ray crystal coordinates of Peroxisome proliferator-activated receptor gamma (PPARγ) in complex with rosiglitazone (PDB ID: 7AWC) with a resolution of 1.74 Å downloaded from protein data bank (https://www.rcsb.org/) was used to perform the

docking calculations. The pdbqt files for both DT13 and ligand-free protein structure were generated for docking. The grid box was generated by selecting grid center base on bound ligand rosiglitazone and the grid size was set to 60 × 60 × 60 xyz points with grid spacing of 0.375 Å. The Lamarckian genetic algorithm available in autodock was used to perform flexible docking between DT13 and PPARγ and the conformation with least binding energy was used for further analysis. The binding mode of DT13 in comparison was co-crystal ligand rosiglitazone were analysed and the representative figures of binding interactions were generated using BIOVIA Discovery Studio Visualizer. The docking was performed with the assistance of Dr. Kakularam Kumar Reddy, Department of Biochemistry, Charité – Universitätsmedizin Berlin.

3.17 Polar Screen PPARγ ligand competitive assay green

Screening of PPARg ligands by evaluating their binding affinities was done using a fluorescent based competitive assay Polarscreen™ PPARγ -Competitor Assay green (Thermofisher Scientific, Massachusetts, US). The assay kit was provided with the following chemicals – a human derived PPARγ ligand binding domain (PPARγ -LBD) tagged with a GST-tag and a selective green fluoromone TRACER (fluorescent PPARγ ligand) called as PPARγ green complex, a separate fluoromone TRACER, and PPARγ screening buffer. The principle of the assay is based on the change in fluorescence polarisation. PPARγ-LBD bound with fluoromone TRACER has high polarisation and when the TRACER is displaced competitively with the test compounds the polarisation is reduced. The assay is performed using manufacturers protocol (Figure 10).

The buffer was diluted with nuclease free water and the other compounds were diluted in DMSO. The assay was performed in a 384 well low volume black plate (max. volume 50 µL per well). The test compounds were serial diluted in 100% DMSO from 1 mM stock solution. Further, test compounds were diluted in PPARγ screening buffer (1:1). Diluted compounds (10 µL) were mixed with (10 µL) PPARγ green complex (RT, 2 h, in dark). Fluorescence polarisation was measured using a spectrophotometer (TECAN Spark Multimode plate reader, Männedorf, Switzerland) with the assistance of Dr. Stefanie Wedepohl in SupraFAB lab, Freie Universität Berlin. The fluorescence polarisation was converted into percent binding where the lowest concentration of compounds was normalised to 100% polarisation.

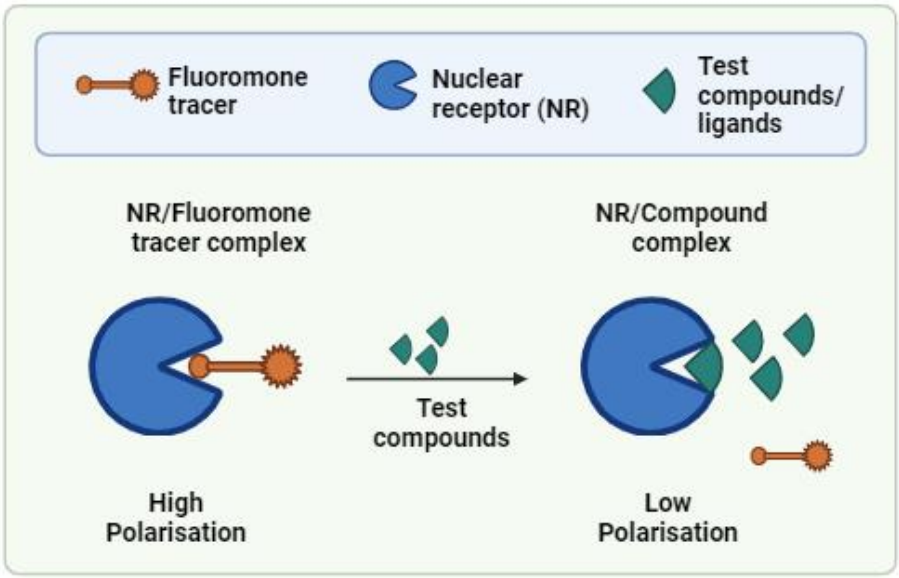

Figure 10: Principle of competitive binding assay for PPARg ligands

The image is adapted as provided by Thermofisher Scientific, created with Biorender.com

3.18 Electrospray ionization and mass spectrometry (ESI-MS)

The dye conjugated saponin was analysed by ESI-MS in the facility of institute of Chemistry, Freie Universität Berlin. The mass spectrum was recorded on modified MAT711 (Varian MAT, Bremen, Germany). The sample was dissolved in methanol and subjected to ionization using electron impact ionization (EI) at 80 eV prior to MS analysis. The mass spectrum shows the mass by charge (m/z) ratio of the analytes plotted against the intensity.

3.19 Statistical analysis

GraphPad prism 9 was used to plot and analyse all the data. Statistical analysis was done by ANOVA and Student t-test. All experiments were done in a minimum of three biological repeats (N) and three technical repeats (n) unless specified otherwise. Outliers were removed using Z-score and the normalised data with standard deviation (SD) was used to calculate the significance. The level of significance is indicated separately for each figure in the results section.

4. Results

4.1 Establishment of an in vitro inflammation model using LPS as a stimulant in RAW264.7 cells

To study the effect of compounds used in the study, an invitro inflammatory model system was established using LPS as an inducer. Macrophages responds to LPS stimulation by mediating activation and release of various inflammatory mediators [127].Therefore, to assess the induction of inflammation in RAW264.7 mouse macrophages, activation of inducible nitric oxide (iNOS) gene was analysed. Furthermore, the viability of cells was also checked to ensure the reliability of the model system.

4.1.1 Effect of LPS on inducible nitric oxide (iNOS) gene expression

Nitric oxide (NO) forms an important mediator in innate immune system [128] and its production is catalysed by iNOS genes [129]. iNOS is known to function as an enhancer of inflammatory response upstream of the LPS induced pathway as well as a target gene for NFkB mediated gene regulation [130]. Therefore, to validate the in vitro inflammation model, expression of iNOS gene was evaluated using real time PCR in LPS stimulated RAW264.7 macrophages. Cells were induced with increasing doses of LPS (0–1000 ng/mL) for 19 h followed by isolation of RNA (Nucleospin RNA isolation kit, Machery-Nagel,Düren,Germany) to convert into complementary DNA(cDNA) (GoScript® Reversetranscriptase, Promega,Wisconsin US). A significant dose dependent increase in the iNOS levels were observed in LPS stimulated cells (Figure 11). This confirmed the establishment of the inflammatory pathway by LPS stimulation. To minimise the possible toxicity, 10 ng/mL of LPS was preferred for effective stimulation of the cells.

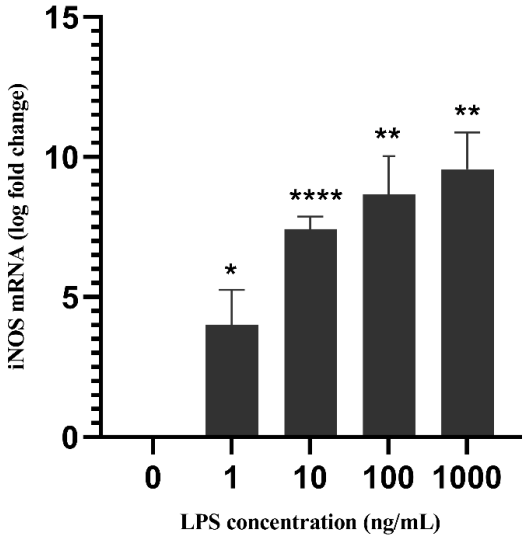

Figure 11 : Inflammation induced in macrophages using LPS as a stimulant

The RAW264.7 cells were stimulated with different concentrations of LPS and iNOS gene expression was analysed using real time PCR. The experiment was performed in triplicates, represented as mean ± SD of three independent experiments *p<0.05, **p<0.01, ***p0.001, 'ns' statistically not significant with respect to untreated cells alone.

4.1.2 Effect of pretreatments on cytotoxicity

In parallel to the induction of inflammation, it is important to check toxicity of the compounds to be used to gain knowledge about their efficacy. In previous studies, mostly crude forms of saponins were used in a concentration range of 50–250 milligrams [131, 132] and defining the dose for the effective drug therapy remained disputed. In this project, micromolar concentrations (equivalent to ng per microlitre) of commercially available purified saponins were used. An MTT assay was performed to check the metabolic activity of the cells, indicating the cytotoxicity of the compounds (Figure 12).

RAW264.7 cells were pre-treated with DT-13, Rk1 and dexamethasone (2 to 30 µM) in a 96 well plate for an hour and then stimulated with 10 ng of LPS for a total of 19 h. Post incubation, an MTT assay was performed according to the assay protocol described earlier. No or minimal change in the metabolic activity of the cells at all concentrations was observed.

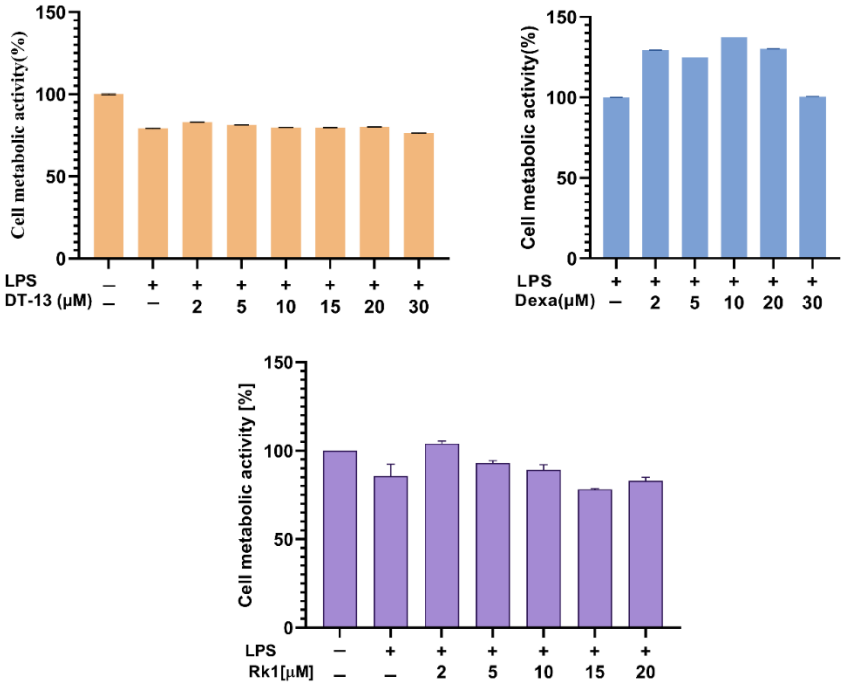

Figure 12 : MTT analysis of compounds in RAW264.7 cells

Macrophages were pretreated with different doses of compounds – dexamethasone, Rk1 and DT-13 – for 1 h and then stimulated with LPS. An MTT assay was performed to analyse the metabolic activity of the cell in the presence of these compounds. Data is represented as mean ± standard deviation (SD) of three independent experiments and normalized with untreated sample as 100% activity.

4.2 Evaluation of proinflammatory cytokines in macrophages pretreated with dexamethasone, DT-13 and Rk1

After establishment of an in-vitro inflammation model system and evaluation of cytotoxicity of the compounds, functional significance of compounds in LPS-stimulated cells were evaluated.

4.2.1 Inhibition of NO release in cells pretreated with DT-13 and Rk1

Significant inhibition of nitric oxide release from the LPS stimulated cells is used to screen potential anti-inflammatory drug candidates [55, 56]. Therefore, in this study, we analysed NO release in LPS stimulated cells pretreated with Rk1 and DT-13 using

Greiss assay. A significant decrease in the production of NO in the cells pretreated with DT-13 and Rk1 with respect to LPS alone was observed. In LPS stimulated cells, DT-13 and Rk1 pre-treatment inhibited the LPS induced NO release in a dose dependent manner (Figure 13). An increase in NO concentration was observed by 5 µM Rk1 pre-treatment but the levels were not significant with respect to LPS alone. These results indicated that in contrast to the high NO induction in cells by LPS, pre-treatment with saponins DT-13 and Rk1 reduced the inflammatory response of the cells.

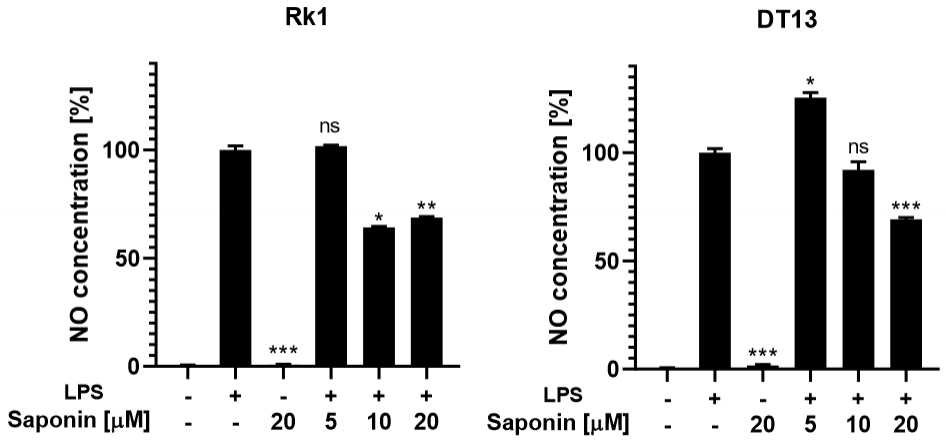

Figure 13 : NO release in DT-13 and Rk1 treated cells prior to LPS stimulation.

NO release in response to DT-13 and Rk1 pretreatment in LPS stimulated cells was analysed using Greiss reagent assay. The bar graph shows the concentration of NO release in percentage normalized with respect to untreated samples considered as 0% and LPS as 100% NO release. The experiment was performed in triplicates, represented as mean ±SD where *p<0.05, **p<0.01, ***p0.001, 'ns' statistically not significant with respect to LPS alone.

4.2.2 Regulation of TICAM and MyD88 genes in cell pretreated with DT-13, Rk1 and dexamethasone

LPS stimulation activates TLR signaling which is further divided into MyD88 dependent or MyD88 independent pathway [133]. MyD88 dependent pathway leads to nuclear translocation of NFκB and activation of the proinflammatory genes [134] whereas MyD88 independent pathway involves toll interleukin receptor containing domain adaptor molecule (TICAM) activation and further release of interferon related genes [135].Therefore, to understand whether DT-13 interferes with the signaling pathway in

MyD88 dependent or independent pathway, we evaluated the expression of TICAM and MyD88 gene using real time PCR in LPS stimulated DT-13 pretreated cells.

LPS alone treatment upregulated the expression of TICAM and MyD88 gene, whereas Rk1 and DT-13 pretreatment downregulated the LPS induced gene expression of MyD88 and TICAM (Figure 14). The inhibition of MyD88 gene was more pronounced than that of TICAM in DT-13 pretreatments (Figure 14). Interestingly, dexamethasone upregulated the expression of MyD88 mRNA. Due to high standard deviations within the experiments, data did not show significant results. Nevertheless, it is still worth noticing that the trend seen in individual experiments were the same i.e., DT-13 and Rk1 exhibited an inhibitory effect on the mRNA levels of MyD88 and TICAM in comparison to treatment with LPS alone.

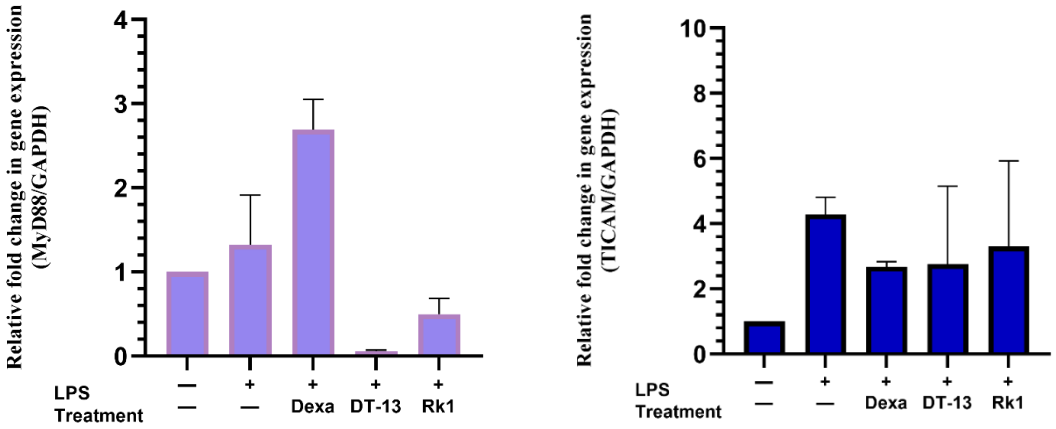

Figure 14 : Gene expression analysis of TICAM and MyD88 in LPS stimulated RAW264.7 cells.

A graphical representation of fold change in mRNA gene expression of TICAM and MyD88 as analysed by real-time PCR. The concentration used for pretreatment were 20 µM and the gene expression values was normalized with respect to GAPDH. The experiment was performed in N=2, n=6, represented as mean ±SD.

4.2.3 Regulation of phosphorylated proteins by pretreatments in LPS stimulated cells

LPS activates a group of kinases in TLR4 pathway that leads to activation by phosphorylation of secondary metabolites involved in LPS mediated inflammatory pathways [136, 137]. Inhibition of these phosphorylated proteins has been implicated

in screening of anti-inflammatory compounds [138]. Previous studies depicted the regulation of LPS induced phosphorylation of NFκB in presence of Rk1[139] and TNFα induced NFκB in DT-13 pretreatments [140]. Therefore, we observed the expression of p-NFκB, IκBα, p-JNK, p-p38 MAPK in LPS stimulated RAW264.7 cells pretreated with DT-13 (10 µM), Rk1 (10 µM) and dexamethasone (10 µM). Macrophages in the presence of LPS alone showed reduced expression of IκBα whereas in cells pre-treated with DT-13 and Rk1, protein expression of IκBα was similar to that of untreated samples (Figure 15A). In LPS stimulated cells, protein expression levels of p-NFκB, p-JNK and p-p38 MAPK proteins was increased in comparison to untreated samples. DT-13, Rk1 and dexamethasone treatment prior to LPS stimulation reduced the expression of p-NFκB, p-JNK proteins. Interestingly, inhibition of p-p38 protein was not observed in DT-13 pretreated cells. However, a dose dependent decrease in expression of p-NFκB protein was observed in DT-13 pretreated LPS stimulated macrophages (Figure 15B).

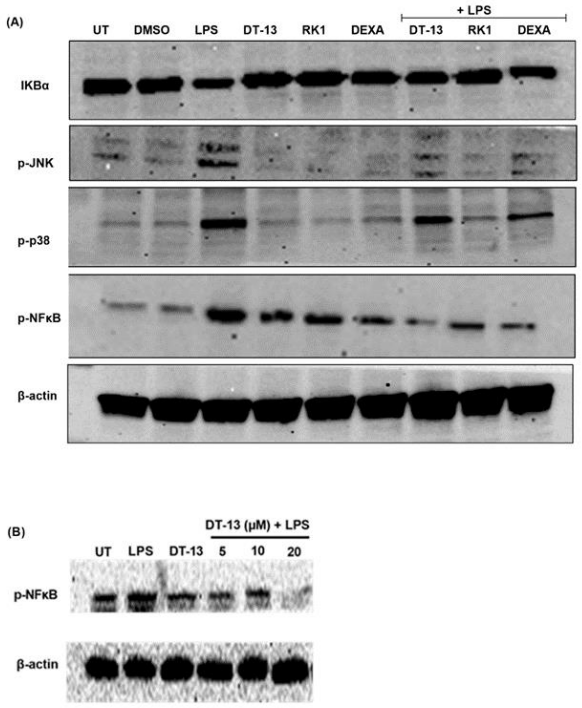

Figure 15 : Protein expression of NFκB signaling proteins in presence of compounds pretreated in LPS stimulated cells

A) Representative image of Western blot of p-JNK, P-NFκB, p-p38 MAPK, IKBα in LPS (10 ng) stimulated RAW 264.7 cells pretreated with DT-13, Rk1, dexamethasone (DEXA) or

untreated (UT). DMSO is used as vehicle control. (B) Western blot of p-NFκB protein in LPS stimulated cells pretreated with different doses of DT-13.

4.2.4 Attenuation of nuclear localisation of NFκB protein

LPS activated NFκB induces its translocation to the nucleus [141]. Since DT-13 inhibited the expression of LPS induced p-NFκB (Section 4.2), we wanted to visualise the effect of DT-13 on nuclear translocation of NFκB in LPS stimulated RAW264.7.

RAW 264.7 cells were stimulated with 200 ng LPS for different time points (0–60 min) and localisation of NFκB was studied by immunofluorescence. The cells were immunostained as described earlier (section 3.12).

As seen in Figure 16, after 5 min of LPS addition, whole cell appeared green due to the FITC conjugated secondary antibody against anti-NFκB antibody. Whereas this colour appears to be localised only in the cytosol as the blue colour of nuclear 4',6-diamidino-2-phenylindole (DAPI)-stain is not affected and remains distinguished when the two channels are merged (FITC + DAPI). However, post 30 min incubation of LPS, an intense green coloured ring like structure is visible in the nuclear region of the cells. The merged channel shows a significantly visible bluish green colour in the nuclear region in contrast to only blue in earlier time frames. This indicates that the NFκB gets more localised into the nucleus within 30 min LPS treatment.

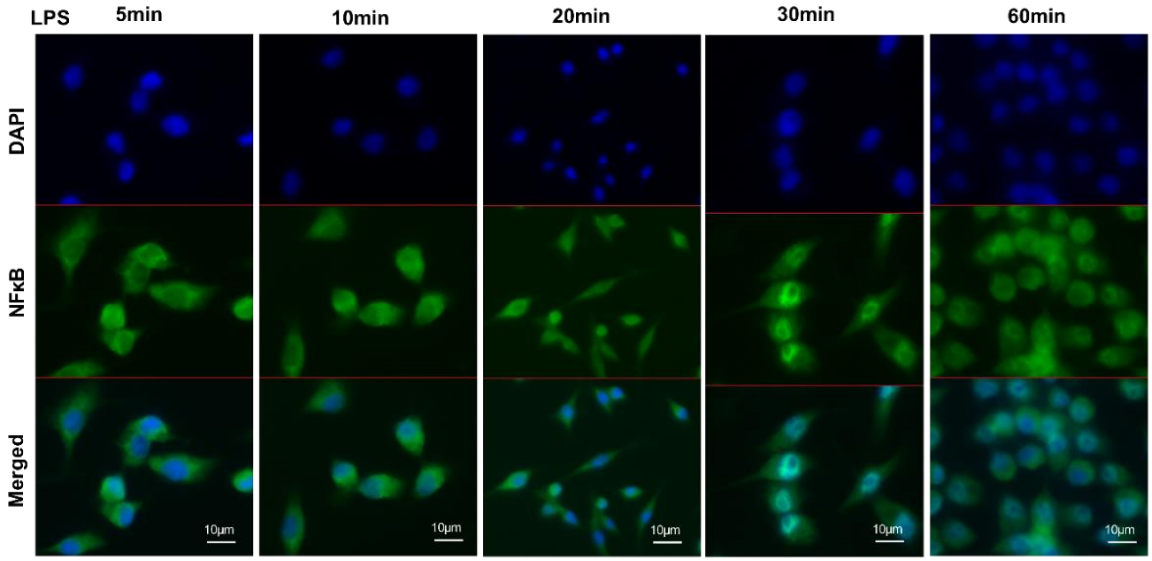

Figure 16 : Time dependent localization of NFκB in LPS stimulated cells

Representative image of macrophages showing a time dependent translocation of NFκB into the nucleus as seen via immunofluorescence microscopy. A visible significant green color ring of FITC labelled NFκB in the nucleus is observed at around 30 minutes of LPS stimulation (Green: FITC labelled NFκB; Blue: DAPI stained nuclei).

DT-13 in contrast to cells treated with LPS alone, did not show expression of NFκB in the nuclear region whereas, in the cells pre-treated with DT-13, the NFκB protein was localised in the cytosolic region only. The two-colour channels were separate from each other, and no bluish-green colour was visualised in the nuclear region (Figure 17). This indeed indicates that DT-13 attenuates the translocation of NFκB into the nucleus.

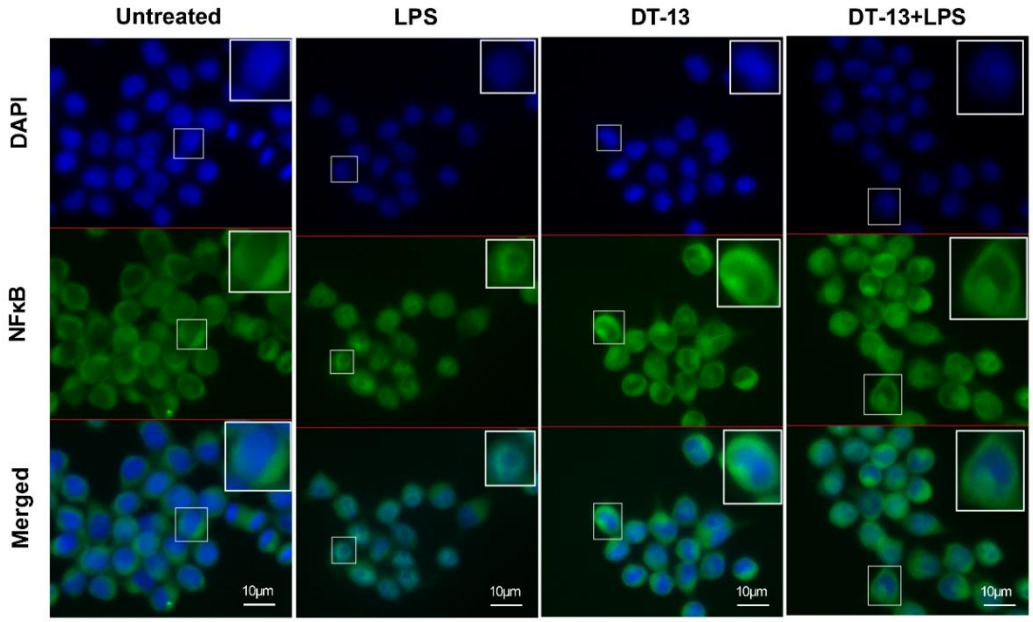

Figure 17 : DT-13 inhibits nuclear localization of NFκB in LPS stimulated cells.

Representative immunofluorescent image of RAW264.7 macrophages showing attenuation of translocation of NFκB into the nucleus. Blue nuclear DAPI staining remains unaltered in DT-13 treated cells and no blue green nucleus is observed in cells treated with DT13 and LPS (Green: FITC labelled NFκB; Blue: DAPI stained nuclei).

Similarly, p-NFκB expression was analysed via immunofluorescence in LPS stimulated cells pre-treated with Rk1, DT-13 and dexamethasone. LPS alone

stimulated cells showed green colour localised to nuclear region only and beautiful bluish green-coloured cells were observed in merged channels (Figure 18) whereas, in DT-13 pre-treated cells, expression of p-NFκB (represented

by green colour) was less in comparison to cells treated with LPS alone and was more like untreated cells. Similar results were seen in Rk1 and dexamethasone pre-treated cells.

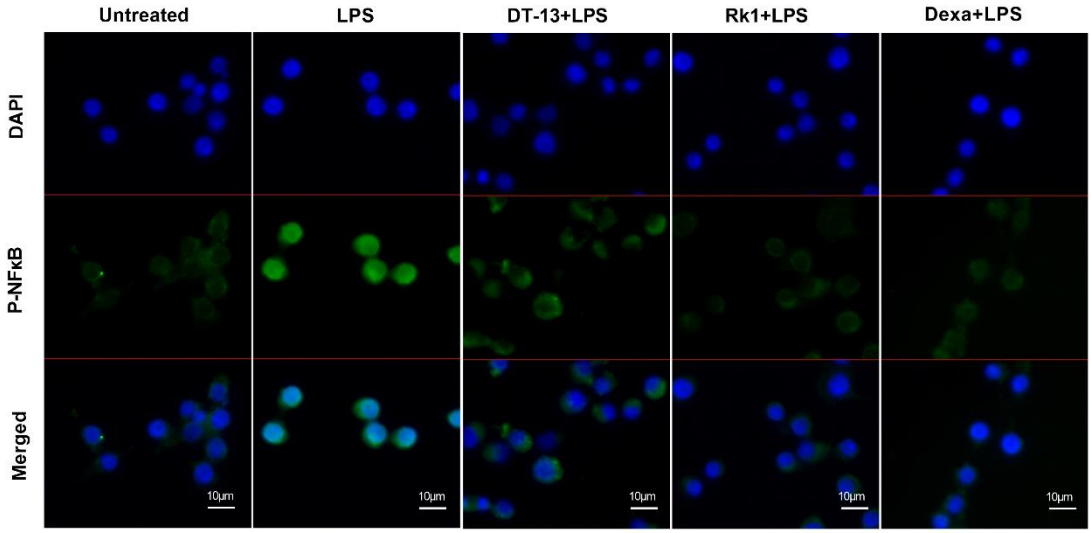

Figure 18 : Pre-treatment of cells inhibits p-NFκB activation

Representative immunofluorescent images of macrophages depicting the effect of DT-13, Rk1 and dexamethasone pre-treatment in LPS stimulated cells (Green: FITC labelled p-NFκB; Blue: DAPI stained nuclei).

4.2.5 Reduced expression of TNFα, COX and IL-6 cytokine in the cells pre-treated with the DT-13, Rk1 and dexamethasone.

LPS mediated activation of NFκB leads to the formation of cytokine storm and increase in proinflammatory markers. The anti-inflammatory property of Rk1, DT-13 and dexamethasone were analysed by evaluating their effect on TNFα, COX-2 gene regulation and IL-6 cytokine release in the LPS stimulated cells. DT-13 and Rk1 inhibited the IL-6 secretion significantly in a dose dependent manner (Figure 19A).

The inhibitory effect of DT-13 on IL-6 was significantly more effective than dexamethasone and Rk1 when equal concentrations were used for pre-treatment (Figure 19B). Additionally, DT-13 showed significant reduction in TNFα-alpha and

COX-2 gene expression in comparison to the Rk1 and dexamethasone (Figure 20) whereas it is worth noting that Rk1 tend to increase the expression of TNFα in comparison to LPS (data not significant).

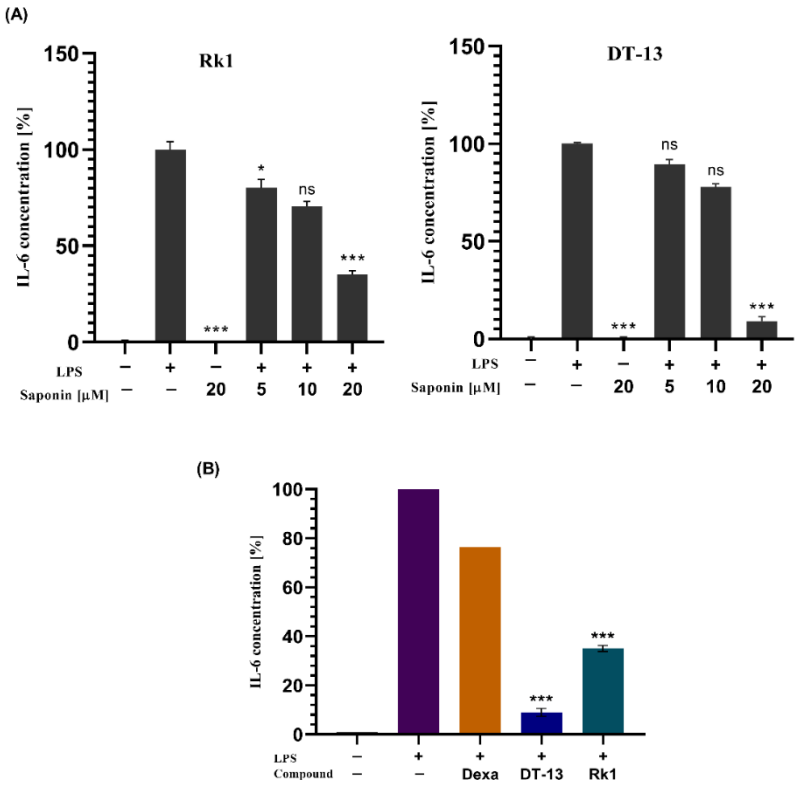

Figure 19 : Pretreatment with DT-13 and Rk1 inhibits LPS stimulated pro-inflammatory cytokines.

(A) IL-6 cytokine release in presence of DT-13 and Rk1 in LPS stimulated cells measured by ELISA. (B) Comparative analysis of DT-13, Rk1 and dexamethasone in terms of IL-6 release at similar concentration. All bars are representative of three biological replicates, mean ± SD, *p<0.05, **p<0.01, ***p0.001, 'ns' statistically not significant with respect to LPS alone.

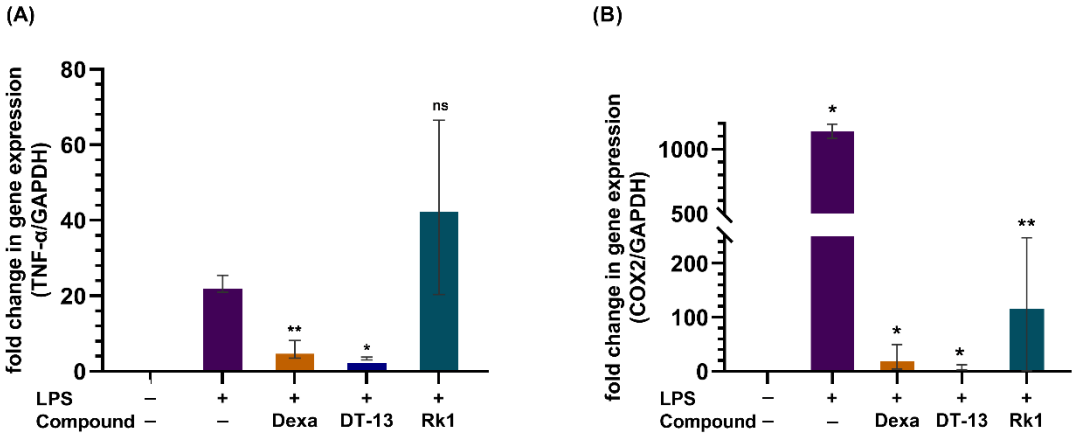

Figure 20 : Gene expression analysis of TNFα and COX-2 in pretreated cells

Bar graph depicting the relative fold change in gene expression of proinflammatory markers. Comparative analysis of DT-13, Rk1 and dexamethasone pre-treatment in LPS stimulated cells as measured by real time PCR. Bars are representative of three independent biological repeats, mean ± SD, *p<0.05, **p<0.01, ***p0.001, 'ns' statistically not significant with respect to LPS alone.

4.3 Attenuation of Inflammasome by DT-13 pretreatment

Protective effects of steroidal saponins via inhibition of NLRP3 inflammasome have been recently implicated in disease physiology [142]. To investigate whether DT-13 has an inhibitory effect on inflammasome activation, the gene expression levels of NLRP3 and IL-1β were measured via real time PCR. It is known that NFκB regulates the expression of NLRP3 gene and therefore is linked with inflammation. DT-13 and Rk1 pre-treatment significantly inhibited IL-1β gene expression in comparison to LPS alone (Figure 21A). DT-13 dose dependent pre-treatments attenuated the release of mature IL-1β protein from the cells as measured by ELISA (Figure 21B). There are studies that states the connection of dexamethasone with NLRP3 inflammasome [143]. Interestingly, our results also confirmed that dexamethasone significantly inhibits NFκB dependent NLRP3 and IL-1β gene expression.

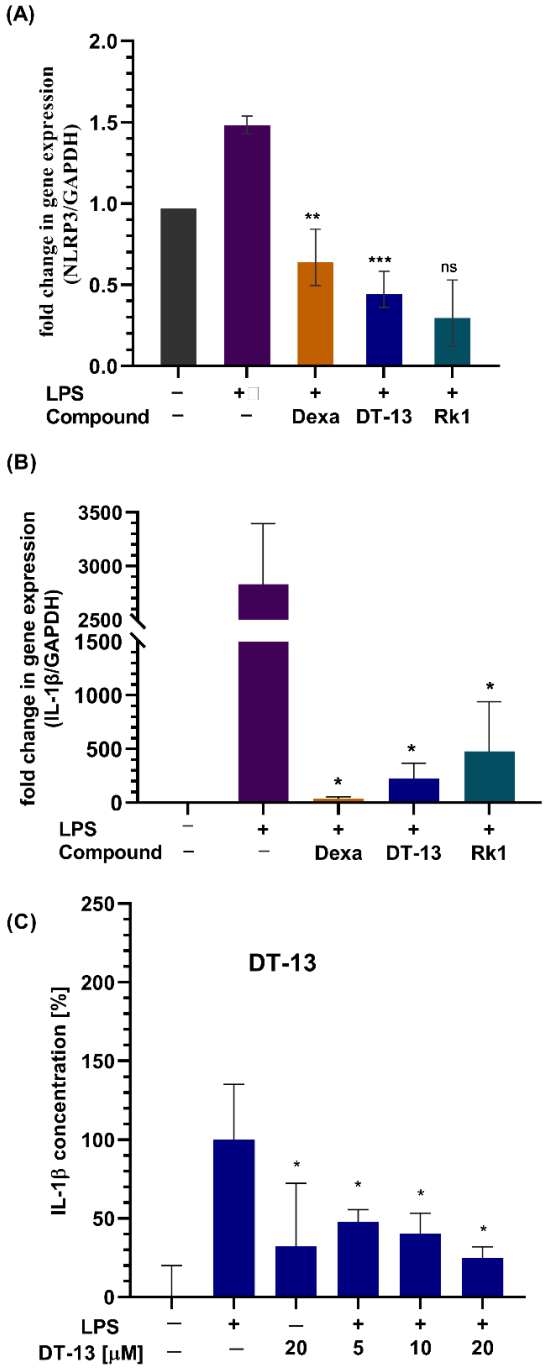

Figure 21: DT-13 inhibits NLRP3 inflammasome related gene expression in LPS stimulated cells.

Gene expression analysis of (A) NLRP3 and (B) IL-1β in cells when pre-treated with DT-13, Rk1 and dexamethasone. (C) IL-1β protein release as measured by ELISA. All data are representative of N ≥3, mean ± SD, *p<0.05, **p<0.01, ***p0.001, 'ns' statistically not significant with respect to LPS alone.

To further validate the role of DT-13 in inflammasome inhibition, a caspase-1 inflammasome assay was performed using cell culture supernatants to quantify the release of caspase-1. In this assay, Ac-YVAD-CHO inflammasome inhibitor was provided as positive control. The assay specificity and efficiency were determined using the positive inhibitor in the cell supernatants treated with LPS alone. In experimental samples, DT-13 and Rk1 pre-treated cells significantly inhibited the release of caspase-1 and hence the inflammasome formation as visualised by decreased luminescence in comparison to LPS alone (Figure 22A).

The protein C5b9 is expressed in membrane attack complex and therefore is utilised as a marker for MAC complex. To measure the activation of the C5b9 protein in response to the saponins, a chemiluminescent assay complement system alternate pathway was performed (section 3.9). Activation of C5b9 was inhibited significantly in a dose dependent manner by DT-13 and Rk1. Saponins at 50 and 100 µg/mL concentration showed a significant decrease in C5b9 protein expression (Figure 22B). Hence all the results infer that DT-13 and Rk1 are involved in inhibiting the NLRP3 inflammasome formation.

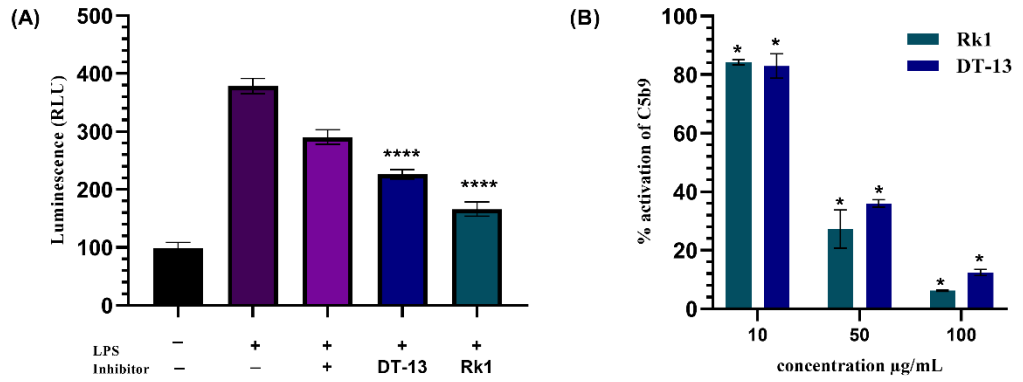

Figure 22 : DT-13 and Rk1 inhibits inflammasome formation and pyroptosis

(A) Bar graph depicting the luminescence corresponding to the activity of caspase-1 in LPS stimulated cells. DT-13 and Rk1 pre-treated cells show significant inhibition of caspase-1 inflammasome formation. (B) Complement alternate pathway assay to analyse the expression of C5b9, a component of the MAC complex responsible for pyroptosis. Data is represented as mean ± SD, N ≥ 3, *p<0.05, **p<0.01, ***p0.001, ‘ns’ statistically not significant with respect to LPS alone (A) and sera positive control in case of (B).

4.4 DT-13 as a ligand for PPARγ

4.4.1 Development of in vitro transfection model system for PPARγ ligand screening in HEK293 cells

To explore the possibility of DT-13 and Rk1 as a ligand for PPARγ, an in vitro HEK293 model system for screening PPARγ ligands was developed using an existing protocol [144]. In this in vitro transfection model system, (1) the PPARγ containing plasmid pcDNA- PPARγ and (2) the PPARγ response element containing plasmid PPRE-Tk-Luc that harbours a luciferase gene for reporting, were transiently transfected into the HEK293 cells. Upon ligand activation of the PPARγ protein, it acts as a transcription factor and binds to its response element gene PPRE-Tk-Luc. The activation of the gene transcription leads to the expression of luciferase protein and this in turn is analysed by the luciferase activity in the cells (Figure 23). The efficiency of the ligand is evaluated by the intensity of the luminescence produced by the cells.

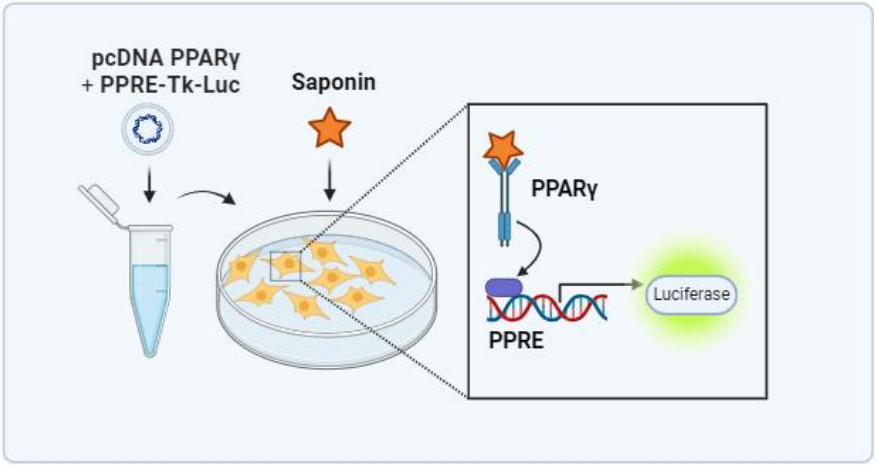

Figure 23 : HEK transfection model system to detect ligand mediated PPARγ activation

A graphical representation of the working principle of in vitro transfection system using HEK293FT cells to detect ligand mediated activation of PPARγ as a cell-based screening method for PPARγ ligands.

The plasmids used for the study were isolated using miniprep kit (section 3.13) and restriction digestion of the plasmid (section 3.14) was done to check the orientation and presence of the gene of interest (Figure S1). Since there was no reporter gene in the plasmid containing PPARγ, the successful transfection was analysed by observing

the expression of PPARγ protein in transfected and non-transfected cells via Western blot. As seen in Figure 24A, the transfected cells showed higher expression of PPARγ protein in comparison to the non-transfected cells. The in vitro transfection model was validated by the addition of known synthetic agonist of PPARγ namely, troglitazone and rosiglitazone. A dose dependent increase in the luciferase activity was observed in just 4 h of incubation of ligands (Figure 24B) although troglitazone (partial agonist) showed minimal activation of PPARγ gene depicted with lower relative light units (RLU) as that of rosiglitazone. For further comparative studies 10 µM concentration of compounds were used.

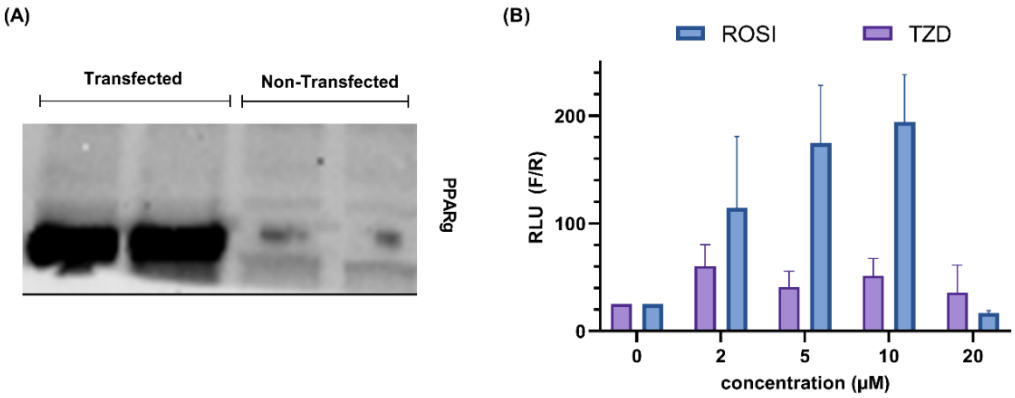

Figure 24 : Development and evaluations of the transfection model system using HEK293FT cell lines.

A) Western blot showing the expression of PPARg protein in transfected and non-transfected cells. (B) Graph depicting the response of PPRE-Tk-Luc gene in presence of increasing doses of troglitazone (TZD), rosiglitazone (ROSI). The data is represented as mean ± standard error mean (SEM)

4.4.2 In vitro studies to evaluate the activity of PPARγ in response to DT-13 and Rk1 induction

To confirm the regulation of PPARγ in LPS stimulated cells, we checked the expression of PPARγ by Western blot in RAW264.7 macrophages pre-treated with DT-13, Rk1 and dexamethasone with or without LPS stimulation. We observed that in comparison to untreated macrophages, the LPS stimulated cells downregulated the expression of

PPARγ protein. In contrast to this, the cells pre-treated with dexamethasone, DT-13, Rk1 alone did not change the levels of PPARγ protein. The effect of LPS was reversed by pre-treatment with dexamethasone, DT-13 and Rk1 in LPS stimulated cells (Figure 25A). This inferred that saponins were somehow mediating the activation of PPARγ expression in LPS induced pathway.

A HEK transfection model system was used to evaluate the activation of PPARγ by DT-13 and Rk1. DT-13 and Rk1 addition showed increased luciferase activity and hence PPARγ activity in comparison to PPARγ ligand troglitazone (Figure 25B). This implies that saponins are acting as a ligand of PPARγ and thereby regulating the LPS induced inflammatory pathway. In this experiment, untreated transfected cells were used as a control for ligands, non-transfected but troglitazone treated as negative control, only troglitazone, rosiglitazone treated transfected cells as positive ligand control and DMSO treated transfected cells for vehicle control.

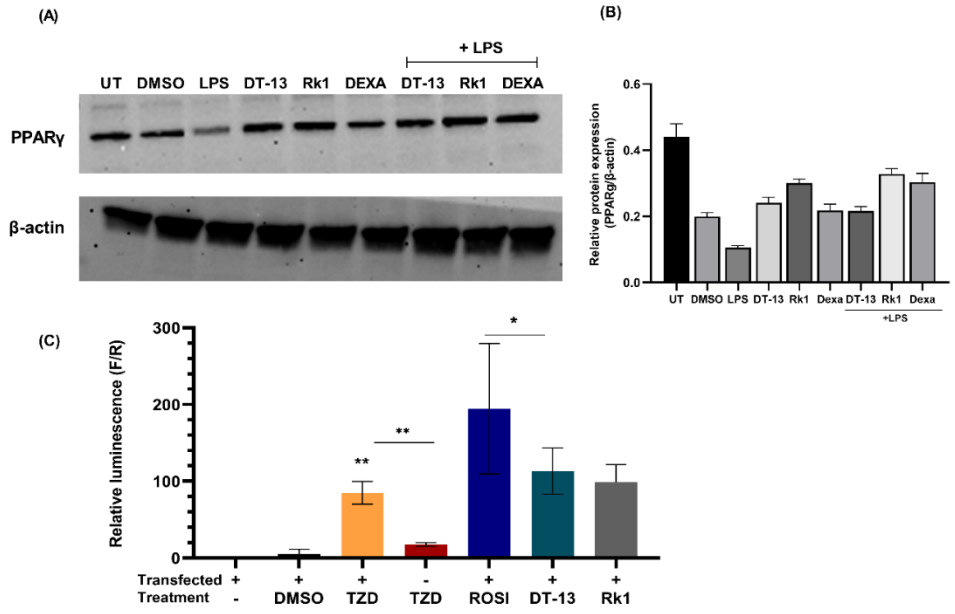

Figure 25 : PPARγ activity in saponin treated cells

(A) Blot depicting the protein expression levels of PPARγ in LPS stimulated RAW264.7 cells with or without pretreatment with dexamethasone and saponins and its quantitative analysis performed using ImageJ (B), (C) Bar graph depicting the PPARg activation in presence of DT-13, Rk1, troglitazone (TZD), and rosiglitazone (ROSI).

We further added different concentration of DT-13 and observed dose dependent increase in luciferase activity of the cells. The observed RLU for DT-13 treatments were in between the values for rosiglitazone and troglitazone treatments (Figure 26)

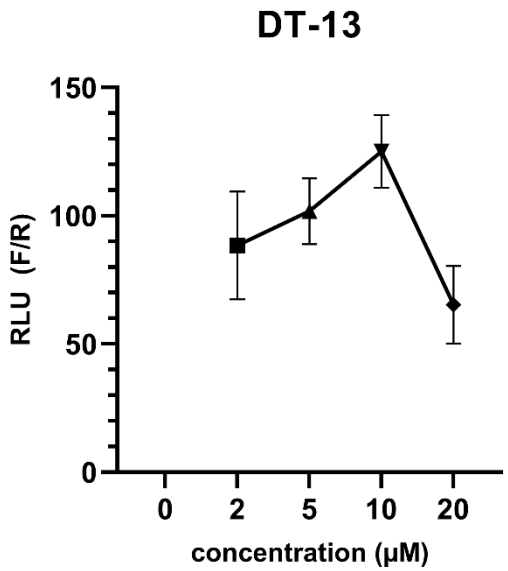

Figure 26 : DT-13 mediated dose dependent activation of PPARγ in vitro

Graph depicting the response of PPRE-Tk-Luc gene in presence of increasing doses of DT-13 as a representative of PPARγ activation in vitro.

PPARγ is known to exist as a heterogenous complex with Retinoid X-Receptor (RXR) protein. To explore whether ligands for RXR in addition to the test ligand compounds further increases the activity of PPARγ, we pre-treated the transfected cells with 9-cis retinoic acid (10 µM) in combination with DT-13, Rk1, and dexamethasone. It is notable that 9-cis retinoic acid (RA) alone was able to increase the luciferase activity. In combination treatment, DT-13/RA showed increased luciferase activity in comparison to DT-13 alone whereas RK1 alone displayed higher luciferase expression than in combination with RA (Figure 27). It cannot be excluded that there is a possibility of both saponins having different binding sites and therefore disparate regulation.

To exclude the possibility that any saponin or natural compound might enhance the activity of luciferase in our experimental setup, we used saponin SO1861 that is

previously described as an endosomal escape enhancer by our lab. Clearly, it was seen that SO1861 did not impart significant increase in luciferase activity (Figure 27). Hence not all, but some saponins like DT-13 and Rk1 may act as an agonist of PPARγ.

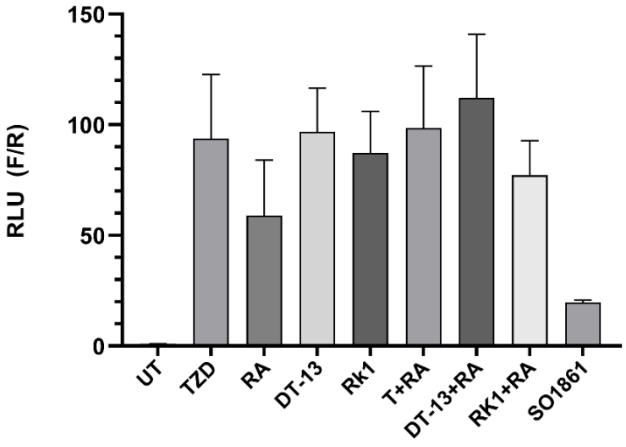

Figure 27 : PPARγ activity in response to pretreatments in combination with 9-cis retinoic acid

Bar graph representation of PPARγ activation in cells treated with DT-13, Rk1 and troglitazone in combination with retinoic acid (RA).

The relative binding affinity of DT-13 to PPARγ receptor was determined using a PPARγ green competitor assay. Synthetic agonists – rosiglitazone, troglitazone and PPARγ inhibitor – GW9662 showed a dose dependent decrease in fluorescence polarisation indicating the increased binding efficiency of these compounds with increasing concentrations. A shift in fluorescence polarisation was observed at around 100 nM concentration of natural ligand 9-hydroxyoctadecadienoic acid (9-HODE). DT-13 and Rk1 did not show a major change in the values. The concentrations of the compounds where 50% of the binding is inhibited (IC50) were calculated as half maximal polarisation values of the compounds and is equivalent to the binding affinity of the molecules. The IC50 value for rosiglitazone and troglitazone was 273.8 nM and 1.42 M respectively. The IC50 value of the PPARγ inhibitor GW9662 was 22.32 nM and for 9-HODE 1.8 µM. DT-13 showed an increase in polarisation values with increasing concentration and an arbitrary IC50 value was obtained. Rk1, on the other hand, appeared to not affect the polarisation values and had an ambiguous IC50 value

(Figure 28) The polarisation values were normalised in percentage by keeping the lower concentration values as max polarisation of 100% and the individual values were calculated with respect to the lower concentration.

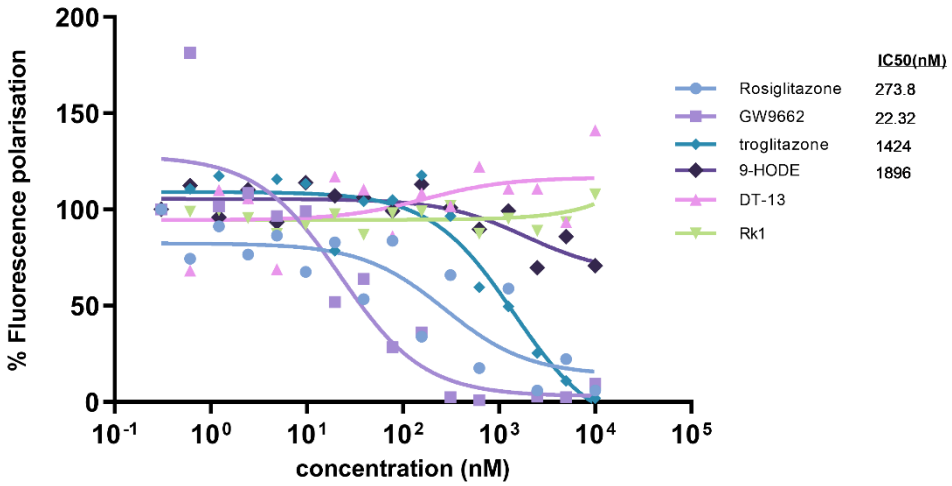

Figure 28 : PPARγ binding efficiency of DT-13 and Rk1 in comparison to known ligands

Graph depicting the fluorescence polarisation values (represented in percentage) with increasing concentrations of PPARγ synthetic ligands rosiglitazone and troglitazone, PPARγ inhibitor- GW9662 and natural PPARγ ligand 9-HODE. Data is represented as mean ±SD, normalised to percentage where the maximum fluorescence polarisation is considered as 100%. A curve fitting graph was obtained using non-linear regression model for log (Inhibitor) vs response option in GraphPad Prism 9.

4.4.3 In-silico binding of DT-13 with PPARγ protein

To study the possible binding interaction of DT-13 with PPARγ protein, molecular docking simulations were performed using Autodoc Vina [145]. Docking calculations showed the possible binding of DT13 at the binding site of PPARγ protein where rosiglitazone binds (Figure 29). The best conformation of DT13 had a binding energy of –5.11 kcal/mol indicating potential binding affinity for PPARγ. The glycosidic part of DT-13 showed three interactions via hydrogen bonding (Ile-281, Cys-285, Leu-340) and two electrostatic interactions (Glu-291, Glu-343) with steroidal part (Figure 29A). Similar interactions were observed for the synthetic ligand rosiglitazone in the co-crystal structure. It forms two hydrogen bond interactions (Tyr-473, Ser-289) with the polar head, two hydrophobic interactions (Leu-330, Arg-288) and one hydrogen bond

(Cys-285) at the aromatic central ring; another two hydrophobic interactions (Cys-285, Ile-341) at the lipophilic tail (Figure 29B). Interestingly, DT-13 and rosiglitazone both showed strong hydrogen bond interactions with cysteine at position 285 of PPARγ. These results suggest the potential binding of DT13 with PPARγ supporting findings of transfection experiments depicting DT-13 as a ligand for PPARγ protein.

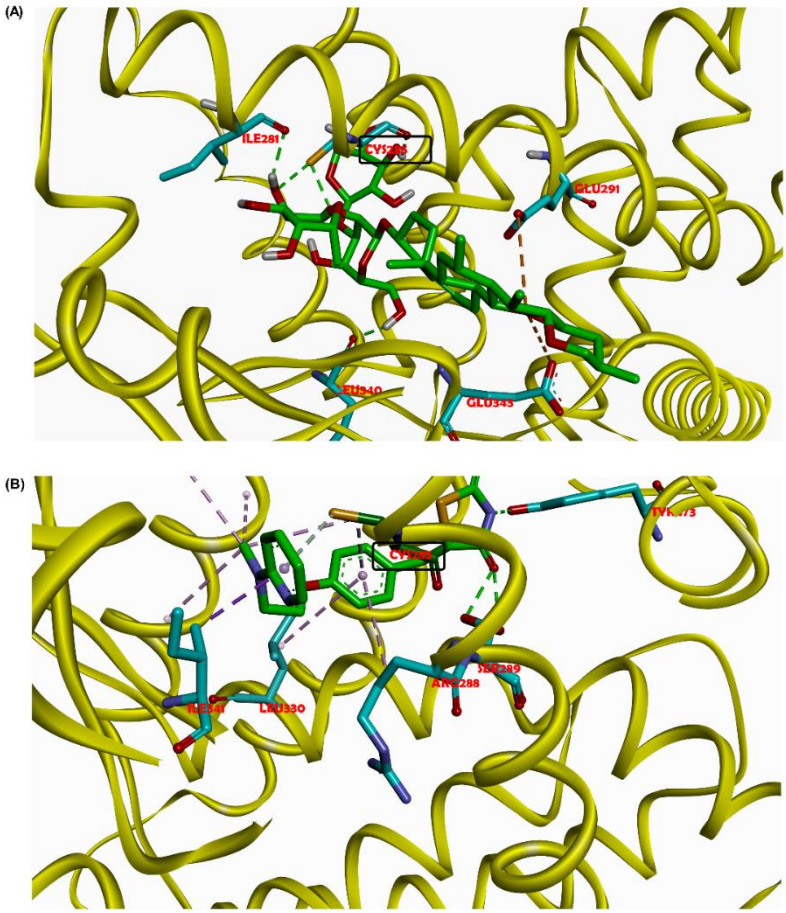

Figure 29 : In silico binding of DT-13 to PPARγ protein

(A) Docked molecule of DT-13 to the ligand binding pocket of PPARγ protein and (B) rosiglitazone bound to the same ligand binding pocket of PPARγ protein as visualised by Discovery studio visualiser. Both the molecules showed similar binding interactions at Cys-285

4.5 Conjugation of saponin Rh3 with Cy3-NHS dye – Localization studies

4.5.1 Analysis of ether precipitated cy3-labelled saponin

It is known that ginseng saponins are anti-inflammatory compounds that inhibit the NFκB/p-AKT/MAPK pathway. The structure function relation of the ginsenosides is widely explored but there is no evidence yet regarding the uptake of these molecules. It is thought that being amphiphilic, it interacts with the cholesterol in the plasma membrane and hence enters the cytosol effecting the cell functioning [146]. To visualize the entry of these small molecules into the cell and thereby enhance the possibility of developing targeted drugs, we wanted to label the saponins.

For conjugation studies, ginseng saponin Rh3 was used. To solubilize Rh3, DMSO was used and for labelling the saponins, Cy3-NHS dye in DMSO was used. Both were mixed in the following reaction ratio mixture.

Cy3:Rh3 (1:3)

Cy3-NHS ester = 1.25 mg (50 µL from 25 mg/mL Stock)

Rh3 = 3.75 mg in 800 µL DMSO

Total = 850 µL

Cy3:Rh3 (5:1)

Cy3-NHS ester = 5 mg (200 µL from 25 mg/mL stock)

Rh3 = 1 mg in 600 µL DMSO

Tota l= 800 µL

The mixture was kept on rotation overnight at room temperature. Next day, the mixture was precipitated in cold ether and further freeze drying was performed using lyophiliser (Alpha 1-2 LD plus lyophiliser (Martin Christ Gefriertrocknungsanlagen GmbH).

The lyophilized mix (GN40) was further analysed by Gregor Nagel (Charité – Universitätsmedizin Berlin). The mix (GN40) was solubilized in methanol and subjected to ESI-MS at Institute for Chemistry and Biochemistry, Freie Universität, Berlin. The sample GN40, showed presence of a lot of free or unconjugated dye (Cy3-COOH) and unconjugated saponin (Rh3-Na). Nevertheless, we observed a peak with

low signal of conjugated saponin (Cy3-Rh3) (Figure 30) in the mass spectrum that relates to the relative abundance of the conjugated molecule.

Figure 30 shows the mass spectrum of dye conjugated Rh3 at a molecular mass of 1043.7 Da with a small peak in addition to peaks for Cy3-COOH and Rh3-Na.

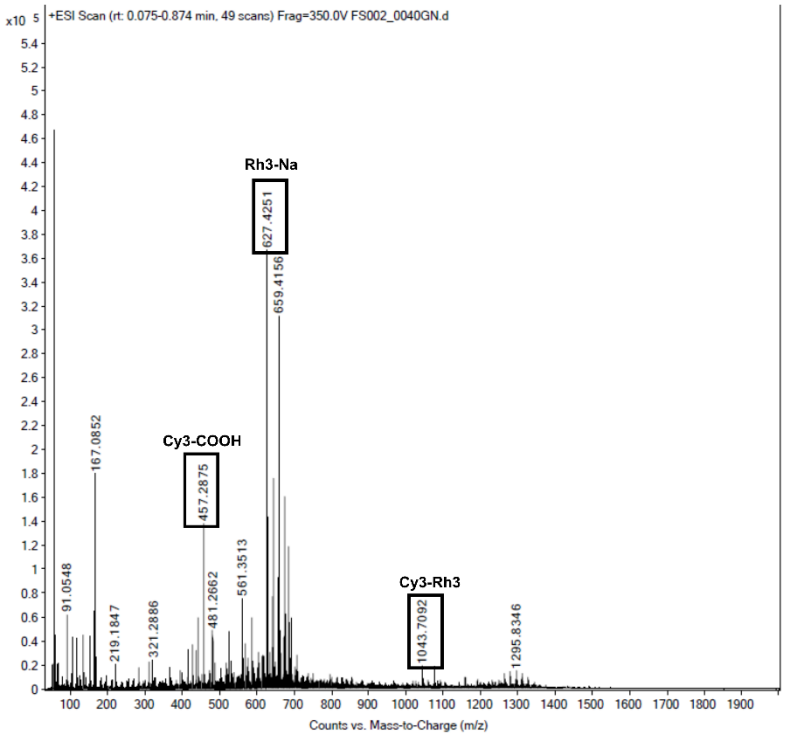

Figure 30 : Massspectrum of dye conjugated saponin (Cy3-Rh3)

To eliminate presence of free dye, dye-conjugated saponin (Cy3-Rh3, 1043.74 g/mol) was subjected to dialysis prior to MS analysis using dialysis membrane with 1K molecular weight cut-off (MWCO), that means molecules with atleast 1 KDa molecular mass will be retained in the membrane. Dye alone (Cy3-NHS, 554.3 g/mol) molecules were expected to be diffused out of the membrane however, no significant difference was observed.

Therefore, to further isolate and purify labelled saponins, reverse phase high performance liquid chromatography (HPLC) (1100 series HPLC, Agilent, Santa Clara, US) was performed using an isocratic method. For mobile phase acetonitrile (ACN)/water (60:40) with 0.1% trifluoroacetic acid (TFA) was used as a solvent and

run time was 60 min. The samples were dissolved in methanol/water (1:1) because they were not soluble in ACN. The results obtained were not clear and the yield was considerably small for further analysis. Nevertheless, we proceeded with the impure fraction to test the activity of the conjugated saponin in vitro.

4.5.2 Greiss reagent assay to evaluate the function of Cy3-Rh3

To investigate the activity of the Cy3 conjugated saponin, Greiss reagent assay was performed to analyse its effect on LPS induced NO release.

LPS stimulated RAW264.7 cells pretreated with the mixture (impure saponin-Cy3 solution) showed a dose dependent decrease in the release of nitric oxide when compared to cells treated with LPS alone (Figure 31). This effect can also be based on the presence of free saponin in the mixture and thus cannot be completely associated with the functionality of the dye conjugated saponin.

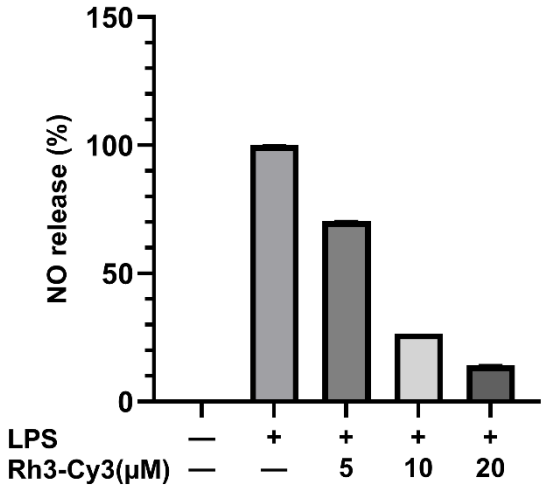

Figure 31 : Greiss reagent assay to measure the NO release by cells pre-treated with Cy3 dye conjugated Rh3.

Bar graph depicting the release of NO by LPs stimulated RAW264.7 cells pretreated with Cy3-Rh3. The data is normalized to percentage where LPS stimulated cells are considered as 100%, represented as mean ± SD of three biological repeats.

4.5.3 Visualizing dye conjugated Rh3 via fluorescence microscopy

To understand and verify the dye conjugation of saponin, we induced RAW264.7 with the impure saponin-Cy3 solution and checked the green fluorescence of Cy3 conjugated Rh3 saponin via fluorescence microscope (Zeiss Axio, Carl Zeiss AG, Jena, Germany). As seen in (Figure 32), Cy3 alone treated cells showed a blurry green fluorescence. This could mean that the dye did not enter the cells or was immediately being secreted out of the cells whereas the cells treated with the mixture showed a significant bright green fluorescence. This infers that even though the dye conjugated saponin was contaminated with free dye, the tendency of the dye inside the cells was low. Therefore, what is visualized, is the small amount of conjugated saponin. The positive outcome of the experiment was that we were able to conjugate the Cy3 dye with saponin Rh3 and were able to visualize it in vitro.

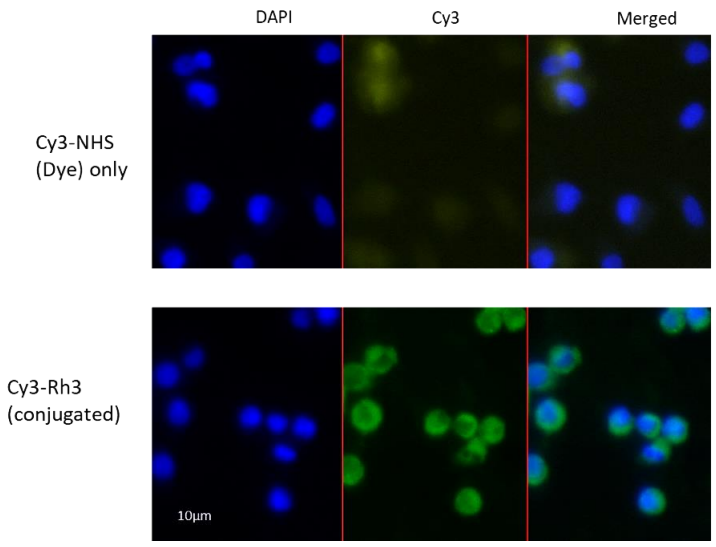

Figure 32 : Fluorescence microscopy images showing the localisation of Cy3 conjugated Rh3 in RAW264.7 cells.

4.5.4 Time dependent localisation of saponin in macrophages

After successful visualisation of Cy3 conjugate saponin in vitro, we analysed its localisation in RAW264.7 macrophages at different time points.

Cells were seeded (2000 cells/well) on a glass coverslip and incubated with Cy3 conjugated saponin (5 µM). The slides were prepared for fluorescence microscopy as described in section 3.12 and observed for dye conjugated saponin localization at various time points using fluorescence microscope (Zeiss Axio, Carl Zeiss AG, Jena, Germany). Within 10 minutes of incubation, all the cells showed green colored fluorescence (Figure 32) uniformly distributed in the cytosolic region as no fluorescence was observed in nucleus. The fluorescence was visibly distinguished from the blue colour of DAPI stained nuclear region. No change was observed post 3 h of incubation, however at 3 h the fluorescence intensity increased and green dots like granular structures were observed in the cells.

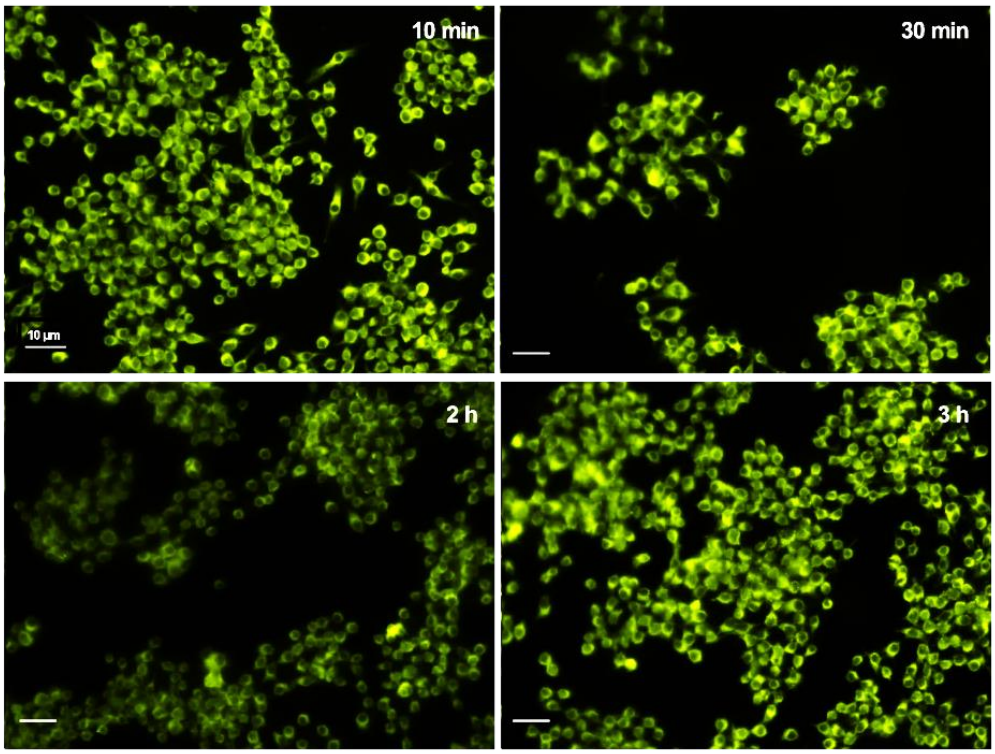

Figure 33 : Localisation of dye conjugated saponin (Cy3-Rh3) at various time points as observed by fluorescence microscopy.

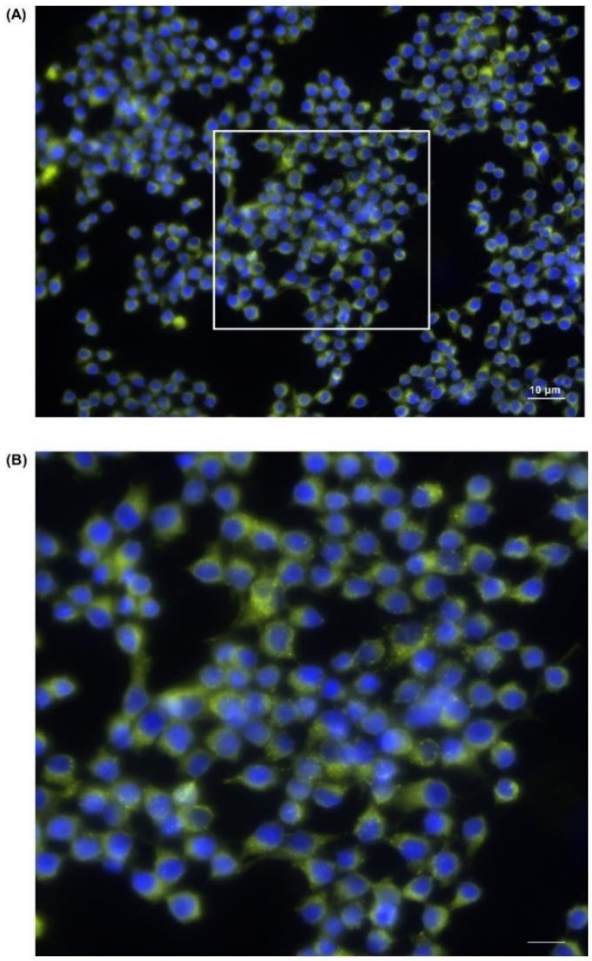

Figure 34 : Localistion of dye conjugated saponin (Cy3-Rh3) after 3 h of incubation in RAW264.7 cells

(A) RAW264.7 cells after 3 h of incubation with Cy3-Rh3 and (B) the zoomed image of cells depicting green fluorescent dots in the cytosol as visualized by fluorescence microscope (Green colour : Cy3-Rh3 and blue : DAPI)

The ultimate goal of current study to understand the mechanism of DT-13 as an anti-inflammatory molecule in comparison to well-known ginseng molecule, Rk1 and anti-inflammatory drug dexamethasone was fully achieved. We elucidated and confirmed the involvement of DT-13 in attenuating inflammation by inhibiting translocation of

NFκB in LPS/TLR4 pathway. Furthermore, we identified DT-13 as ligand for the activation of PPARγ mediated trans repression of inflammatory genes in macrophages. Although we were partially successful in labelling saponin with fluorescent dye, we did observe the localisation of conjugated saponin in vitro.

5. Discussion

5.1 Toxicity testing of compounds used in vitro.

Saponins are well known anti-inflammatory natural compounds that are widely used as dietary supplements. They are known to act via interfering with the NFκB pathway. During inflammation, in the LPS-TLR4/NFκB signalling pathway, localisation of activated NFκB into the nucleus regulates the expression of various inflammatory responsive genes [147]. Proinflammatory cytokines like TNFα, COX2 and IL-6 tends to increase marking the beginning of inflammation. These markers upon accumulation initiate and regulate other parallel pathways leading to excessive production of these cytokines and chronic inflammation. Saponins on the other hand are known to inhibit production of these cytokines [148]. Saponins like ginsenosides are widely researched for their anti-inflammatory, anti-cancer properties in various disease physiology including neurological disorders [149-152]. Nevertheless, there is still no clear information on the mechanism of action of various saponins and therefore indicates the scope of research.

Substantial references show that induction of inflammation by LPS in the macrophages has been used a model system to understand various inflammatory pathways [153, 154]. The cellular response is therefore dependent on the dose of LPS used to stimulate the cells [155]. Honda T *et al*. summarised that LPS at high dose (100 ng/mL to 1 µg/mL) are used to study inflammatory response whereas low dose LPS (50 pg/mL to 50 ng/mL) induces inhibition of pro-inflammatory cytokines [156]. They showed that LPS (0.1 ng/mL) stimulated-THP1 cells reduced the vascular endothelial inflammation [157]. Shi H *et al.* used LPS (0.1 to 10.0 µg/mL) to induce oxidative stress in bovine mammary epithelial cells and showed LPS induced toxicity in dose dependent manner. However, no significant difference was observed in cells treated with 0.1 µg/mL and 10.0 µg/mL LPS with respect to induction of oxidative stress [158]. These studies depicted the effect of different LPS doses in vitro but did not include any anti-inflammatory compound. Antonicelli *et al.* used 10 µg/mL LPS in vitro and 1 µg/mL in vivo to study the anti-IL-8 effect of new thiol antioxidant [159]. In our experiments, we treated RAW264.7 cells with LPS (0–1000 ng/mL) and checked the induction of inflammation by analysing the iNOS gene expression levels by real time PCR. A dose

dependent increase was observed in mRNA levels of iNOS gene (Figure 11). We continued our experiments further with low dose (10 ng/mL) of LPS. No toxicity assay was performed on cells treated with different doses of LPS, however morphology of cells treated with LPS (10 ng/mL) was checked with simple visualisation in bright field using light microscope (Figure S2). Cells showed similar morphology (extended projections) as that of untreated cells but with more cytoplasmic vacuoles, although this could be the ingested LPS by the macrophages [160]. To evaluate the effect of LPS (10 ng/mL) on the activation of the TLR4, immunofluorescence was performed in LPS stimulated macrophages at various time points. An increased expression was observed post 30 min of LPS incubation (Figure S3) but the effect was not observed in subsequent experiments.

Most of the studies previously were done with crude plant extracts containing a mixture of bioactive saponins and the concentration up to 100 µg/mL were used to study therapeutic effects in vitro [131, 132]. Fracasso J.A.R *et al*, showed that the effect of saponin are cell type specific and depicted no cytotoxicity in fibroblasts treated with 1600 µg/mL of pomegranate and sisal residue extracts [161]. In search of a new drug molecule, preclinical studies majorly focus on pure isolated plant metabolites investigating their effects in vitro [162, 163]. Zhu J *et al*, used purified saikosaponin A in micromolar concentrations in RAW264.7 cells [164]. In the present study, purified anti-inflammatory compounds – DT-13, Rk1, dexamethasone (1–20/30 µM) – were used and their toxicity were analysed in vitro by MTT assay. No or minimal change in the metabolic activity was observed in cells pre-treated with DT-13, Rk1 and dexamethasone (Figure 12). These results depicted the non-toxic concentration of the compounds to be used for further experiments and eliminated the possibility of false positive results in our experiments.

5.2 Is DT-13 more effective anti-inflammatory compound? Is it pan-inhibitor or selective?

Traditional NSAIDs which are mostly COX inhibitors, possess side effects underlying various gastrointestinal toxicity [165, 166]. Current strategies involve gastroprotective NSAIDs with selective COX-2 inhibition, COX/LOX inhibition or NO release mediating NSAIDs [167]. However, due to rapid absorption of plant derived molecules via passive diffusion in intestinal lining [168, 169], they are considered more safer and

less toxic as an anti-inflammatory agent [170]. Joseph C. Maroon *et* al, summarized the benefits of natural anti-inflammatory compounds over traditional NSAIDs [171]. Rk1 is known to inhibit NO release and proinflammatory cytokines IL-6, TNFα expression via JAK2/STAT3 pathway [172] whereas dexamethasone is known to inhibit COX-2 via p38/MAPK pathway [173]. DT-13 on the other hand is known to inhibit TNFα induced inflammation via NFκB/MAPK pathway [140, 174]. In our experiments, we tried to understand the inhibitory action of DT-13 on various inflammation associated genes and proteins in comparison to dexamethasone and Rk1. DT-13 significantly inhibited LPS induced NO release from macrophages (Figure 13) and downregulated the mRNA levels of MyD88 and TICAM (Figure 14) however dexamethasone attenuated TICAM gene expression and increased the expression of MyD88. Similar observation was reported in a study on pig alveolar macrophages by Sun P et al. [175]. This could imply a different mode of action of the dexamethasone compared to saponins. Although dexamethasone is known to inhibit MyD88 expression as well but by far has been used in combination with other drug molecules [176]. Further expression of secondary metabolites was analysed via Western blotting. DT-13 inhibited LPS induced p-NFκB proteins and p-JNK in a dose dependent manner. Similar inhibition was observed for Rk1 pre-treated cells (Figure 19). In the presence of LPS, phosphorylated NFκB translocation is crucial with respect to the gene regulation of inflammatory cytokines and other inflammation responsive genes [25]. Cells pre-treated with DT-13 inhibited LPS induced accumulation of NFκB in the nuclear region (Figure 17). Also, activated NFκB (p-NFκB) was visualized in cells pretreated with DT-13, Rk1 and dexamethasone (Figure 18). DT-13 showed more inhibitory effect with 32%, dexamethasone 26% and Rk1 19% of p-NFκB expression when compared to LPS alone (normalized to 100% with respect to untreated) (Table 4).

Additionally, DT-13 inhibited IL-6 cytokine release with an efficiency of 90% whereas Rk1 showed 78% inhibition of IL-6 release. Dexamethasone attenuated IL-6 cytokine, but the inhibition was only 24% (Figure 19). Dexamethasone is known to follow a different pathway of IL-6 regulation involving glucocorticoid receptor (GR) [177] that might be the reason of its varied inhibition efficiency. Additionally, DT-13 reduced the expression of TNF-α and COX-2 by 85% and 99% respectively (Figure 20). The

inhibition was significantly more than that of dexamethasone and Rk1. Table 4 summaries the inhibition efficiency of DT-13, Rk1 and dexamethasone.

Table 4 : Inhibition efficiency of Rk1, DT-13 and dexamethasone

The values are represented in percentages and normalized with respect to LPS.

Markers	**Inhibition Efficiency (%)**		
	DT-13	**Rk1**	**Dexamethasone**
NO	**69.2**	**68.8**	**—**
IL-6	**89.9**	**77.7**	**23.7**
TNF-α	**85.3**	**—**	**14.7**
COX-2	**99.5**	**94.5**	**97.5**
p- NFκB	**31.8**	**19.2**	**26.3**

Although to delve into the interpretation of DT-13 as a better inhibitor molecule, we must address the major question that whether a drug inhibiting multiple pathways (pan-inhibition) is preferred over a targeted selective inhibitor like COX-2 inhibitors. Skye Montoya *et al*, reviewed various pros and cons of a selective and non-selective inhibitor molecule. They stated that in addition to less toxicity and easy detection of mode of action, targeted drug inhibitors however have more possibility of drug resistance. Pan-inhibitors on the other hand are less likely to develop drug resistance and more efficient due to control over multiple pathways but sometimes show unpredictable toxicity [178]. Lei Zhong *et al*, also concluded the importance of combination drug over targeted therapy to treat drug resistance in cancer malignancies [179]. In the present study, in addition to anti-inflammatory effect, our results showed that DT-13 attenuated inflammasome related genes. In DT-13 pretreated cells, NLRP3 and IL-1β gene expression was downregulated in comparison to LPS (Figure 21A). We also observed reduction in IL-1β (Figure 21C) and caspase-1 (Figure 22A) release in the presence of DT-13. Additionally, the inhibitory effect of DT-13 on C5b9 component of MAC complex (Figure 22B) depicts its role as a pan-inhibitor of inflammation and inflammasome. Although more in-depth knowledge is

required to analyse the toxicity and side effects of DT-13 for example effect on expression of COX-1 enzyme that mainly is the cause of GI related toxicity from NSAIDs inhibition [180].

5.3 Does DT-13 activate PPARγ mediated transrepression of NFκB?

To further understand the anti-inflammatory mechanism of DT-13 we delved more into finding the possible targets of DT-13. The literature research illuminated the importance of PPARγ in NFκB mediated inflammation and lead to the hypothesis that DT-13 acts as a ligand for PPARγ to suppress LPS stimulated inflammation.

In the current study, a transfection model system was developed using HEK 293 cells to evaluate the ligand mediated activation of PPARγ. Increased PPARγ expression was seen in transfected cells compared to non-transfected cells, confirming the efficient transfection of the cells (Figure 24A).To confirm the working efficiency of the assay, agonists for PPARγ namely troglitazone and rosiglitazone were used as positive controls. We observed a dose dependent increase in PPARγ activation in cells treated with rosiglitazone and troglitazone (Figure 24B) however the effect of rosiglitazone was more pronounced than that of troglitazone. These variations within the thiazolidinedione class of drugs are already reviewed [181]. It is known that LPS stimulation leads to downregulation of PPARγ [182]. Conversely, ligand activated PPARγ indirectly downregulates LPS stimulated pro-inflammatory cytokines by a mechanism called as trans-repression [109]. In our experiments, LPS induction decreased the PPARγ levels in total cell protein whereas its expression was increased by pre-treatments with DT-13 and Rk1 (Figure 25A). Utilising HEK transfection model, we observed that in presence of DT-13 PPARγ was activated in a dose dependent manner as seen by increased luciferase expression (Figure 26). Zhang *et al*, summarized the in silico studies of saponins as ligand of different nuclear receptors [183]. Patrik F. Schwarz *et al*, showed a novel steroidal sapogenin directly binding to the retinoic acid associated orphan receptor α/γ (ROR α/γ) [184]. They used RORγ-Gal4 in addition to tk-Luc plasmid to check the ROR specific activation via luciferase activity. Their approach was different, but the outcome was similar to our transfection experiments. In addition to luciferase activity, they also measured gene expression of RORγ related target genes (Interleukin 17 A and glucose 6 phosphatase) via realtime

PCR. We could have utilized similar approach to check the localization or activation of NFκB in PPARγ overexpressed cells.

Moreover, PPARγ is known to exist as a heterogenous complex with Retinoid X receptor (RXR) [185] ; therefore, transfected HEK cells were treated with RXR ligand retinoic acid (RA) in combination with DT-13, Rk1 and troglitazone. Interestingly, cells treated with Rk1, Rk1/ RA, T/RA, DT-13, DT-13/RA all showed luciferase activity amongst which DT-13 and DT-13/RA showed significantly more pronounced increase in luciferase activity (Figure 27). It was remarkable to see that when another saponin SO1861 (saponin shown to possess endosomal escape enhancer activity by our Lab [186]) was added, no significant luminescence was observed. This proved that the assay was specific, and addition of any compound does not elicit the luciferase activity.

We further performed molecular docking studies and showed the probable binding affinity of DT-13 molecule in the ligand binding pocket of PPARγ protein. The best conformation of docked DT-13 molecule into PPARγ macromolecule was obtained in the same pocket as that of rosiglitazone. However, we could observe a similar hydrogen bond interaction of DT-13 and rosiglitazone with Cys-285 of PPARγ protein. The interactions were mostly governed by hydrogen bonding in DT-13, similar to that of rosiglitazone (Figure 29). A binding energy of -5.11 kcal/mol revealed a strong binding of DT-13 with that of PPARγ, confirming our hypothesis of DT-13 as a ligand for PPARγ protein.

To corroborate the findings of DT-13 binding to PPARγ in vitro, we performed a cell free fluorescence polarisation-based assay to screen PPARγ ligands. The binding efficiency of DT-13 was analysed in addition to rosiglitazone, troglitazone, PPARγ inhibitor GW9662 and PPARγ natural ligand 9-HODE. The assay involves measuring the change in fluorescence polarisation values of the nuclear receptor bound with fluoromone tracer in presence of test compounds The fluorescence polarisation is high when the fluoromone tracer is bound to the PPARγ ligand binding domain and it decreases as the test compound competes for the binding and fluoromone tracer is released. The ligands and inhibitor of PPARγ showed a dose response curve as expected (Figure 28). DT-13, in contrast to other compounds showed a gradual decrease in binding affinity with increasing concentration and the shift in the curve was minimal. On the other hand, Rk1 showed high polarisation values independent of concentration leading to ambiguous binding affinity. The binding curve of DT-13

implies that it could not compete with the attached fluoromone tracer for the ligand binding site of PPARγ although it could also indicate a different mechanism and binding site for DT-13. The tendency of saponins to form micelles in the solution [187] could be the reason of the varying results at higher concentrations. Nevertheless, these results indicate that DT-13 binds to PPARγ and activates an anti-inflammatory pathway via PPARγ mediated transrepression of proinflammatory cytokines.

5.4 Localisation of saponins in cells

In plants, saponins are usually localised in mesophyll, primary and secondary phloem layer of leaves, stem and roots respectively [188]. In mammalian cells, they are mostly used as permeabilisers [189] and emulsifiers [190] for the uptake of lipid based bioactive compounds [191]. Additionally, studies performed on lipid membranes mimicking mammalian cells highlighted the interaction of saponins with the cell membranes [192]. Nataliya Frenkel *et al*, showed the importance of cholesterol in the uptake of saponin [193]. Currently no studies have been done so far to visualize the uptake of saponins via fluorescence labelling directly however Weng *et al*, radiolabelled saponin saponinum album (SA) from Gypsophila paniculate L. with [^{3}H]-acetic anhydride to investigate the kinetics of SA [194]. In our project, we tried to conjugate ginseng saponin Rh3 with the fluorescent dye Cy3-NHS (section 4.5) to understand and visualise the localisation of Rh3 saponin in vitro using fluorescence microscopy. Rh3 saponin consists of hydrophilic part with one glucose molecule and a hydrophobic triterpene backbone. The possibility of saponin forming an ester bond linkage with the dye is via four hydroxyl groups present in glycosidic part and one in the triterpene part of the saponin. Such complex reaction would possibly lead to binding of one or more dye conjugates to the saponin but might lead to steric hindrance. According to the mass spectrum of the dye-conjugated saponin sample, we were successful in conjugating the dye to the saponin (peak at 1043 g/mol) (Figure 30) however the purification of the dye conjugated saponin was not completely achieved with dialysis and HPLC. Limited UV detection of saponins [195] in HPLC added to the complexity of our purification. Yi Wang *et al*, reviewed various methods including thin layer chromatography (TLC), mass spectrometry to separate and analyse saponins [196]. In our experiments we performed reverse phase HPLC (RP-HPLC) using an isocratic method whereas in a study to investigate the saponins in

mango peel by Imran e*t al,* RP-HPLC with gradient elution mode was used instead of isocratic method [197]. Another interesting approach was depicted by Shuai Li *et* al, using an online preparative HPLC method for efficient purification of saponins from Panax notoginseng saponins. They used four different elution modes consisting of five separation columns, eighteen trap columns and six enrichment steps. Liu *et al*, incorporated diode array detectors to HPLC (HPLC-DAD) for quantitative determination of saponins [198]. Although we were unable to purify the conjugated saponin, we continued with the evaluation of its functionality whilst keeping in mind the presence of free saponin and free dye in the sample. Greiss reagent assay was performed to check NO release in presence of Cy3-Rh3 in LPS stimulated macrophages. There was a dose dependent inhibition of NO release from the cells treated with dye conjugated Rh3 (Figure 31). This effect could have been due to the presence of free saponin in the sample therefore we further analysed cells under fluorescence microscope to investigate the localization of Cy3-Rh3. We were able to see the localization of saponin even with the minimal yield of conjugated saponin via fluorescence microscopy (Figure 32). A bright green fluorescence was observed in cells treated with Cy3-Rh3 at various time points (Figure 33). We observed that saponin localises into the cytosolic region mostly and is distributed equally. Post 3 h of incubation, cells showed green fluorescence as dot-like structures (Figure 34) whereas this could be aggregation of saponin molecules inside the vacuoles.

6. Conclusion and Outlook

Our aim was to investigate the inhibitory mechanism of DT-13 in LPS stimulated inflammatory pathway and to identify its targets. For the same we implied a top-down approach of evaluating secondary metabolites from the start of the LPS/TLR4 signaling pathway until the end (release of proinflammatory cytokines and pyroptosis). We confirmed the inhibition of nuclear translocation of activated NFκB followed by downregulation of TNFα, COX-2, IL-6, IL-1β and NLRP3 inflammasome related genes in cells pretreated with DT-13.

We proposed a pan-inhibition mechanism of DT-13 due to its anti-inflammatory and anti-inflammasome properties. This gives it an advantage in regulating inflammation via multiple pathways but additionally might possess unknown toxicity. For the same reason more in-depth toxicity studies need to be done in vitro and in vivo to analyse further side effects of DT-13. To understand the effect of DT-13 in other disease conditions, different cell types need to be included. This study demonstrated the anti-inflammatory effect of DT-13 to be more pronounced than that of dexamethasone and ginseng saponin Rk1 at the same concentration. Additionally, we showed a direct binding mechanism of DT-13 to PPARγ receptor mediating transrepression of proinflammatory cytokine with the help of an HEK transfection model system. Although DT-13 mediated direct regulation of PPARγ dependent genes (for example, Rab9 recently implicated in NLRP3 inflammasome in asthmatic condition [199]) should be performed to have a broader view of its binding efficiency. With the help of in silico docking studies, we successfully predicted a putative binding site for DT-13 and investigated its binding efficiency using fluorescent polarization-based assay. We did not observe a dose response curve for DT-13 and therefore a different approach, for example surface plasmon response should be applied to visualise the binding interaction. Furthermore, we were successful in conjugating saponin with fluorescent dye but were unable to purify it. Therefore, modifications should be done for achieving better purification of the conjugated saponin to track the subcellular localization of saponins. Considering the benefits reaped from ancient traditional herbal plant medications, current study shows valuable insights for preclinical studies involving optimization of DT-13 as a new anti-inflammatory drug candidate.

Bibliography

1. Chaplin, D.D., *Overview of the immune response.* J Allergy Clin Immunol, 2010. **125**(2 Suppl 2): p. S3-23.
2. Woodell-May, J.E. and S.D. Sommerfeld, *Role of Inflammation and the Immune System in the Progression of Osteoarthritis.* Journal of Orthopaedic Research, 2020. **38**(2): p. 253-257.
3. Bonilla, F.A. and H.C. Oettgen, *Adaptive immunity.* J Allergy Clin Immunol, 2010. **125**(2 Suppl 2): p. S33-40.
4. Chen, L., et al., *Inflammatory responses and inflammation-associated diseases in organs.* Oncotarget, 2018. **9**(6): p. 7204-7218.
5. Liehn, E.A. and H.A. Cabrera-Fuentes, *Inflammation between defense and disease: impact on tissue repair and chronic sickness.* Discoveries (Craiova), 2015. **3**(1): p. e42.
6. Germolec, D.R., et al., *Markers of Inflammation.* Methods Mol Biol, 2018. **1803**: p. 57-79.
7. Hannoodee, S. and D.N. Nasuruddin, *Acute Inflammatory Response*, in *StatPearls*. 2024, StatPearls Publishing Copyright © 2024, StatPearls Publishing LLC.: Treasure Island (FL).
8. Franceschi, C. and J. Campisi, *Chronic Inflammation (Inflammaging) and Its Potential Contribution to Age-Associated Diseases.* The Journals of Gerontology: Series A, 2014. **69**(Suppl_1): p. S4-S9.
9. Furman, D., et al., *Chronic inflammation in the etiology of disease across the life span.* Nature Medicine, 2019. **25**(12): p. 1822-1832.
10. Drayton, D.L., et al., *Lymphoid organ development: from ontogeny to neogenesis.* Nature Immunology, 2006. **7**(4): p. 344-353.
11. Ribeiro, L.S., L. Migliari Branco, and B.S. Franklin, *Regulation of Innate Immune Responses by Platelets.* Frontiers in Immunology, 2019. **10**.
12. José Luis, M.-C., et al., *Cytokine Profiling Plays a Crucial Role in Activating Immune System to Clear Infectious Pathogens*, in *Immune Response Activation and Immunomodulation*, K.T. Rajeev and S.B. Prakash, Editors. 2018, IntechOpen: Rijeka. p. Ch. 2.
13. Tsalamandris, S., et al., *The Role of Inflammation in Diabetes: Current Concepts and Future Perspectives.* Eur Cardiol, 2019. **14**(1): p. 50-59.
14. Singh, N., et al., *Inflammation and cancer.* Ann Afr Med, 2019. **18**(3): p. 121-126.
15. Liu, C.H., et al., *Biomarkers of chronic inflammation in disease development and prevention: challenges and opportunities.* Nature Immunology, 2017. **18**(11): p. 1175-1180.
16. Banerjee, C. and M.I. Chimowitz, *Stroke Caused by Atherosclerosis of the Major Intracranial Arteries.* Circulation Research, 2017. **120**(3): p. 502-513.

17. Konsman, J.P., *Cytokines in the Brain and Neuroinflammation: We Didn't Starve the Fire!* Pharmaceuticals (Basel), 2022. **15**(2).

18. Chen, W.W., X. Zhang, and W.J. Huang, *Role of neuroinflammation in neurodegenerative diseases (Review).* Mol Med Rep, 2016. **13**(4): p. 3391-6.

19. Wellen, K.E. and G.S. Hotamisligil, *Inflammation, stress, and diabetes.* J Clin Invest, 2005. **115**(5): p. 1111-9.

20. Megha, K.B., et al., *Cascade of immune mechanism and consequences of inflammatory disorders.* Phytomedicine, 2021. **91**: p. 153712.

21. Jiang, Y., et al., *Inflammatory pathways in COVID-19: Mechanism and therapeutic interventions.* MedComm (2020), 2022. **3**(3): p. e154.

22. Kawai, T. and S. Akira, *Signaling to NF-kappaB by Toll-like receptors.* Trends Mol Med, 2007. **13**(11): p. 460-9.

23. Kuzmich, N.N., et al., *TLR4 Signaling Pathway Modulators as Potential Therapeutics in Inflammation and Sepsis.* Vaccines (Basel), 2017. **5**(4).

24. Siebenlist, U., G. Franzoso, and K. Brown, *Structure, Regulation and Function of NF-kappaB.* Annual Review of Cell and Developmental Biology, 1994. **10**(Volume 10, 1994): p. 405-455.

25. Oeckinghaus, A. and S. Ghosh, *The NF-kappaB family of transcription factors and its regulation.* Cold Spring Harb Perspect Biol, 2009. **1**(4): p. a000034.

26. Hu, L.-F., et al., *The Regulation of Seventeen Inflammatory Mediators are Associated with Patient Outcomes in Severe Fever with Thrombocytopenia Syndrome.* Scientific Reports, 2018. **8**(1): p. 159.

27. Martín-Sánchez, F., et al., *Inflammasome-dependent IL-1β release depends upon membrane permeabilisation.* Cell Death & Differentiation, 2016. **23**(7): p. 1219-1231.

28. Ting, J.P., et al., *The NLR gene family: a standard nomenclature.* Immunity, 2008. **28**(3): p. 285-7.

29. Jimenez-Duran, G., et al., *Complement membrane attack complex is an immunometabolic regulator of NLRP3 activation and IL-18 secretion in human macrophages.* Front Immunol, 2022. **13**: p. 918551.

30. Miao, E.A., J.V. Rajan, and A. Aderem, *Caspase-1-induced pyroptotic cell death.* Immunol Rev, 2011. **243**(1): p. 206-14.

31. Triantafilou, M., et al., *Complementing the inflammasome.* Immunology, 2016. **147**(2): p. 152-64.

32. Laudisi, F., et al., *Cutting edge: the NLRP3 inflammasome links complement-mediated inflammation and IL-1beta release.* J Immunol, 2013. **191**(3): p. 1006-10.

33. Seok, J.K., et al., *Therapeutic regulation of the NLRP3 inflammasome in chronic inflammatory diseases.* Archives of Pharmacal Research, 2021. **44**(1): p. 16-35.

34. Latz, E., T.S. Xiao, and A. Stutz, *Activation and regulation of the inflammasomes.* Nature Reviews Immunology, 2013. **13**(6): p. 397-411.

35. Li, Z., et al., *Activation of the NLRP3 inflammasome and elevation of interleukin-1β secretion in infection by sever fever with thrombocytopenia syndrome virus.* Scientific Reports, 2022. **12**(1): p. 2573.

36. Kelley, N., et al., *The NLRP3 Inflammasome: An Overview of Mechanisms of Activation and Regulation.* Int J Mol Sci, 2019. **20**(13).

37. Bergsbaken, T., S.L. Fink, and B.T. Cookson, *Pyroptosis: host cell death and inflammation.* Nature Reviews Microbiology, 2009. **7**(2): p. 99-109.

38. Liu, Y., et al., *Impeding the combination of astrocytic ASCT2 and NLRP3 by talniflumate alleviates neuroinflammation in experimental models of Parkinson's disease.* Acta Pharm Sin B, 2023. **13**(2): p. 662-677.

39. Ising, C., et al., *NLRP3 inflammasome activation drives tau pathology.* Nature, 2019. **575**(7784): p. 669-673.

40. Zhang, Y., Z. Dong, and W. Song, *NLRP3 inflammasome as a novel therapeutic target for Alzheimer's disease.* Signal Transduct Target Ther, 2020. **5**(1): p. 37.

41. Chi, W., et al., *Caspase-8 promotes NLRP1/NLRP3 inflammasome activation and IL-1beta production in acute glaucoma.* Proc Natl Acad Sci U S A, 2014. **111**(30): p. 11181-6.

42. Perrone, L., et al., *Thioredoxin interacting protein (TXNIP) induces inflammation through chromatin modification in retinal capillary endothelial cells under diabetic conditions.* J Cell Physiol, 2009. **221**(1): p. 262-72.

43. Tseng, W.A., et al., *NLRP3 inflammasome activation in retinal pigment epithelial cells by lysosomal destabilization: implications for age-related macular degeneration.* Invest Ophthalmol Vis Sci, 2013. **54**(1): p. 110-20.

44. Zheng, Q., et al., *Reactive oxygen species activated NLRP3 inflammasomes initiate inflammation in hyperosmolarity stressed human corneal epithelial cells and environment-induced dry eye patients.* Exp Eye Res, 2015. **134**: p. 133-40.

45. Orecchioni, M., et al., *Olfactory receptor 2 in vascular macrophages drives atherosclerosis by NLRP3-dependent IL-1 production.* Science, 2022. **375**(6577): p. 214-221.

46. Schunk, S.J., et al., *Genetically determined NLRP3 inflammasome activation associates with systemic inflammation and cardiovascular mortality.* Eur Heart J, 2021. **42**(18): p. 1742-1756.

47. Coll, R.C., et al., *A small-molecule inhibitor of the NLRP3 inflammasome for the treatment of inflammatory diseases.* Nat Med, 2015. **21**(3): p. 248-55.

48. Albornoz, E.A., et al., *SARS-CoV-2 drives NLRP3 inflammasome activation in human microglia through spike protein.* Molecular Psychiatry, 2023. **28**(7): p. 2878-2893.

49. Mieres-Castro, D. and F. Mora-Poblete *Saponins: Research Progress and Their Potential Role in the Post-COVID-19 Pandemic Era*. Pharmaceutics, 2023. **15**, DOI: 10.3390/pharmaceutics15020348.

50. Zarghi, A. and S. Arfaei, *Selective COX-2 Inhibitors: A Review of Their Structure-Activity Relationships.* Iran J Pharm Res, 2011. **10**(4): p. 655-83.

51. Useini, L., et al., *Carboranyl Analogues of Mefenamic Acid and Their Biological Evaluation.* ACS Omega, 2022. **7**(28): p. 24282-24291.

52. Maroon, J.C., J.W. Bost, and A. Maroon, *Natural anti-inflammatory agents for pain relief.* Surg Neurol Int, 2010. **1**: p. 80.

53. Sultana, N. and Z.S. Saify, *Naturally occurring and synthetic agents as potential anti-inflammatory and immunomodulants.* Antiinflamm Antiallergy Agents Med Chem, 2012. **11**(1): p. 3-19.

54. Bunte, K., A. Hensel, and T. Beikler, *Polyphenols in the prevention and treatment of periodontal disease: A systematic review of in vivo, ex vivo and in vitro studies.* Fitoterapia, 2019. **132**: p. 30-39.

55. Mandegary, A., et al., *Alkaloid and flavonoid rich fractions of fenugreek seeds (Trigonella foenum-graecum L.) with antinociceptive and anti-inflammatory effects.* Food and Chemical Toxicology, 2012. **50**(7): p. 2503-2507.

56. Thoh, M., et al., *Azadirachtin interacts with the tumor necrosis factor (TNF) binding domain of its receptors and inhibits TNF-induced biological responses.* J Biol Chem, 2010. **285**(8): p. 5888-95.

57. Peng, Y., et al., *Anti-Inflammatory Effects of Curcumin in the Inflammatory Diseases: Status, Limitations and Countermeasures.* Drug Des Devel Ther, 2021. **15**: p. 4503-4525.

58. Mahendran, S., et al., *Antioxidant, analgesic and anti-inflammatory properties of new ninhydrin adduct of embelin.* Pharmaceutical Chemistry Journal, 2011. **45**(9): p. 547-551.

59. Donnelly, L.E., et al., *Anti-inflammatory effects of resveratrol in lung epithelial cells: molecular mechanisms.* Am J Physiol Lung Cell Mol Physiol, 2004. **287**(4): p. L774-83.

60. Kleemann, R., et al., *Anti-inflammatory, anti-proliferative and anti-atherosclerotic effects of quercetin in human in vitro and in vivo models.* Atherosclerosis, 2011. **218**(1): p. 44-52.

61. Rajkumar, S.V., et al., *Phase III Clinical Trial of Thalidomide Plus Dexamethasone Compared With Dexamethasone Alone in Newly Diagnosed Multiple Myeloma: A Clinical Trial Coordinated by the Eastern Cooperative Oncology Group.* Journal of Clinical Oncology, 2006. **24**(3): p. 431-436.

62. Fanlo, P., et al., *Efficacy and Safety of Anakinra Plus Standard of Care for Patients With Severe COVID-19: A Randomized Phase 2/3 Clinical Trial.* JAMA Network Open, 2023. **6**(4): p. e237243-e237243.

63. Carlisi, D., et al., *Parthenolide and Its Soluble Analogues: Multitasking Compounds with Antitumor Properties.* Biomedicines, 2022. **10**(2).

64. Ridker, P.M., et al., *Antiinflammatory Therapy with Canakinumab for Atherosclerotic Disease.* N Engl J Med, 2017. **377**(12): p. 1119-1131.

65. Xu, S., et al., *Inflammasome inhibitors: promising therapeutic approaches against cancer.* J Hematol Oncol, 2019. **12**(1): p. 64.

66. *Non-steroidal anti-inflammatory drugs (NSAIDs) — mechanisms of action*, in *Dictionary of Rheumatology*, J. Rovenský and J. Payer, Editors. 2009, Springer Vienna: Vienna. p. 146-148.

67. Elkordy, A.A., et al., *An overview on natural product drug formulations from conventional medicines to nanomedicines: Past, present and future.* Journal of Drug Delivery Science and Technology, 2021. **63**: p. 102459.

68. Atanasov, A.G., et al., *Natural products in drug discovery: advances and opportunities.* Nature Reviews Drug Discovery, 2021. **20**(3): p. 200-216.

69. Atanasov, A.G., et al., *Natural products in drug discovery: advances and opportunities.* Nat Rev Drug Discov, 2021. **20**(3): p. 200-216.

70. Dorota, K., et al., *Saponin-Based, Biological-Active Surfactants from Plants*, in *Application and Characterization of Surfactants*, N. Reza, Editor. 2017, IntechOpen: Rijeka. p. Ch. 6.

71. Podolak, I., A. Galanty, and D. Sobolewska, *Saponins as cytotoxic agents: a review.* Phytochemistry Reviews, 2010. **9**(3): p. 425-474.

72. Divekar, P.A., et al., *Plant Secondary Metabolites as Defense Tools against Herbivores for Sustainable Crop Protection.* Int J Mol Sci, 2022. **23**(5).

73. Singh, D. and P.K. Chaudhuri, *Structural characteristics, bioavailability and cardioprotective potential of saponins.* Integrative Medicine Research, 2018. **7**(1): p. 33-43.

74. Peng, S., et al., *Improving curcumin solubility and bioavailability by encapsulation in saponin-coated curcumin nanoparticles prepared using a simple pH-driven loading method.* Food & Function, 2018. **9**(3): p. 1829-1839.

75. Wang, P., *Natural and Synthetic Saponins as Vaccine Adjuvants.* Vaccines (Basel), 2021. **9**(3).

76. Chen, C., et al., *Comparative Transcriptome and Phytochemical Analysis Provides Insight into Triterpene Saponin Biosynthesis in Seeds and Flowers of the Tea Plant (Camellia sinensis).* Metabolites, 2022. **12**(3).

77. Thakur, M., et al., *Chemistry and pharmacology of saponins: special focus on cytotoxic properties.* Botanics: Targets and Therapy, 2011. **1**(null): p. 19-29.

78. Moses, T., K.K. Papadopoulou, and A. Osbourn, *Metabolic and functional diversity of saponins, biosynthetic intermediates and semi-synthetic derivatives.* Crit Rev Biochem Mol Biol, 2014. **49**(6): p. 439-62.

79. Navarro del Hierro, J., et al., *The gastrointestinal behavior of saponins and its significance for their bioavailability and bioactivities.* Journal of Functional Foods, 2018. **40**: p. 484-497.

80. Yu, K., F. Chen, and C. Li, *Absorption, disposition, and pharmacokinetics of saponins from Chinese medicinal herbs: what do we know and what do we need to know more?* Curr Drug Metab, 2012. **13**(5): p. 577-98.

81. He, Y., et al., *Recent Advances in Biotransformation of Saponins.* Molecules, 2019. **24**(13).

82. Passos, F.R.S., et al., *Anti-inflammatory and modulatory effects of steroidal saponins and sapogenins on cytokines: A review of pre-clinical research.* Phytomedicine, 2022. **96**: p. 153842.

83. Jang, K.-J., et al., *Anti-inflammatory effects of saponins derived from the roots of Platycodon grandiflorus in lipopolysaccharide-stimulated BV2 microglial cells.* Int J Mol Med, 2013. **31**(6): p. 1357-1366.

84. Keller, A.C., et al., *Saponins from the traditional medicinal plant Momordica charantia stimulate insulin secretion in vitro.* Phytomedicine, 2011. **19**(1): p. 32-7.

85. Patel, S.B., et al., *Anti-hyperglycemic and Anti-hyperlipidemic Effects of Bryonia Laciniosa Seed Extract and its Saponin Fraction in Streptozotocin-induced Diabetes in Rats.* Journal of Young Pharmacists, 2012. **4**(3): p. 171-176.

86. Zhang, H., et al., *Steroidal saponins and sapogenins from fenugreek and their inhibitory activity against α-glucosidase.* Steroids, 2020. **161**: p. 108690.

87. Podolak, I., A. Galanty, and D. Sobolewska, *Saponins as cytotoxic agents: a review.* Phytochem Rev, 2010. **9**(3): p. 425-474.

88. Moalic, S., et al., *A plant steroid, diosgenin, induces apoptosis, cell cycle arrest and COX activity in osteosarcoma cells.* FEBS Lett, 2001. **506**(3): p. 225-30.

89. Avato, P., et al., *Activity of Saponins from Medicago species Against HeLa and MCF-7 Cell Lines and their Capacity to Potentiate Cisplatin Effect.* Anti-Cancer Agents in Medicinal Chemistry- Anti-Cancer Agents), 2017. **17**(11): p. 1508-1518.

90. Yan, X.-J., et al., *Triterpenoids as reversal agents for anticancer drug resistance treatment.* Drug Discovery Today, 2014. **19**(4): p. 482-488.

91. Serra-Burriel, M., et al., *Impact of multi-drug resistant bacteria on economic and clinical outcomes of healthcare-associated infections in adults: Systematic review and meta-analysis.* PLoS One, 2020. **15**(1): p. e0227139.

92. Omokpariola, D.O., et al., *Phytochemical and Anti-Microbial Analysis of Metabolites in seeds of Moringa oleifera grown in Nigeria.* Progress in Chemical and Biochemical Research, 2021. **4**(3): p. 268-277.

93. Monte, J., et al., *Antimicrobial Activity of Selected Phytochemicals against Escherichia coli and Staphylococcus aureus and Their Biofilms.* Pathogens, 2014. **3**(2): p. 473-98.

94. Maeng, Y.S., et al., *Rk1, a ginsenoside, is a new blocker of vascular leakage acting through actin structure remodeling.* PLoS One, 2013. **8**(7): p. e68659.

95. Khan, G.J., et al., *Pharmacological effects and potential therapeutic targets of DT-13.* Biomedicine & Pharmacotherapy, 2018. **97**: p. 255-263.

96. Zhang, Y., et al., *The saponin DT-13 Attenuates Tumor Necrosis Factor-α-induced Vascular Inflammation Associated with Src/NF-κB/MAPK Pathway Modulation.* International Journal of Biological Sciences, 2015. **11**(8): p. 970-981.

97. Lee, J.-O., et al., *Korean Red Ginseng saponin fraction exerts anti-inflammatory effects by targeting the NF-κB and AP-1 pathways.* Journal of Ginseng Research, 2022. **46**(3): p. 489-495.

98. Villapol, S., *Roles of Peroxisome Proliferator-Activated Receptor Gamma on Brain and Peripheral Inflammation.* Cell Mol Neurobiol, 2018. **38**(1): p. 121-132.

99. Bouhlel, M.A., et al., *PPARgamma activation primes human monocytes into alternative M2 macrophages with anti-inflammatory properties.* Cell Metab, 2007. **6**(2): p. 137-43.

100. Kapadia, R., J.H. Yi, and R. Vemuganti, *Mechanisms of anti-inflammatory and neuroprotective actions of PPAR-gamma agonists.* Front Biosci, 2008. **13**: p. 1813-26.

101. Heneka, M.T., T. Klockgether, and D.L. Feinstein, *Peroxisome proliferator-activated receptor-gamma ligands reduce neuronal inducible nitric oxide synthase expression and cell death in vivo.* J Neurosci, 2000. **20**(18): p. 6862-7.

102. Medina-Gomez, G., et al., *PPAR gamma 2 prevents lipotoxicity by controlling adipose tissue expandability and peripheral lipid metabolism.* PLoS Genet, 2007. **3**(4): p. e64.

103. Moller, D.E. and J.P. Berger, *Role of PPARs in the regulation of obesity-related insulin sensitivity and inflammation.* Int J Obes Relat Metab Disord, 2003. **27 Suppl 3**: p. S17-21.

104. Hevener, A.L., et al., *Muscle-specific Pparg deletion causes insulin resistance.* Nat Med, 2003. **9**(12): p. 1491-7.

105. Goldstein, J.T., et al., *Genomic Activation of PPARG Reveals a Candidate Therapeutic Axis in Bladder Cancer.* Cancer Res, 2017. **77**(24): p. 6987-6998.

106. Feinstein, D.L., *Therapeutic potential of peroxisome proliferator-activated receptor agonists for neurological disease.* Diabetes Technol Ther, 2003. **5**(1): p. 67-73.

107. Chiarelli, F. and D. Di Marzio, *Peroxisome proliferator-activated receptor-gamma agonists and diabetes: current evidence and future perspectives.* Vasc Health Risk Manag, 2008. **4**(2): p. 297-304.

108. Bailey, S.T. and S. Ghosh, *'PPAR'ting ways with inflammation.* Nature Immunology, 2005. **6**(10): p. 966-967.

109. Pascual, G., et al., *A SUMOylation-dependent pathway mediates transrepression of inflammatory response genes by PPAR-gamma.* Nature, 2005. **437**(7059): p. 759-63.

110. Jennewein, C., et al., *Sumoylation of peroxisome proliferator-activated receptor gamma by apoptotic cells prevents lipopolysaccharide-induced NCoR removal from kappaB binding sites mediating transrepression of proinflammatory cytokines.* J Immunol, 2008. **181**(8): p. 5646-52.

111. Li, W., et al., *Anti-Inflammatory and PPAR Transactivational Effects of Oleanane-Type Triterpenoid Saponins from the Roots of <italic>Pulsatilla koreana</italic&gt.* Biomolecules & Therapeutics, 2014. **22**(4): p. 334-340.

112. Montanari, R., et al., *Screening of saponins and sapogenins from Medicago species as potential PPARgamma agonists and X-ray structure of the complex PPARgamma/caulophyllogenin.* Sci Rep, 2016. **6**: p. 27658.

113. Salah El Dine, R., et al., *PPARalpha and gamma Activation Effects of New Nor-triterpenoidal Saponins from the Aerial Parts of Anabasis articulata.* Planta Med, 2019. **85**(4): p. 274-281.

114. Al Sharif, M., et al., *Molecular determinants of PPARγ partial agonism and related in silico/in vivo studies of natural saponins as potential type 2 diabetes modulators.* Food and Chemical Toxicology, 2018. **112**: p. 47-59.

115. Guasch, L., et al., *Identification of PPARgamma partial agonists of natural origin (II): in silico prediction in natural extracts with known antidiabetic activity.* PLoS One, 2013. **8**(2): p. e55889.

116. Krskova-Tybitanclova, K., et al., *Short term 13-cis-retinoic acid treatment at therapeutic doses elevates expression of leptin, GLUT4, PPARgamma and aP2 in rat adipose tissue.* J Physiol Pharmacol, 2008. **59**(4): p. 731-43.

117. Monden, T., et al., *p120 acts as a specific coactivator for 9-cis-retinoic acid receptor (RXR) on peroxisome proliferator-activated receptor-gamma/RXR heterodimers.* Mol Endocrinol, 1999. **13**(10): p. 1695-703.

118. Kevser Bali, S., et al., *The effect of PFASs on PPAR-gamma/RXR-alpha heterodimer.* Biophysical Journal, 2023. **122**: p. 20a.

119. Park, J.Y., et al., *Ascofuranone inhibits lipopolysaccharide-induced inflammatory response via NF-kappaB and AP-1, p-ERK, TNF-α, IL-6 and IL-1β in RAW 264.7 macrophages.* PLoS One, 2017. **12**(2): p. e0171322.

120. Lakhan, R., et al., *Local administration of AAV-DJ pseudoserotype expressing COX2 provided early onset of transgene expression and promoted bone fracture healing in mice.* Gene Ther, 2015. **22**(9): p. 721-8.

121. Moser, V.A., M.F. Uchoa, and C.J. Pike, *TLR4 inhibitor TAK-242 attenuates the adverse neural effects of diet-induced obesity.* J Neuroinflammation, 2018. **15**(1): p. 306.

122. Yan, F., et al., *Corilagin Ameliorates Con A-Induced Hepatic Injury by Restricting M1 Macrophage Polarization.* Front Immunol, 2021. **12**: p. 807509.

123. Liu, Y., et al., *Angiotensin-(1-7) Suppresses Hepatocellular Carcinoma Growth and Angiogenesis via Complex Interactions of Angiotensin II Type 1 Receptor, Angiotensin II Type 2 Receptor and Mas Receptor.* Mol Med, 2015. **21**(1): p. 626-36.

124. Zhu, X., et al., *Inhibition of pyroptosis attenuates Staphylococcus aureus-induced bone injury in traumatic osteomyelitis.* Ann Transl Med, 2019. **7**(8): p. 170.

125. Hauser, S., et al., *Degradation of the peroxisome proliferator-activated receptor gamma is linked to ligand-dependent activation.* J Biol Chem, 2000. **275**(24): p. 18527-33.

126. Kim, J.B., et al., *ADD1/SREBP1 activates PPARgamma through the production of endogenous ligand.* Proc Natl Acad Sci U S A, 1998. **95**(8): p. 4333-7.

127. Takashiba, S., et al., *Differentiation of monocytes to macrophages primes cells for lipopolysaccharide stimulation via accumulation of cytoplasmic nuclear factor kappaB.* Infect Immun, 1999. **67**(11): p. 5573-8.

128. Garcia, X. and F. Stein, *Nitric Oxide.* Seminars in Pediatric Infectious Diseases, 2006. **17**(2): p. 55-57.

129. Aktan, F., *iNOS-mediated nitric oxide production and its regulation.* Life Sciences, 2004. **75**(6): p. 639-653.

130. Nakazawa, H., et al., *iNOS as a Driver of Inflammation and Apoptosis in Mouse Skeletal Muscle after Burn Injury: Possible Involvement of Sirt1 S-Nitrosylation-Mediated Acetylation of p65 NF-κB and p53.* PLoS One, 2017. **12**(1): p. e0170391.

131. Park, J.S., et al., *Anti-inflammatory mechanism of ginseng saponins in activated microglia.* J Neuroimmunol, 2009. **209**(1-2): p. 40-9.

132. Lee, J.O., et al., *Korean Red Ginseng saponin fraction exerts anti-inflammatory effects by targeting the NF-kappaB and AP-1 pathways.* J Ginseng Res, 2022. **46**(3): p. 489-495.

133. Akira, S. and K. Takeda, *Toll-like receptor signalling.* Nature Reviews Immunology, 2004. **4**(7): p. 499-511.

134. Kagan, J.C. and R. Medzhitov, *Phosphoinositide-mediated adaptor recruitment controls Toll-like receptor signaling.* Cell, 2006. **125**(5): p. 943-55.

135. Yamamoto, M., et al., *TRAM is specifically involved in the Toll-like receptor 4-mediated MyD88-independent signaling pathway.* Nat Immunol, 2003. **4**(11): p. 1144-50.

136. Procyk, K.J., et al., *Lipopolysaccharide induces Jun N-terminal kinase activation in macrophages by a novel Cdc42/Rac-independent pathway involving sequential activation of protein kinase C ζ and phosphatidylcholine-dependent phospholipase C.* Blood, 2000. **96**(7): p. 2592-2598.

137. Weinstein, S.L., et al., *Bacterial lipopolysaccharide induces tyrosine phosphorylation and activation of mitogen-activated protein kinases in macrophages.* Journal of Biological Chemistry, 1992. **267**(21): p. 14955-14962.

138. Zong, Y., et al., *Resveratrol inhibits LPS-induced MAPKs activation via activation of the phosphatidylinositol 3-kinase pathway in murine RAW 264.7 macrophage cells.* PLoS One, 2012. **7**(8): p. e44107.

139. Yu, Q., et al., *Ginsenoside Rk1 suppresses pro-inflammatory responses in lipopolysaccharide-stimulated RAW264.7 cells by inhibiting the Jak2/Stat3 pathway.* Chinese Journal of Natural Medicines, 2017. **15**(10): p. 751-757.

140. Zhang, Y., et al., *The saponin DT-13 attenuates tumor necrosis factor-α-induced vascular inflammation associated with Src/NF-κB/MAPK pathway modulation.* Int J Biol Sci, 2015. **11**(8): p. 970-81.

141. Bagaev, A.V., et al., *Elevated pre-activation basal level of nuclear NF-κB in native macrophages accelerates LPS-induced translocation of cytosolic NF-κB into the cell nucleus.* Scientific Reports, 2019. **9**(1): p. 4563.

142. Cheng, G., et al., *Polyphyllin II inhibits NLPR3 inflammasome activation and inflammatory response of Mycobacterium tuberculosis-infected human bronchial epithelial cells.* Allergol Immunopathol (Madr), 2024. **52**(1): p. 16-23.

143. Hooftman, A. and L.A.J. O'Neill, *Can NLRP3 inhibitors improve on dexamethasone for the treatment of COVID-19?* Curr Res Pharmacol Drug Discov, 2021. **2**: p. 100048.

144. Ma, J.J., et al., *Establishment of a cell-based drug screening model for identifying agonists of human peroxisome proliferator-activated receptor gamma (PPARgamma).* J Pharm Pharmacol, 2012. **64**(5): p. 719-26.

145. Willems, S., et al., *Endogenous vitamin E metabolites mediate allosteric PPARgamma activation with unprecedented co-regulatory interactions.* Cell Chem Biol, 2021. **28**(10): p. 1489-1500 e8.

146. Smith, W.S., et al., *Membrane cholesterol is essential for triterpenoid saponin augmentation of a saporin-based immunotoxin directed against CD19 on human lymphoma cells.* Biochimica et Biophysica Acta (BBA) - Biomembranes, 2017. **1859**(5): p. 993-1007.

147. Tak, P.P. and G.S. Firestein, *NF-kappaB: a key role in inflammatory diseases.* J Clin Invest, 2001. **107**(1): p. 7-11.

148. Khan, M.I., et al. *Therapeutic Effects of Saponins for the Prevention and Treatment of Cancer by Ameliorating Inflammation and Angiogenesis and Inducing Antioxidant and Apoptotic Effects in Human Cells*. International Journal of Molecular Sciences, 2022. **23**, DOI: 10.3390/ijms231810665.

149. Sun, Y., et al., *New Therapeutic Approaches to and Mechanisms of Ginsenoside Rg1 against Neurological Diseases.* Cells, 2022. **11**(16).

150. Zhu, Y., et al., *Ginsenoside Rg1 as a promising adjuvant agent for enhancing the anti-cancer functions of granulocytes inhibited by noradrenaline.* Frontiers in Immunology, 2023. **14**.

151. She, L., et al., *Ginsenoside Rk3 ameliorates Aβ-induced neurotoxicity in APP/PS1 model mice via AMPK signaling pathway.* Biomedicine & Pharmacotherapy, 2023. **158**: p. 114192.

152. Gao, Q., et al., *Ginsenoside Rg1 alleviates ANIT-induced cholestatic liver injury by inhibiting hepatic inflammation and oxidative stress via SIRT1 activation.* Journal of Ethnopharmacology, 2024. **319**: p. 117089.

153. Yang, L.L., et al., *Endotoxin molecule lipopolysaccharide-induced zebrafish inflammation model: a novel screening method for anti-inflammatory drugs.* Molecules, 2014. **19**(2): p. 2390-409.

154. Seehase, S., et al., *LPS-induced lung inflammation in marmoset monkeys - an acute model for anti-inflammatory drug testing.* PLoS One, 2012. **7**(8): p. e43709.

155. Inagawa, H., C. Kohchi, and G. Soma, *Oral administration of lipopolysaccharides for the prevention of various diseases: benefit and usefulness.* Anticancer Res, 2011. **31**(7): p. 2431-6.

156. Honda, T. and H. Inagawa, *Utility of In Vitro Cellular Models of Low-Dose Lipopolysaccharide in Elucidating the Mechanisms of Anti-Inflammatory and Wound-Healing-Promoting Effects of Lipopolysaccharide Administration In Vivo.* Int J Mol Sci, 2023. **24**(18).

157. Honda, T. and H. Inagawa, *Suppression of Inflammatory Cytokine Genes Expression in Vascular Endothelial Cells by Super-low Dose Lipopolysaccharide-activated Macrophages.* Anticancer Res, 2022. **42**(8): p. 4049-4054.

158. Shi, H., et al., *The in vitro effect of lipopolysaccharide on proliferation, inflammatory factors and antioxidant enzyme activity in bovine mammary epithelial cells.* Anim Nutr, 2016. **2**(2): p. 99-104.

159. Antonicelli, F., et al., *Regulation of LPS-mediated inflammation in vivo and in vitro by the thiol antioxidant Nacystelyn.* Am J Physiol Lung Cell Mol Physiol, 2004. **286**(6): p. L1319-27.

160. Garlito-Diaz, H., et al., *A New Antifungal-Loaded Sol-Gel Can Prevent Candida albicans Prosthetic Joint Infection.* Antibiotics (Basel), 2021. **10**(6).

161. Fracasso, J.A.R., et al., *Toxicological Profile and Anti-Inflammatory Effect of Mucoadhesive Gel from Residues of Agave sisalana and Punica granatum.* Gels, 2023. **9**(12): p. 942.

162. Prabhakar, G., et al., *In vitro biological evaluation of Steroidal Saponins from seeds of Crotalaria verrucosa L. for cancer studies.* Environmental Advances, 2024. **15**: p. 100471.

163. Bachran, C., et al., *Chapter 9 - Preclinical Studies of Saponins for Tumor Therapy*, in *Recent Advances in Medicinal Chemistry*, R. Atta ur, M.I. Choudhary, and G. Perry, Editors. 2014, Elsevier. p. 272-302.

164. Zhu, J., et al., *Saikosaponin A mediates the inflammatory response by inhibiting the MAPK and NF-κB pathways in LPS-stimulated RAW 264.7 cells.* Exp Ther Med, 2013. **5**(5): p. 1345-1350.

165. Patrignani, P., et al., *Managing the adverse effects of nonsteroidal anti-inflammatory drugs.* Expert Rev Clin Pharmacol, 2011. **4**(5): p. 605-21.

166. Fortun, P.J. and C.J. Hawkey, *Nonsteroidal antiinflammatory drugs and the small intestine.* Curr Opin Gastroenterol, 2007. **23**(2): p. 134-41.

167. Sohail, R., et al., *Effects of Non-steroidal Anti-inflammatory Drugs (NSAIDs) and Gastroprotective NSAIDs on the Gastrointestinal Tract: A Narrative Review.* Cureus, 2023. **15**(4): p. e37080.

168. Liu, W., et al., *Anti-Inflammatory Function of Plant-Derived Bioactive Peptides: A Review.* Foods, 2022. **11**(15).

169. Kuang, G., et al., *Study of Absorption Characteristics of the Total Saponins from Radix Ilicis Pubescentis in an In Situ Single-Pass Intestinal Perfusion (SPIP) Rat Model by Using Ultra Performance Liquid Chromatography (UPLC).* Molecules, 2017. **22**(11).

170. Nemudzivhadi, V. and P. Masoko, *In Vitro Assessment of Cytotoxicity, Antioxidant, and Anti-Inflammatory Activities of Ricinus communis (Euphorbiaceae) Leaf Extracts.* Evidence-Based Complementary and Alternative Medicine, 2014. **2014**: p. 625961.

171. Maroon, J.C., et al., *Natural antiinflammatory agents for pain relief in athletes.* Neurosurg Focus, 2006. **21**(4): p. E11.

172. Yu, Q., et al., *Ginsenoside Rk1 suppresses pro-inflammatory responses in lipopolysaccharide-stimulated RAW264.7 cells by inhibiting the Jak2/Stat3 pathway.* Chin J Nat Med, 2017. **15**(10): p. 751-757.

173. Chuang, T.Y., et al., *Suppression of LPS-induced inflammatory responses by the hydroxyl groups of dexamethasone.* Oncotarget, 2017. **8**(30): p. 49735-49748.

174. Fan, R., et al., *DT-13 ameliorates TNF-α-induced nitric oxide production in the endothelium in vivo and in vitro.* Biochemical and Biophysical Research Communications, 2018. **495**(1): p. 1175-1181.

175. Sun, P., et al., *Matrine inhibits IL-1β secretion in primary porcine alveolar macrophages through the MyD88/NF-κB pathway and NLRP3 inflammasome.* Veterinary Research, 2019. **50**(1): p. 53.

176. Zhou, J., et al., *Effect of dexamethasone on TLR4 and MyD88 expression in monocytes of patients with tuberculous meningitis.* European Journal of Inflammation, 2017. **15**(2): p. 107-112.

177. Chang, W.-T., et al., *Mutant glucocorticoid receptor binding elements on the interleukin-6 promoter regulate dexamethasone effects.* BMC Immunology, 2021. **22**(1): p. 24.

178. Montoya, S., et al., *Targeted Therapies in Cancer: To Be or Not to Be, Selective.* Biomedicines, 2021. **9**(11).

179. Zhong, L., et al., *Small molecules in targeted cancer therapy: advances, challenges, and future perspectives.* Signal Transduction and Targeted Therapy, 2021. **6**(1): p. 201.

180. Bjarnason, I. and B. Thjodleifsson, *Gastrointestinal toxicity of non-steroidal anti-inflammatory drugs: the effect of nimesulide compared with naproxen on the human gastrointestinal tract.* Rheumatology (Oxford), 1999. **38 Suppl 1**: p. 24-32.

181. Lebovitz, H.E., *Differentiating members of the thiazolidinedione class: a focus on safety.* Diabetes Metab Res Rev, 2002. **18 Suppl 2**: p. S23-9.

182. Zhou, M., et al., *Endotoxin downregulates peroxisome proliferator-activated receptor-gamma via the increase in TNF-alpha release.* Am J Physiol Regul Integr Comp Physiol, 2008. **294**(1): p. R84-92.

183. Zhang, T., et al., *Saponins as modulators of nuclear receptors.* Crit Rev Food Sci Nutr, 2020. **60**(1): p. 94-107.

184. Schwarz, P.F., et al., *Identification of the Natural Steroid Sapogenin Diosgenin as a Direct Dual-Specific RORα/γ Inverse Agonist.* Biomedicines, 2022. **10**(9).

185. Kilu, W., et al., *Heterodimer formation with retinoic acid receptor RXRα modulates coactivator recruitment by peroxisome proliferator-activated receptor PPARγ.* J Biol Chem, 2021. **297**(1): p. 100814.

186. Fuchs, H., et al., *Glycosylated Triterpenoids as Endosomal Escape Enhancers in Targeted Tumor Therapies.* Biomedicines, 2017. **5**(2): p. 14.

187. Schreiner, T.B., et al., *Saponins as Natural Emulsifiers for Nanoemulsions.* Journal of Agricultural and Food Chemistry, 2022. **70**(22): p. 6573-6590.

188. Zannino, L., et al., *Histochemical and ultrastructural localization of triterpene saponins in Medicago truncatula.* Microsc Res Tech, 2024.

189. Jacob, M.C., M. Favre, and J.C. Bensa, *Membrane cell permeabilization with saponin and multiparametric analysis by flow cytometry.* Cytometry, 1991. **12**(6): p. 550-8.

190. Schreiner, T.B., et al., *Saponins as Natural Emulsifiers for Nanoemulsions.* J Agric Food Chem, 2022. **70**(22): p. 6573-6590.

191. Ozturk, B., et al., *Formation and stabilization of nanoemulsion-based vitamin E delivery systems using natural surfactants: Quillaja saponin and lecithin.* Journal of Food Engineering, 2014. **142**: p. 57-63.

192. Korchowiec, B., et al., *The Molecular Bases of the Interaction between a Saponin from the Roots of Gypsophila paniculata L. and Model Lipid Membranes.* Int J Mol Sci, 2022. **23**(6).

193. Frenkel, N., et al., *Mechanistic investigation of interactions between steroidal saponin digitonin and cell membrane models.* J Phys Chem B, 2014. **118**(50): p. 14632-9.

194. Weng, A., C. Görick, and M.F. Melzig, *Enhancement of toxicity of saporin-based toxins by Gypsophila saponins--kinetic of the saponin.* Exp Biol Med (Maywood), 2009. **234**(8): p. 961-6.

195. Negi, J.S., et al., *High-performance liquid chromatography analysis of plant saponins: An update 2005-2010.* Pharmacogn Rev, 2011. **5**(10): p. 155-8.

196. Wang, Y., et al., *Recent Advances in Separation and Analysis of Saponins in Natural Products.* Separations, 2022. **9**(7): p. 163.

197. Imran, M., et al., *Quantification of mangiferin by high pressure liquid chromatography; physicochemical and sensory evaluation of functional mangiferin drink.* Journal of Food Processing and Preservation, 2016. **40**(4): p. 760-769.

198. Liu, G., et al., *Isolation, Identification, and Quantitative Determination of Saponin in Apostichopus japonicus by HPLC-DAD.* Journal of Ocean University of China, 2022. **21**(2): p. 473-478.

199. Xu, C., et al., *IL-4 activates ULK1/Atg9a/Rab9 in asthma, NLRP3 inflammasomes, and Golgi fragmentation by increasing autophagy flux and mitochondrial oxidative stress.* Redox Biol, 2024. **71**: p. 103090.

Appendix

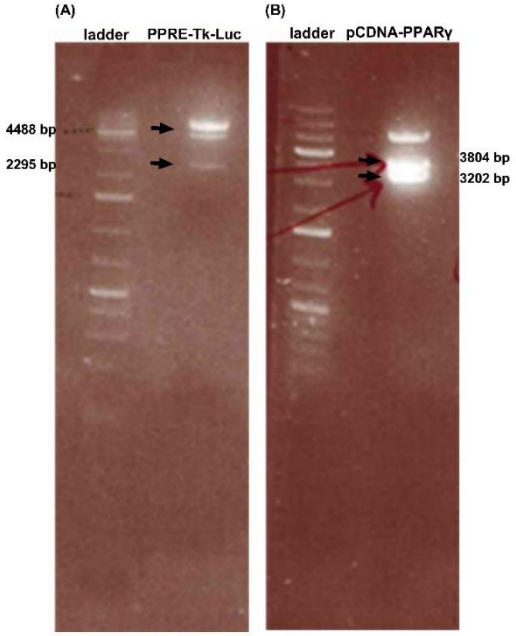

Figure S1: Restriction digestion of plasmids

To validate the presence of pure and intact plasmid post isolation of plasmids from bacterial pellet, double restriction digestion of plasmids was performed.

The agarose gels depict the presence of two partially digested fragments of PPRE-Tk-Luc (A)and (B) pCDNA-PPARg plasmids.

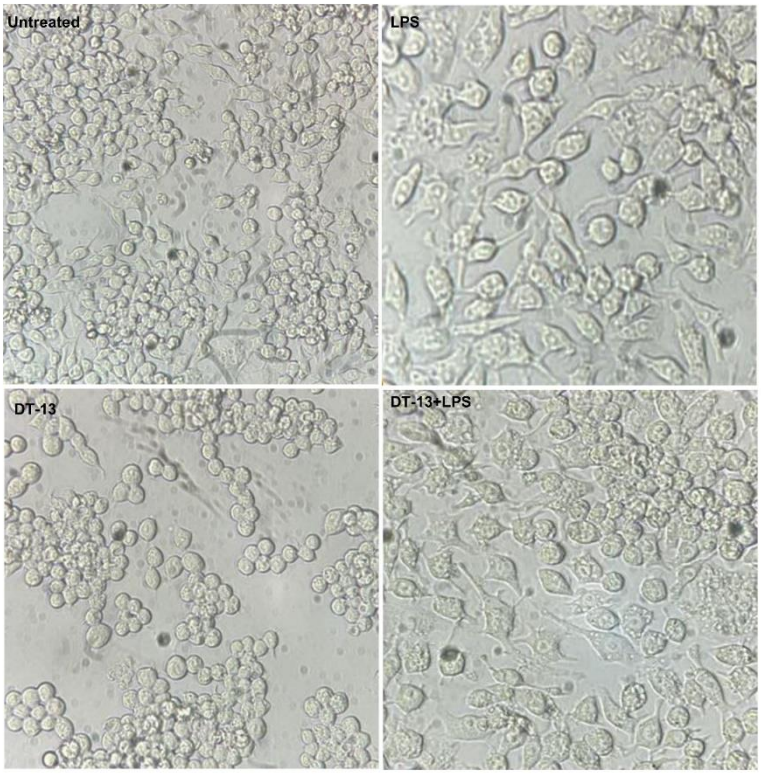

Figure S2 : Images of RAW264.7 cells in presence of DT-13 and LPS as observed under light microscope.

Morphological changes in pre-treated RAW264.7 cells

RAW264.7 cells were maintained until confluency 80% before splitting for experiments. The morphological changes of cells in presence of cell treatments were visualised under light microscope. As seen in supplemental figure, untreated cells appeared normal without any extensions and change in shape. Cells treated with 10 ng of LPS had star like appearance with elongated cell extensions and more vacuoles inside the cytoplasmic region. These increased number of intercytoplasmic vacuoles indicate cell under stress. Cells pre-treated with DT-13 did not show any change in morphology of the cells, whereas DT-13 pre-treated LPS stimulated cells again showed vacuoles inside the cells. The images depicted that DT-13 pre-treatment did not improve the morphological appearance of the cells in contrast to the physiological changes observed with cell culture experiments.

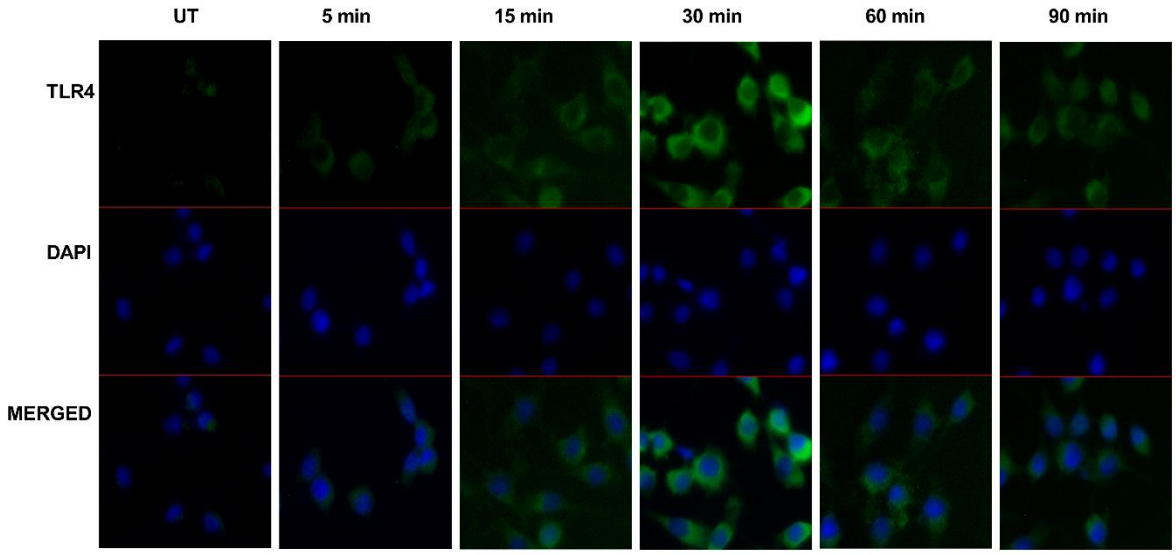

Figure S3 : TLR4 expression in response to LPS in RAW26.7 at various time points as observed by immunofluorescence.

To determine the effect of LPS on the expression of TLR4 receptor protein in RAW264.7 macrophages, cells were incubated with 200 ng LPS at different time points. With the help of immunofluorescence, green FITC labelled TLR4 was visualised to be highly expressed after 30 min of LPS incubation. However, the TLR4 expression diminished in further LPS incubations at 60 and 90 min. This effect corresponded with the high expression of NFκB protein post 30 min of LPS incubation in macrophages.

List of Publications

Publication I

DT-13 attenuates inflammation by inhibiting NLRP3-inflammasome related genes in RAW264.7 macrophages

Raina, S., Hübner, E., Samuel, E., Nagel, G., & Fuchs, H. (2024)

Biochemical and biophysical research communications, *708*, 149763. https://doi.org/10.1016/j.bbrc.2024.149763

Publication II

DT-13 Mediates Ligand-Dependent Activation of PPARγ Response Elements In Vitro

Raina, Shikha, Esther Samuel, and Hendrik Fuchs. (2024)

Biology, *13*(12), 1015. https://doi.org/10.3390/biology13121015